MIXED BATTERY ARRAY ENERGY STORAGE SYSTEM

By

Xiaoyang Ning

Submitted in partial fulfillment of the requirements for the degree of Master of Applied Science

at

Dalhousie University
Halifax, Nova Scotia
June 2024

Dalhousie University is located in Mi'kma'ki, the ancestral and unceded territory of the Mi'kmaq. We are all Treaty people.

TABLE OF CONTENTS

LIST OF TABLES

LIST OF FIGURES

ABSTRACT

This research proposes and studies aspects of a mixed battery array composed of used electric vehicle (EV) batteries repurposed into a second life in both a theoretical and experimental fashion. The research seeks to address five key objectives.

Battery pack performance analysis and battery pack grouping: The primary focus is to assess individual electric vehicle battery pack state of health conditions performance and devise optimal grouping strategies for a mixed battery array configuration. The research intends to examine system energy efficiency, battery capacity degradation, and the implications of different lithium-ion battery types in operation within a mixed battery array context.

Battery pack interconnection comparison between the DC-couple and AC-couple power conversion system: This aspect of the study will compare the energy efficiency of DC and AC coupling methods for interconnecting battery packs within the mixed battery array energy system.

Battery management system (BMS) component comparison between original equipment manufacturer and third-party equipment: This research section focused on a comparative study between utilizing the original BMS installed in EV battery packs or replacing BMS for the second-life application. Thus, this part of the research also developed several BMS replacement methods to facilitate different original BMS types and battery pack designs.

Energy management system (EMS) integration: This research project installed a centralized battery management system for each battery pack to obtain full access to the battery pack; thus, the scope of this part of the research included developing an energy management system and a digital communication system between the battery management system and the energy management system.

Battery Thermal Management System (TMS) Comparison: The work described in this thesis evaluated three types of TMS for their feasibility in mixed battery systems: one passive TMS and two active TMS systems utilizing forced air and liquid cooling. The research aimed to consolidate the TMS based on the maximum operational power rate of the battery packs. The testing results indicated that the battery pack could be passively cooled if the discharge power rate is lower than 2 hours. However, liquid cooling is highly recommended for operation power rates exceeding the 2-hour rate. Due to the complex air vent design, forced air TMS is not recommended for mixed battery array systems.

The demonstration system built during this project aims to validate the design options recommended for the mixed battery array system. Hence, the single-pack operation testing at the end of this project presented the operation capability from the demonstration unit. All battery packs were cycled at a 3-hour rate during the testing stage using constant power for an initial condition evaluation. The Tesla Model 3 long-range battery pack provided 57 kWh of usable energy; the Tesla Model 3 standard-range battery pack provided 54 kWh of usable energy; the Bolt battery pack provided 54 kWh of usable energy; the GV 60 battery pack provided 69 kWh of usable energy. In addition, the AC-coupled power architecture demonstrated the flexibility of the mixed battery array system in accepting the various EV battery packs and further proved the adaptive scalability of such design for battery systems in the future. Finally, the selected battery management system proved the communication reliability and cell balancing function during single-pack testing cycling.

LIST OF ABBREVIATIONS

BESS	Battery Energy Storage System
BMS	Battery Management System
CG	Cell Group
CTC	Cell to Chassis
CTP	Cell to Pack
EA	Energy Arbitrage
EIA	US Energy Information Administration
EMS	Energy Management System
EV	Electric Vehicle
FR	Frequency Regulation
GV60	Genesis GV60 Battery
IR	Internal Resistance
LFP	Lithium Iron Phosphate
LIB	Lithium-ion Battery
LMO	Lithium-Manganese Oxide
M3LR	Tesla Model 3 Long-Range Battery
M3SR	Tesla Model 3 Standard-Range Battery
MBA	Mixed Battery Array
MCU	Master Controller Unit
MTC	Module to Chassis
MTP	Module to Pack
NCA	Nickel Cobalt Aluminum Oxide
NMC	Nickel-Manganese-Cobalt
ODB2	On-Board Diagnostic II
OEM	Original Equipment Manufacturer
PCM	Phase Changing Materials
PNNL	Pacific Northwest National Labs
PS	Peak Shaving
RESL	Renewable Energy Storage Laboratory
RPT	Reference Performance Testing
SLD	Single Line Diagram
STC	Standalone Test Container
TMS	Thermal Management System
VPC	Voltage Per Cell

GLOSSARY

- **Battery Management System (BMS):** A system that reports cell group voltages, pack current, pack voltage, temperature, and alarms and provides cell voltage balancing.
- **Cell:** The basic unit of a battery consists of positive and negative electrodes, an electrolyte, a separator, and an enclosure.
- **Cell Group:** Multiple cells forming a parallel group with the same voltage by connecting in parallel.
- **DC-DC Converter:** Devices that convert DC electrical power bi-directionally from different voltages to a uniform voltage on the DC Bus.
- **Energy Efficiency:** The ratio of the energy output from a battery to the energy input during one charging and discharging cycle, which starts and ends at the same state of charge.
- **Energy Management System (EMS):** Computer software manages BESS operations, overseeing tasks such as battery status monitoring, power conversion system control, energy demand response, thermal management, etc.
- **Hour Rate:** The ratio of rated energy capacity (kWh or Ah) to the operation power rate (kW or A) describes the time required to fully discharge a battery.
- **Internal Resistance (IR):** The electrical resistance within a battery cell is caused by the cell design or cell chemistry, which affects its energy efficiency.
- **Module:** A group of battery cells connected in series in a single enclosure.
- **Open Circuit Voltage (OCV):** The battery terminal voltage measured at the non-operation state.
- **Pack:** An assembly of multiple modules or cells, including additional components such as thermal and battery management systems and safety features.
- **Power Conversion System (PCS):** Devices that convert electrical power bi-directionally between DC and AC to facilitate energy transfer entering and leaving the battery system.
- **State of Charge (SOC):** A measurement indicating the remaining coulombic capacity of a battery as a percentage of its rate capacity.
- **State of Health (SOH):** A percentage calculation of the maximum usable energy capacity with respect to the rate of energy capacity.

ACKNOWLEDGEMENTS

I extend my deepest gratitude to Dr. Lukas Swan, whose invaluable guidance has enriched my journey toward earning this degree and profoundly impacted my development as a diligent and thoughtful engineer. His relentless support and exceptional mentorship have significantly enhanced my professional skills and personal growth. Dr. Swan's role as a supervisor and mentor has been truly remarkable.

I am also deeply thankful to my supervisory committee, Dr. Pegg and Dr. Doman, for their indispensable advice and meticulous review of my project. Their insights and feedback have been critical to the advancement of my work.

My heartfelt thanks go out to my colleagues, friends, and family, whose unwavering support and encouragement have made my academic journey a memorable and enjoyable experience. I want to extend special thanks to Riley Roache, Blair Bresson, and Rikuto Nakayasu, whose dedicated assistance in the lab was pivotal to the success of this project. Their tireless and committed efforts have been instrumental in bringing this work to fruition.

This research would not have been possible without the financial support from the Natural Sciences and Engineering Research Council of Canada and the generous funding from Dr. Lukas Swan's Discovery Grant, LES Create Grant, and the Canadian Innovation Foundation. Their support has been crucial in enabling the research and its achievements.

1 INTRODUCTION

The growing global interest in variable renewable energy systems, such as wind and solar power, is driving an increasing demand for innovative energy storage solutions. Consequently, battery energy storage systems (BESS) have emerged as crucial supports for the electricity sector amid this transition. BESS has attracted considerable attention due to its rapid deployment, flexible integration, and high compatibility with new and existing electrical infrastructures. However, the current global lithium-ion batteries (LIB) production mainly supplies the electric vehicle (EV) industry, which is projected to constrain the rate of BESS installations due to insufficient battery supply. This challenge has sparked interest in repurposing EV batteries for second-life applications in energy storage. As many LIBs are anticipated to reach end-of-life in the near future, this approach offers a promising solution to meet market demand in the coming decades.

According to the International Energy Agency (IEA), the global EV battery demand in 2022 was around 550.5 GWh, which consumed 78.6% of total LIB production in 2022 [1], and McKinsey also projected the battery demands for EVs will continue to grow by about six times, reaching around 3.38 TWh by 2030 [2]. Therefore, even more EV batteries will become available for second-life applications. Most automakers expect more than 15 years or 100,000-mile lifespan on their EV batteries [3]. After the primary applications in EVs, most LIBs still contain a substantial amount of energy capacity in most cases; therefore, these batteries still have a lot of remaining economic potential if used in second-life applications. According to the US Advanced Battery Consortium, Lithium-ion batteries would only lose an average of 20 to 25% of rated capacity after fifteen years of regular operation as EV batteries, which converts to 75% state of health (SOH) at the end of its life in an EV [4]. However, as the battery technology improves over the years, and battery capacity increase in the EV industry the battery pack end of life energy capacity also projected to increase as shown in Figure 1.1 [5].

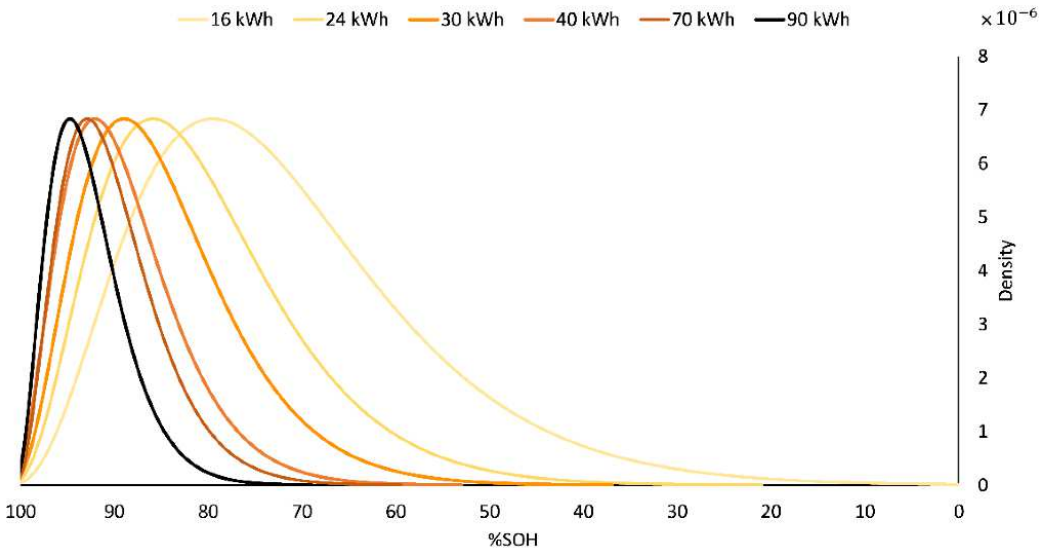

Figure 1.1: EV Battery End of Life Capacity Projection By Energy Density

. This data suggested the potential to reuse the retired EV batteries for BESS, as they are currently recycled after their EV life, forming a large amount of wasted material and lost economic value.

On the other hand, the 2023 Energy Storage Market Outlook published by Bloomberg stated that their market analysis showed a 27% compound annual growth rate in LIB demand for stationary BESS in the next six years [6]. Hence, the current global LIB production capacity will not support the future battery demand for the electricity sector without expanding production capacity or exploring new energy storage solutions. Thus, this imbalanced demand and supply have led to a rapidly growing interest in repurposing EV batteries for secondary applications, contributing to a more sustainable and circular economy.

1.1 CURRENT CHALLENGES OF REPURPOSING EV BATTERIES

Repurposing EV batteries opens numerous opportunities but is accompanied by several challenges. These include battery cell degradation, the diversity in battery pack designs, SOH variations, communication protocols, geometry, thermal management solutions, and power capabilities. Any of these issues can significantly affect the performance and energy efficiency of energy storage systems utilizing second-life EV batteries. Due to the lack of support from the original equipment manufacturer (OEM), these challenges are more profound for independent battery system integrators. As such, aftermarket EV battery application developers often need to open and modify the EV battery packs to repurpose

them for BESS, and this process will pose additional safety risks and labour costs for third-party developers.

Furthermore, the developed standardized testing protocols, repurposing guidelines, and potential safety risks hamper the broader acceptance of this technology [7]. In North America, UL 1974 is the primary regulation for repurposing EV batteries, offering extensive testing protocol guidance[8]. However, this regulation is criticized for being excessively conservative and onerous.

Moreover, financial groups analyzing the battery storage system market are raising concerns about the economic hurdles in repurposing EV batteries. While it is commonly acknowledged that retired EV batteries cost considerably less than new ones, the cumulative expenses of evaluating, refurbishing, and deploying these batteries remain considerable [9]. The repurposed EV battery packs require sophisticated energy management technology and robust system safety design, and these batteries must be meticulously operated to ensure battery safety and reliability for second-life applications. Right now, these expenses may outweigh the economic benefits of choosing second-life batteries over new ones [9].

Finally, logistical challenges introduce additional costs and complexities, such as collecting, transporting, and storing used batteries. Given the hazardous nature of lithium-ion batteries, these logistics must be managed with the utmost care, adhering to stringent safety standards, thus inflating the costs and logistical burdens associated with repurposing efforts. Overcoming these economic barriers is crucial for the successful integration and broader adoption of second-life EV batteries in various applications.

1.2 MIXED BATTERY ARRAY CONCEPT INTRODUCTION

This thesis develops a new approach to repurposing second-life EV batteries by implementing different EV battery packs into one BESS with a flexible power, communication, and control system. Instead of uniformed battery pack installation, MBA integrates battery packs from various auto manufacturers, model, model year, chemistry type, configuration, and SOH into a large-scale, centralized-controlled, and low-cost stationary energy storage system. The proposed MBA architecture will increase the opportunities for EV batteries in second-life applications, overcome the differences in EV

battery pack design, and increase battery supply by diverting recycling EV batteries to second-life applications for the urgent battery energy storage market.

The key innovation from this research for the second-life EV batteries application is the mixed battery pack architecture. While existing academic and commercial projects focus on using the same type of battery for the entire battery system, a mixed battery array allows second-life EV batteries from different vehicle manufacturers, models, and model years to be integrated into the same system. This approach significantly improves the EV battery reuse rate after their first life. Additionally, this research project focuses on pack-level integration, which reduces the complexity of disassembling and regrouping the battery modules to form the battery system.Research Statement

In light of the burgeoning interest in the second-life applications of EV batteries and understanding the EV battery system integration process, this research aims to propel the MBA concept forward by evaluating and comparing four major BESS design options, including battery pack evaluation, AC and DC-coupled power structure comparison, Battery Management System (BMS) and Energy Management System (EMS) integration evaluation, and thermal management system comparison.

- Battery pack SOH analysis and installation requirements: This study evaluated the initial SOH condition of the EV battery packs, focusing on battery pack usable capacity, energy efficiency, voltage balance conditions, and thermal response. It also aims to study the installation requirements for each battery pack, which defines the battery pack integration requirements in the MBA environment.
- Battery pack interconnection method comparison: This part of the research compares DC and AC-couped PCS for battery pack interconnection methods. The comparison aims to provide insights into the energy efficiency, complexity, and scalability between the two approaches. The selected coupling method must provide a wide range of battery pack voltage adaptability and flexibility to add and remove battery packs quickly.
- BMS comparison study: This study compares OEM and third-party BMS for reusability, accessibility, and reliability. This study aims to understand the purpose of the BMS in the EV battery pack and compare the advantages and disadvantages between the OEM and third-party BMS. Also, demonstrate the OEM BMS replacement process for a third-party BMS.

- Thermal Management System Requirements: This part of the research reviews three thermal management systems available for a BESS; however, the MBA system might not be suitable for all solutions due to its unique integration and operation requirements. Hence, this research project explores the advantages and limitations of each thermal management solution and provides recommendations based on the power requirements of the MBA system.

In addition, this research project built a demonstration and piloted an MBA unit to verify the selected design option and tested battery pack performance under the constructed MBA system. Hence, this research project designed, built, and tested a small-scale MBA system to exemplify the practical process of repurposing EV battery packs for BESS.

Moreover, the research will culminate in a detailed demonstration of a single-pack operation managed by an Energy Management System (EMS). This demonstration MBA unit showcased the operational viability of the MBA concept and its potential for future development of control strategies, including advanced signalling for grid support functions. By aligning practical demonstrations with theoretical research, this project contributes substantively to the domain of EV battery repurposing, offering scalable solutions for energy storage that leverage the untapped potential of second-life batteries. This endeavour not only addresses the immediate technical challenges but also paves the way for innovative control strategies that can significantly enhance grid support applications in the future.

2 LITERATURE REVIEW

Several commercial pilot projects led by EV manufacturers and academic research studies have previously explored the concept of EV battery repurposing, but on a smaller scale or in simulation. EV manufacturers such as BMW and Nissan have already demonstrated the possibility of repurposing their EV battery pack for BESS on a commercial scale [10], [11]. In addition, independent BESS developers such as Cactos Energy Storage System and B2U have developed their battery systems using EV packs from Tesla and Nissan [12], [13]. Several recent commercial EV battery second-life projects led by EV manufacturers are reviewed in section 2.1.

Research projects have focused on various aspects of EV battery performance and degradation in the academic field. One experimental research project tested the mixed battery array concept, while another study examined cell-level degradation in second-life EV batteries. Additionally, investigations have been conducted into EV battery pack-level thermal performance and degradation. Furthermore, there are simulation research projects focused on EV battery pack-level degradation under mixed Energy Arbitrage (EA) and Frequency Regulation (FR) signals, advancing second-life EV battery research closer to real-life applications. Lastly, a simulation study comparing different MBA system architectures was published by Bauer et al. 2018. This study analyzed the energy efficiency of various DC-coupled and AC-coupled systems. Bauer et al. suggested that the battery interconnection method can affect the BESS energy efficiency; however, their simulation results only showed less than 2 percent difference between AC-coupled and DC-coupled systems [14]. However, when paralleling multiple packs under the same DC string, the DC-coupled system delivered five percent higher energy efficiency [14]. Hence, Bauer et al. suggested the DC-coupled BESS exhibits the best overall performance based on their sensitivity analysis of battery system reliability during power distributions [14]. The academic research contributions mentioned above are discussed in sections 2.2 to 2.6.

Therefore, the following subsections will review the most recent EV battery performance and application studies in the second-life pertinent to this research project.

2.1 RECENT EV BATTERY REPURPOSING PROJECTS

Several major electric vehicle manufacturers have already developed a few testing projects using their EV battery packs. For instance, a five-year duration battery second-life pilot project joint initiative by Vattenfall, BMW, and Bosch was launched in 2013 [10]. The objective was to understand the aging and storage capabilities of second-life LIBs, and a 2 MW/2.8 MWh energy storage system was developed in Hamburg, Germany, to test the battery energy efficiency and degradation [10]. BMW supplied over 100 EV battery packs from new and retired BMW i3 for this project, of which 32 kWh energy capacity was from the new packs, and approx. 22 kWh was used for the reused packs. Bosch developed the EMS to control the operation of the battery system, which provided reliable energy support for the local electricity grid [10].

Other automakers are also actively investing and exploring opportunities to reuse their EV batteries for stationary energy storage systems. Nissan Motor Corp. and Renault SA are increasing efforts to repurpose old EV batteries and tap surging demand for battery energy storage demand [11], according to Holger and Petroni's business analysis article. In March 2022, an energy storage system composed of 30 new and 48 used Nissan LEAF EV battery packs was installed in Melilla, Spain, to provide a 15-minute emergency backup power supply for a local power plant [15]. Automakers often receive retired EV packs by providing warranty or buy-back options for their customers; for example, Renault offered battery pack rental and lease services to maintain the ownership of their batteries while keeping Renault EVs on the roads. Renault has rented out more than 250,000 EV batteries that will come back for second-life applications in the future; meanwhile, Renault has built several energy storage systems in France, Germany, and the UK with their used and new EV batteries [9] [13]. Renault launched the Advanced Battery Storage (ABS) project at the end of 2018, aiming to create a stationary energy storage system by repurposing EV batteries. The first ABS installation was at the George Besse Renault factory in Douai, France, with a capacity of 4.9 MWh in 2018. A second site in Elverlingsen, Germany, was commissioned at the end of 2022, which included a BESS with 2.9 MWh capacity using 72 new Renault ZOE batteries [16].

Most EV battery repurpose projects are currently being developed by EV manufacturers since they can access a large amount of retired EV batteries more quickly. However, a few

private companies in North America have started to enter the BESS market with second-life EV batteries, such as Moment Energy in BC, Canada, Smartville and B2U Storage Solution in CA, USA. These independent developers have designed or commissioned BESS using repurposed EV batteries. For example, Moment Energy developed a second-life EV battery energy storage system for Vancouver International Airport [17], Smartville published their modular EV battery BESS unit ranging from 100 kW to 100+ MW [18], and B2U is operating a 12 MWh EV battery BESS in California [13].

2.2 MIXED BATTERY ARRAY CONCEPT DEVELOPMENT

Recent academic studies have predominantly focused on introducing the MBA concept, which has enabled some independent developers to integrate a variety of batteries into a BESS. The initial concept-proof projects entailed experimental testing with mixed EV battery modules operated by self-developed BMS and EMS. In a recent study, Thompson explored the EV battery thermal performance, power capability, and energy capacity degradation by applying different operation profiles via different operation power rates, temperature, and depth of discharge (DOD) [19]. Thompson's research only focused on the battery module level and pack level performance analysis; however, more recent projects have presented simulation and analytical results for the pack level and the system level in an MBA system based on Thompson's research findings [19].

Thompson tested five different EV battery modules using protocols suggested by the Pacific Northwest National Labs (PNNL) to evaluate the performance of second-life batteries in relation to grid services [19]. Thompson's research found that repurposed EV battery modules performed well in peak shaving (PS) and FR applications.

For the PS application, Thompson cycled the battery modules for peak shaving applications between 95% SOC to 5% SOC and over 4-hour, 1-hour, and 0.5-hour discharge rates. Thompson's data suggested that the hour rate positively correlates with energy efficiency, meaning battery modules are more energy efficient at lower power rates, which is agreed upon in all tested battery modules, as shown in Table 2.1.

Table 2.1: EV Battery Module Energy Efficiency by Discharge Hour Rate For Peak Shaving [19]

Hour Rate	Manufacturer	Battery	Rate (kW)	Energy Efficiency (%)	Discharge Energy (kWh)	Rated Energy (kWh)
4 hour	LG Chem	Volt	1.5	98.8	6.2	6.0
	Panasonic	Tesla	1.2	94.6	4.0	4.8
	AESC	2012 Leaf	3.8	97.5	13.9	15.0
	AESC	2015 Leaf	0.4	98.0	1.4	1.4
	EnerDel	Moxie+	1.0	98.7	3.8	3.9
1 Hour	LG Chem	Volt	6.0	96.6	5.7	6.0
	Panasonic	Tesla	4.8	87.1	3.4	4.8
	AESC	2012 Leaf	15.0	94.0	11.6	15.0
	AESC	2015 Leaf	1.4	94.7	1.2	1.4
	EnerDel	Moxie+	3.9	96.6	3.6	3.9
0.5 Hour	LG Chem	Volt	2.0	94.4	0.94	1.0[14]
	Panasonic	Tesla	6.0	82.4	2.9	4.8
	AESC	2012 Leaf	30.0	88.4	7.8	15.0
	AESC	2015 Leaf	3.0	92.3	0.7	1.4
	EnerDel	Moxie+	7.8	95.8	2.7	3.9

DC energy efficiency for the Tesla battery module increased from 82.4% to 94.6% when the hour rate increased from 0.5 to 4 hours via the discharge power was decreased. Similarly, the discharged energy from a single module was increased from 2.9 kWh to 4.0 kWh as the hour rate was reduced by about four times. In addition, energy efficiency was also affected by battery manufacturing and cell chemistry. Panasonic cells in Tesla had the lowest energy efficiency at a higher hour rate as the cell chemistry was Lithium Nickel-Cobalt-Aluminum Oxide (NCA). Alternatively, LG, AESC and EnerDel had higher energy efficiency because the cell chemistry was Lithium-Nickel-Manganese-Cobalt-Oxide (NMC).

Table 2.2: EV Battery Module Temperature by Discharge Hour Rate For Peak Shaving [19]

Hour Rate	Manufacturer	Battery	Dis. Duration (h)	Dis. Temperature (°C)	Dis. Rest Duration (h)
4 Hour	LG Chem	Volt	4.16	27.3	0.16
	Panasonic	Tesla	3.37	29.7	0.17
	AESC	2012 Leaf	3.65	23.0	0.16
	AESC	2015 Leaf	3.32	29.3	0.16
	EnerDel	Moxie+	3.79	25.8	0.17
1 Hour	LG Chem	Volt	0.95	31.4	0.16
	Panasonic	Tesla	0.72	44.5	1.49
	AESC	2012 Leaf	0.77	36.0	1.97
	AESC	2015 Leaf	0.87	38.7	1.24
	EnerDel	Moxie+	0.92	31.3	0.27
0.5 Hour	LG Chem	Volt	0.47	33.3	0.17
	Panasonic	Tesla	0.48	50.6	2.75
	AESC	2012 Leaf	0.26	39.0	2.37
	AESC	2015 Leaf	0.25	43.3	1.34
	EnerDel	Moxie+	0.34	32.3	0.27

Furthermore, Thompson suggested that the energy efficiency reduction at a lower hour rate was caused by the energy loss to heat generation during high-power cycling. Table 2.2 shows the supporting data of the Tesla module temperature increased from 29.7 °C to 50.6 °C during the discharge process.

The FR testing aims to determine the peak power capability and energy efficiency of the EV battery modules selected in Thompson's project. FR services involve a contracted maximum power value with the grid operator, and the battery system must be able to deliver the contracted maximum power in the agreed time frame. Hence, Thompson's test setup put the test battery modules into 24-hour normalized cycles defined by PNNL and progressively increased the peak power value until the battery failed to complete the 24-hour cycle for the FR application [19]. Given the PNNL test requirements, Thomson's FR test setup is shown in Table 2.3 and energy efficiency and thermal performance results are shown in Table 2.4.

Table 2.3: Test Cycling Power Single Over 24h For Frequency Regulation [19]

Manufacturer	Battery	Peak Power (kW)	Peak Power Equivalent Hour Rate (h)	Lowest SOC in test (%)	24 h Energy Throughput (kWh)	Number Equivalent Cycles by Rated Energy
LG Chem	Volt	2.0	0.50	32.6	14.4	7.2
Panasonic	Tesla	6.0	0.84	5.2	43.5	4.5
AESC	2012 Leaf	30.0	0.46	5.5	215.8	7.2
AESC	2015 Leaf	2.6	0.52	14.2	18.6	6.7
Enerdel	Moxie+	7.8	0.39	25.2	56.0	7.2

Table 2.4: Energy Efficiency Test Results for Frequency Regulation [13]

Manufacturer	Battery	Energy Efficiency (%)	Recharge Factor (%)	Lowest Average Cell Voltage (V)	Highest Temperature (°C)
LG Chem	Volt	97.8	102.2%	3.52	31.3
Panasonic	Tesla	92.9	107.6%	3.22	37.3
AESC	2012 Leaf	95.8	104.4%	3.51	38.0
AESC	2015 Leaf	96.7	103.4%	3.51	34.0
Enerdel	Moxie+	98.0	102.0%	3.07	27.0

The testing results in Tables 2.3 and 2.4 highlight that battery usable energy capacity is crucial in FR applications. As such, the 2012 Leaf module demonstrated superior performance compared to other tested modules, attributed to its highest-rated energy capacity of 15 kWh, as listed in Table 2.1. In comparison, the 2012 Leaf module processed 215.8 kWh of energy over 24 hours, far outstripping the 2015 Leaf module, which only processed 2.6 kWh over 24 hours due to its limited 1.4 kWh energy capacity; thus, the usable capacity significantly impacts the energy throughput in the FR application. However, both modules recorded similar levels of energy efficiency and peak temperatures during the 24-hour testing cycle, as shown in Table 2.4. Thus, Thompson's data suggested that the larger available energy capacity gives a wider operation window for the battery to stay in FR service, and the FR singles relatively required lower hour rate operation compared to the EA singles, which results in higher energy efficiency.

Thompson's study showed that repurposed EV battery modules can be used outside their automotive life. In addition, the NMC cell-based EV batteries perform exceptionally well in second-life applications due to the lower degradation in their first-life operation [19].

2.3 EV BATTERY CELL DEGRADATION IN GRID SERVICES

Another research on EV battery repurposing was conducted by Elliott et al. (2020) [20]. Elliott concentrated on battery cell-level energy degradation and efficiency analysis in EA and FR services. Specifically, Elliott focused on two types of lithium-ion cells for his studies: Lithium Nickel Manganese Cobalt Oxide blended with Lithium Manganese Oxide (NMC+LMO) cells and lithium iron phosphate (LFP) cells. These two batteries are most commonly used in the EV industry. Cell performance evaluation was conducted by tracking energy degradation and energy efficiency at different stages of the testing cycles. Half-cell testing and electrochemical voltage spectroscopy processes were employed during the testing cycles to investigate the origins of lithium plating and the loss of lithium inventory.

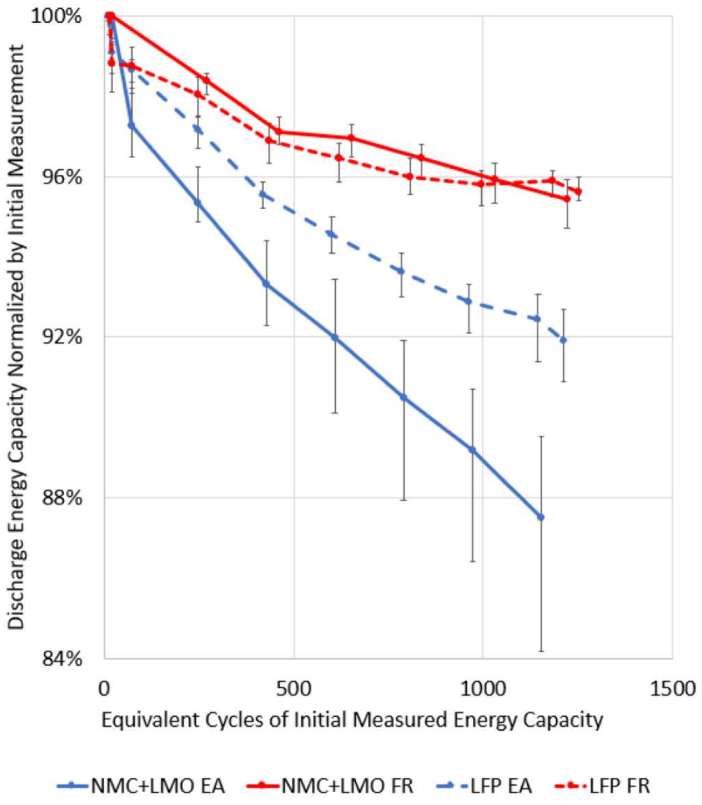

Figure 2.1: NMC+LMO & LFP Cell Discharged Energy Under EA and FR Services [20]

As shown in Figure 2.1, the discharge energy capacity results revealed that cells repurposed for EA applications degraded twice as fast as those used for FR applications, regardless of the cell type. Hence, the more prominent degradation factor was attributed to the deep cycling process, which caused higher lithium plating and accelerated the loss of lithium

inventory [20]. Moreover, NMC + LMO cells degraded twice as quickly as LFP cells due to the higher cut-off voltage and lack of cobalt content in the NMC + LMO cells, leading to faster solid electrolyte interface (SEI) growth and quicker lithium inventory loss.

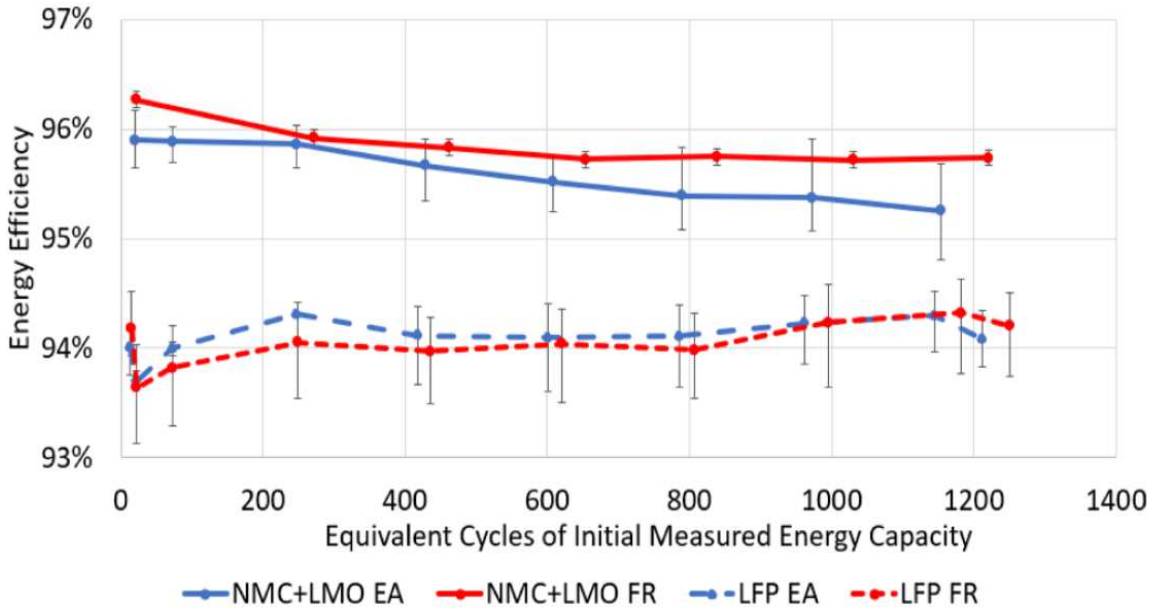

Figure 2.2: Energy Efficiency Comparison Between NMC&LMO Cells Vs LFP Cells [20]

Despite the rapid energy degradation of NMC+LMO cells compared to LFP cells, the former proved higher energy efficiency, as shown in Figure 2.2. Moreover, Elliott observed almost no reduction in energy efficiency in both cells in the first 1200 cycle equivalents, making these cells well suited for energy arbitrage applications [20].

Elliott et al. suggested that the second-life application for an EV battery should based on the cell chemistry. Applications requiring long life cycles and deep cycling would benefit more from LFP cells. Conversely, operation cost or energy-efficiency sensitive services should consider NMC +LMO cells as the primary battery choice [20].

2.4 EV BATTERY GRID SERVICE PERFORMANCE ANALYSIS

White and Swan (2021) published a series of in-depth and targeted studies focusing on the thermal performance analysis of EV battery packs. Specifically, they published two articles on EV battery performance analysis for FR and EA services [21], [22].

In FR services, White et al. selected six EV battery packs with different configurations and chemistries. Each pack was independently operated under the same FR power signal in sequential tests to assess trends in energy efficiency and thermal performance. White et

al.'s data suggested that the battery-positive electrode material plays a significant role in determining its energy efficiency, with NMC cells showing higher energy efficiency than NCA cells. Furthermore, they found that the pack thermal performance during FR service was primarily influenced by the design of the thermal management system, such as whether it used active or passive cooling. Finally, cell chemistry did not significantly impact the overall pack thermal performance [21].

White et al.'s study on EA services involved a comparison of seven EV battery packs, varying in shape, size, chemistry, and thermal management method. They evaluated second-life battery performance based on six metrics: two energy metrics (usable energy capacity and charge-discharge energy efficiency), one volume metric (energy density), and three thermal metrics (average temperature rise, peak temperature rise, and cycle time). Each battery underwent cycling at different power rates to simulate grid energy arbitrage demand profiles. White et al. suggested that EV packs with a liquid cooling design are preferable for EA applications due to the higher cooling capacity, which better supports temperature regulation during the deep cycling process. Additionally, packs with NMC cells demonstrated higher usable energy capacity and energy efficiency than those with NCA cells, making them more suitable for low-cost charging and high-revenue discharging in energy arbitrage [21].

2.5 DEGRADATION OF EV CELLS FOR EA AND FR APPLICATION

Lithium-ion batteries are used in a large range of energy storage applications, which can be divided into two major service types: energy-intensive service applications and power-intensive service applications. Energy-intensive services, such as peak shaving and energy arbitrage, often operate the batteries in a wider SOC range, and the batteries are operated between 20% to 80% SOC or higher. Yet, power-intensive services operate the batteries in a tighter delta SOC band, such as frequency regulation. Hence, Ellis et al.'s study focused on battery cell-level degradation by comparing single-signal services with mixed-signal services [23] and examined how simultaneous service calls could affect battery degradation. Ellis et al. also used two lithium-ion chemistries in this study, NMC and LFP, and they picked three new battery cells from each chemistry.

The research method involved creating simultaneous service profiles by superimposing different proportions of EA and FR service signals over a period of time. This approach

aimed to understand how varying the proportion of these services affects battery degradation over time. Ellis et al. structured the same experimental procedures for NMC and LFP cells to assess capacity degradation, degradation rate, and energy efficiency changes with respect to these two cell chemistries.

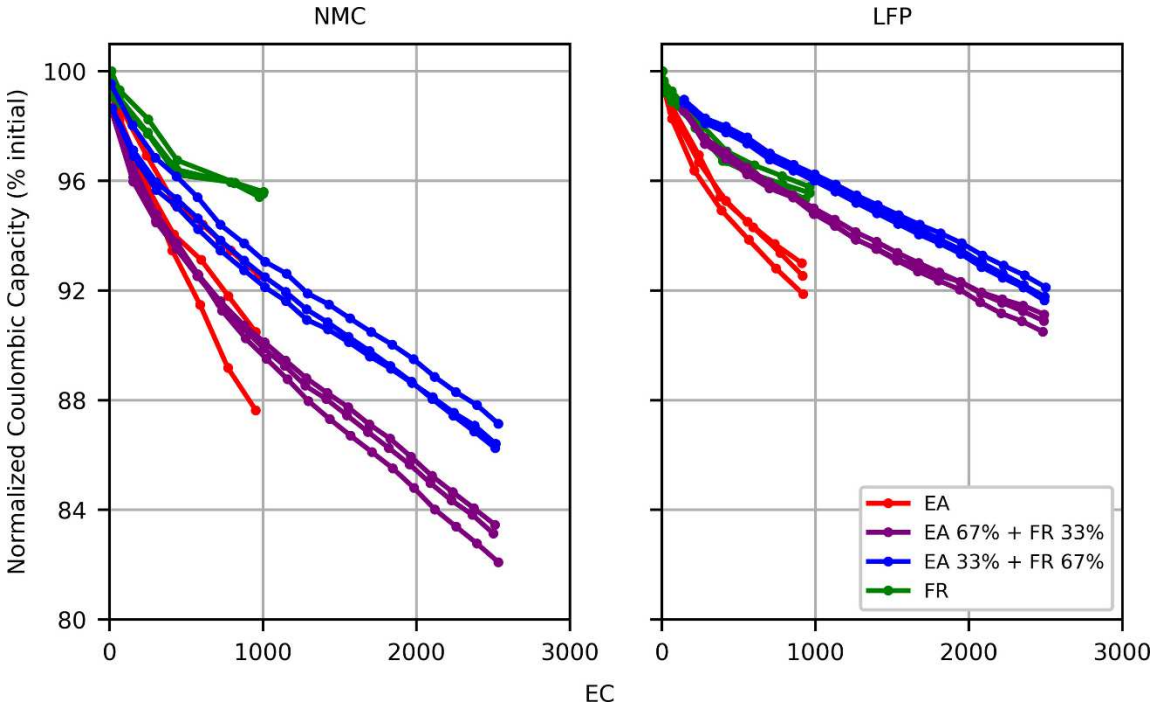

Figure 2.3: NMC and LFP Cell Capacity Degradation Under FR and EA Services [23]

The capacity degradation results are shown in Figure 2.3, where two mixed service signals were compared with EA and FR services for NMA and LFP cells. The EA service caused the highest capacity degradation for both cell chemistries, followed by the two mixed singles and the FR services. Between the two mixed singles, the cells that called for 67% EA services had higher degradation than those with 33% EA services. Hence, the experiment results by Ellis et al. suggested that high DOD applications cause faster capacity degradation than low DOD applications [23].

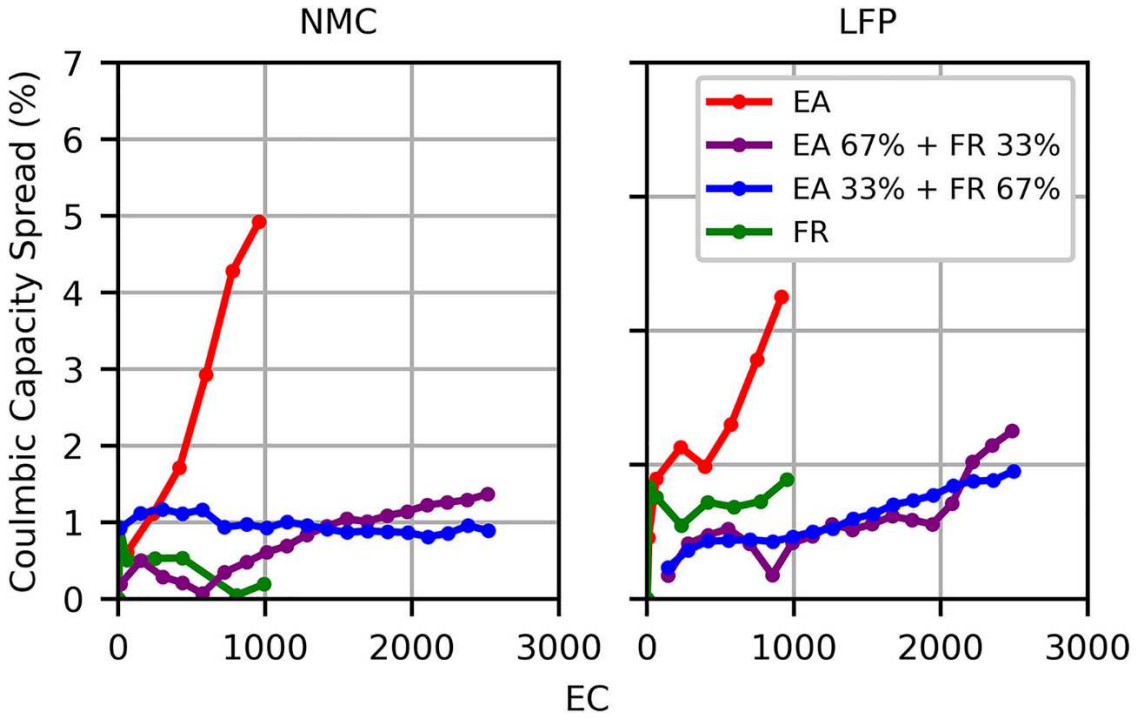

Figure 2.4: NMC & LFP Cell Degradation Rate under EA and FR Services [23].

Furthermore, Ellis et al. observed that the degradation rate becomes constant after 1000 cycles (up to 2500 cycles tested), indicating a diminishing sensitivity to service profiles as batteries age. Additionally, the study found that frequency regulation alone caused the least capacity degradation among the services tested for NMC cells. Yet, LFP cells are less sensitive to service type, as shown in Figure 2.4 [23].

The study concludes that simultaneous servicing of multiple grid services can significantly impact the degradation patterns of LIB, with the mix of services and the battery chemistry playing crucial roles. It suggests that while simultaneous services can increase degradation, understanding these patterns allows for better economic and operational strategies to maximize battery use and longevity. This article advances the understanding of NMC and LFP battery degradation under complex service conditions and provides valuable insights for EV battery degradation expectations in second-life applications. Therefore, optimizing these types of cell usage in grid services would contribute to the future development of EV batteries in energy storage systems.

2.6 MIX BATTERY ARRAY SYSTEM ARCHITECTURE COMPARISON

A research project from the University of Munich in Germany, led by Bauer et al. (2018), proposed a novel method for evaluating EV battery stationary system architectures,

focusing primarily on system-wide energy efficiency simulation over three different power conversion system (PCS) integration methods [14]. This study also incorporated an energy efficiency sensitivity analysis, highlighting distinctions based on integration methods and power distribution within the PCS.

Bauer et al. introduced three PCS integration topologies for new and repurposed EV batteries. The first topology connects a single battery pack to the electricity grid through a DC-DC, DC-AC converter, and a centralized step-up transformer called a DC-coupled system. In contrast, the second topology only employed a DC-AC converter and a step-up transformer for each battery pack, known as an AC-coupled system. The third topology kept the same PCS integration method as the second but increased the system energy capacity by allowing multiple battery packs to be connected in series [14]. Single-line diagrams for these topologies are shown in Figure 2.5 to Figure 2.7.

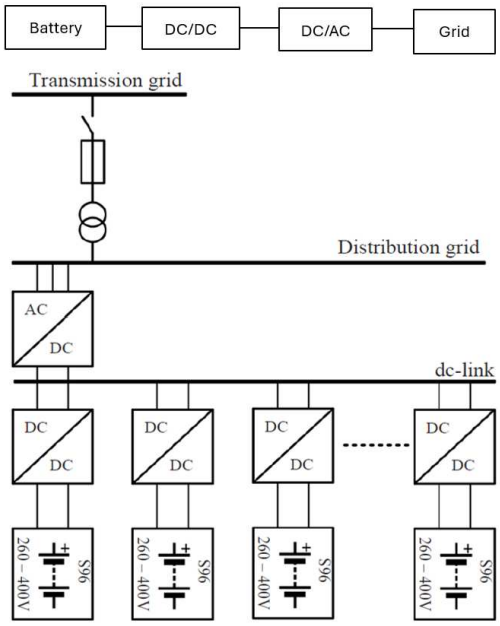

Figure 2.5: Topology 1 - DC-coupled PCS [14]

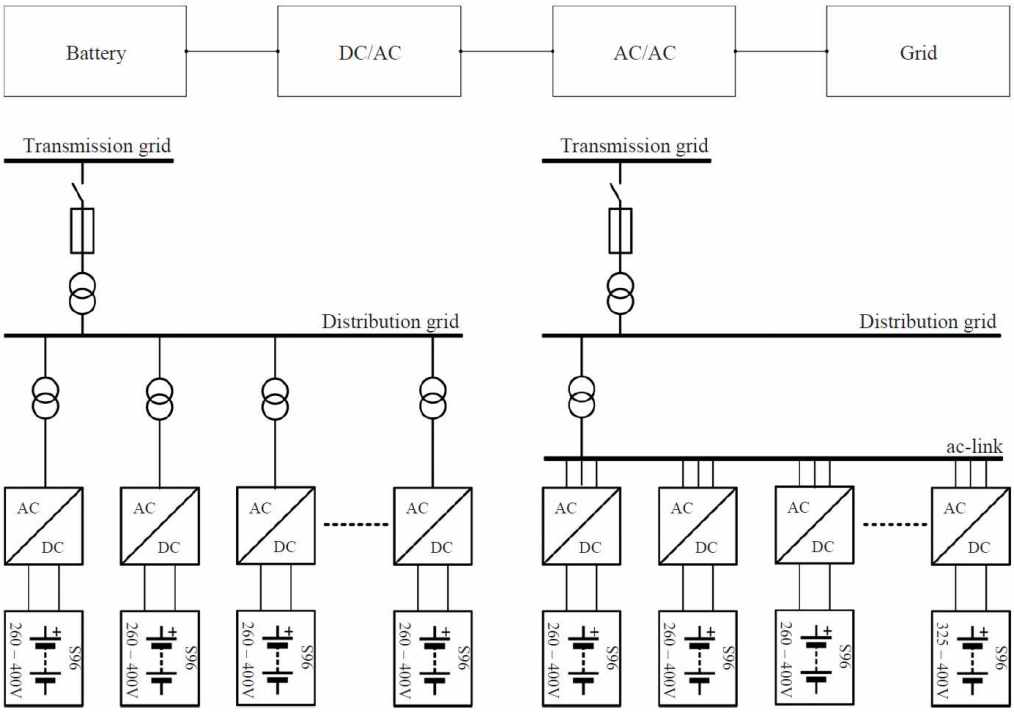

Figure 2.6: Topology 2 - AC-coupled PCS [14]

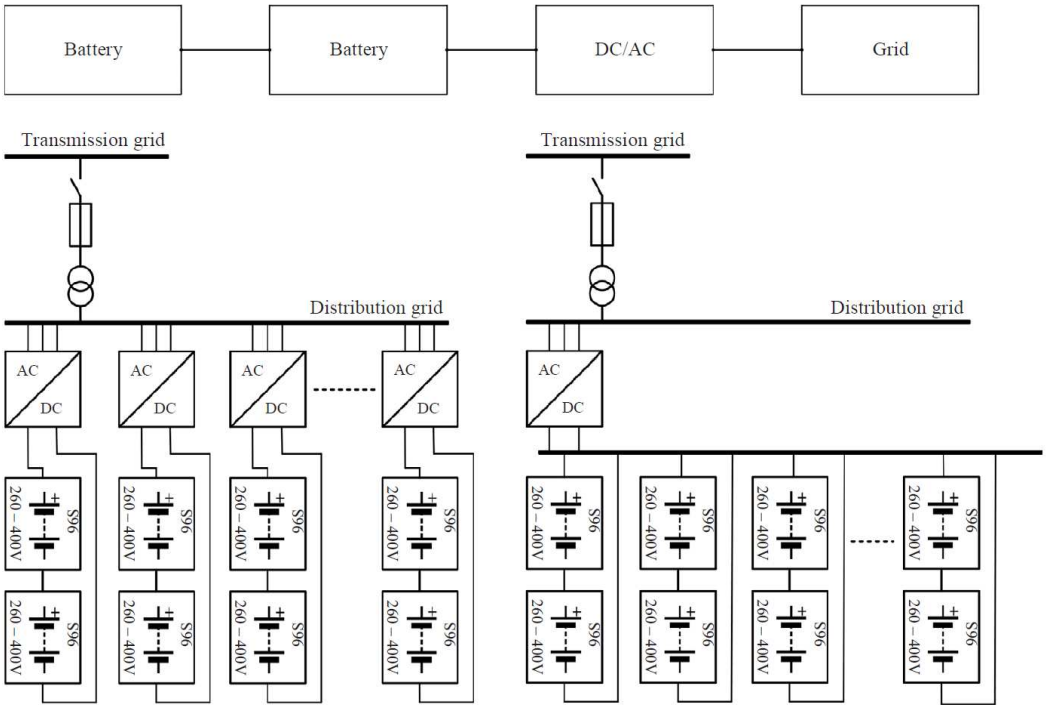

Figure 2.7: Topology 3 - AC-coupled PCS with Dual Battery Packs [14]

Bauer's simulation results indicate only minor energy efficiency differences, ranging from one to two percent, among the three topologies when operated at full power load. However,

Bauer et al. also discovered that the DC-DC converter can improve system energy efficiency in lower power ranges. As such, Bauer's simulation results showed that topology 1 had higher energy efficiency than topology 2 when the PCSs mainly operated in low power load distributions; however, the energy efficiency difference gradually reduced as the power load distribution concentrated to the higher power load [14]. Figure 2.8 shows the topology 1 and 2 energy efficiency comparison between three power load distributions from ±15 kW to ± 200 kW.

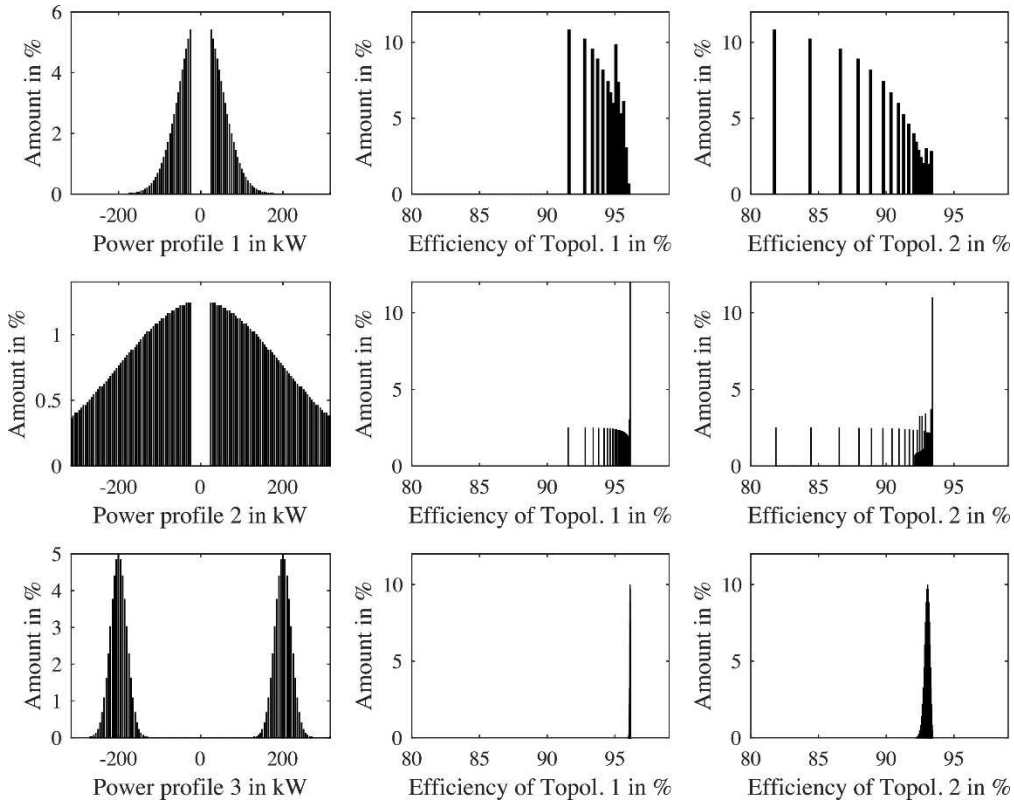

Figure 2.8: Three Power Distribution Vs. PCS Energy Efficiency [14].

Power profile 1 illustrates the PCS power distribution focused on the lower range where the maximum energy efficiency difference between topology 1 and 2 is 6%; however, the maximum energy efficiency difference reduced to 2% when the power distribution approached the rated capacity at 200 kW, as shown in power profile 3 [14].

Finally, considering the system efficiency sensitivity analysis, the DC-coupled system, consisting of a DC-DC converter connected to a centralized DC-AC inverter, showcased a better performance based on the simulation results [14].

2.7 KEY MBA RESEARCH INTEREST POINTS

The research discussed above by Thompson, Elliott, White, and Ellis et al. explored the performance of EV batteries at various levels, including cell, module, and pack. The promising results concerning energy efficiency, capacity degradation, and thermal behaviour in second-life EV batteries underscore the potential of the MBA concept for further academic exploration, especially in MBA system integration using EV battery packs. Therefore, this research project offers the opportunity to verify the mixed battery array energy storage system-level performance concerning the same technical aspect mentioned above. The results provided by the system-level testing provide additional values for MBA solution verification before the larger second-life EV battery energy system roll-out.

Additionally, the simulation results presented by Bauer et al. suggested that the PCS efficiency between DC-coupled and AC-coupled systems is comparable in a traditional BESS, where each battery string has the same energy capacity. However, the MBA system introduces unique challenges by connecting a different battery pack to each PCS, requiring enhanced voltage and connection flexibility, which may necessitate reconsidering the preferred PCS connection approach. Thus, this research project verifies the energy efficiency between DC-coupled and AC-coupled power systems using market-available components and further analyzes the impact on the MBA system performance and reliability from each power system option.

Lastly, this project will explore and assess various design options throughout development to select a viable and efficient EV battery repurposing solution. A significant focus will be on the documentation of the MBA development process and the positive and negative aspects of the four design options. These will provide invaluable real-life insights for enhancing future scaled-up systems and establish a methodological framework for similar initiatives for future projects.

3 MIXED BATTERY ARRAY DESIGN OPTIONS

3.1 EV BATTERY PACK DESIGN STUDY

Modern EV battery packs exhibit a range of design characteristics and specifications. This section explores four different modern EV battery pack designs, examining how variations in battery cell type, module layout, and pack configuration influence their integration into the MBA system.

In the current EV market, most EV battery packs follow a design commonly known as the "Flat pack" or "Floor Pack," where the battery pack integrates into the vehicle floor. Despite this standard approach, numerous variations within the pack design are tailored to meet different vehicle body types, price ranges, travel ranges, and performance levels. Most EV manufacturers utilize two primary pack structure designs: module-to-pack (MTP) and cell-to-pack (CTP); however, several EV manufacturers have already started to explore new pack integration strategies, such as cell-to-chassis (CTC) and module-to-chassis (MTC) to improve pack-level energy density.

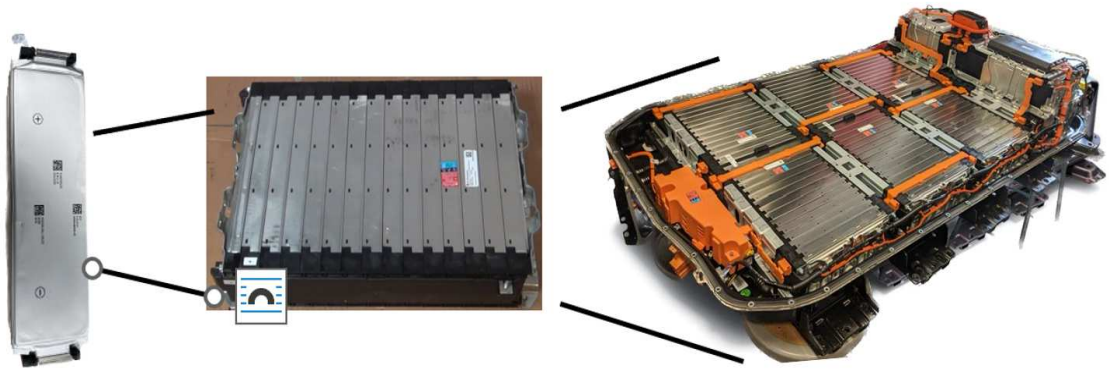

Figure 3.1: Module-to-Pack Design from Chevrolet Bolt EV

The Module-to-Pack (MTP) design adopts a modular approach where cell groups are first assembled into battery modules; these modules are then connected in series to form the pack. This design offers several key advantages: robustness, repairability, and lower voltage levels per module. The structural integrity of the MTP design not only strengthens the vehicle body but also simplifies maintenance and repair processes. Its versatility is particularly beneficial for integrating various vehicle platforms, making it ideal for retrofitting existing models. An example of an MTP-designed EV is the Chevrolet Bolt,

shown in Figure 3.1. From a technical perspective, typical EV battery modules operate within a voltage range of 30 V to 100 V. This range is influenced by factors such as pack-level energy capacity and voltage platform, balancing electrical safety, weight, and replacement costs.

The current EV industry is highly adapted to the MTP design, and it allows for easier repurposed access for second-life applications due to the modular design. As for MBA systems, the MTP design also allows for more accessible pack modifications, such as bypassing damaged modules and reducing the pack service time. Although MTP is a robust design, multiple levels of packaging have reduced the peck-level energy density; given this, EV manufacturers are moving forward to CTP or CTC designs to achieve higher energy density for their vehicles.

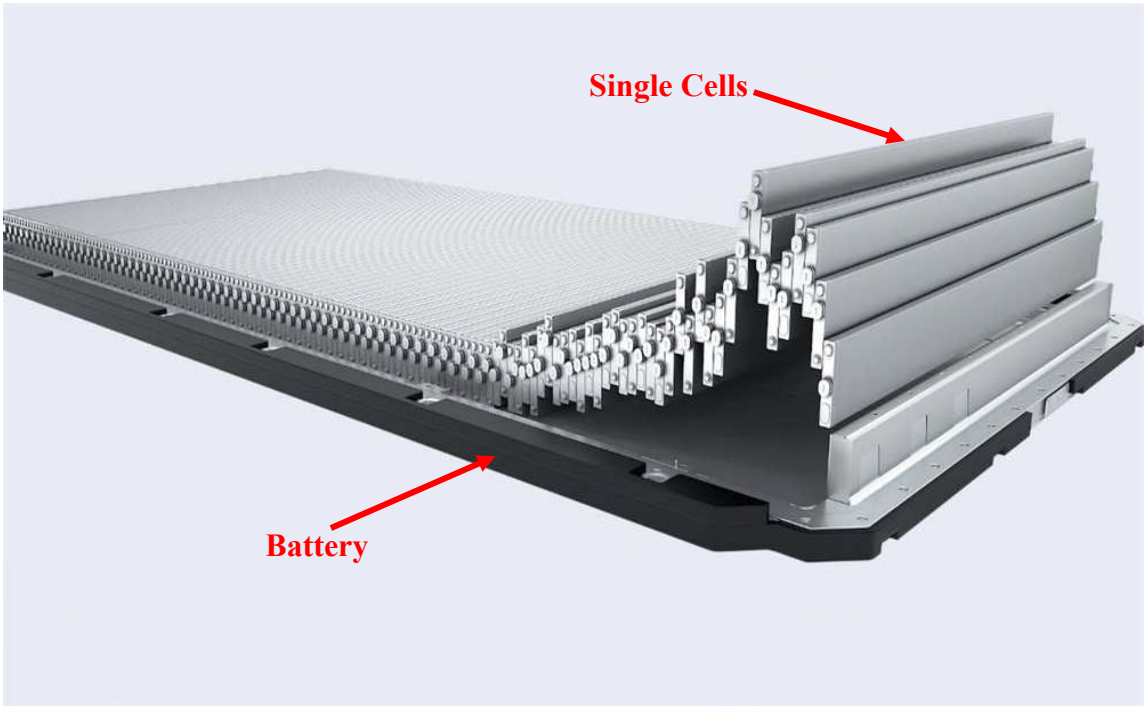

Figure 3.2: BYD Blade Battery Cell-to-Pack Design [24]

The CTP design removes the need for battery modules by integrating cells directly into the pack frame. This approach significantly improves volumetric energy density (Wh/L), reduces component count by about 40%, and increases space volume utilization by 15-50% [25]. These efficiencies can lead to notable cost reductions in battery production. Companies like CATL and BYD have been at the forefront of this technology, utilizing prismatic and pouch cells [26]. Figure 3.2 shows a CTP pack design by BYD.

Consequently, the primary benefits of the CTP design are its higher energy density, reduced production costs, and fewer points of hardware failure. While energy density may not be a critical factor for the MBA system, the advantages of lower production costs and reduced failure points make CTP-designed packs valuable in secondary life applications, where they can help minimize capital and operational expenses. However, the CTP design presents a few notable disadvantages compared to the MTP design in terms of repairability and maintenance voltage. Since the CTP design integrates cells directly into the pack frame, it limits the accessibility for repairing or replacing damaged cells, potentially rendering the entire battery pack unusable for second-life applications. Additionally, the maintenance voltage for a CTP-designed pack corresponds to the full-pack or half-pack voltage if a mid-pack disconnect is included. In contrast, the MTP design allows for maintenance at the module level, significantly lowering safety risks for technicians.

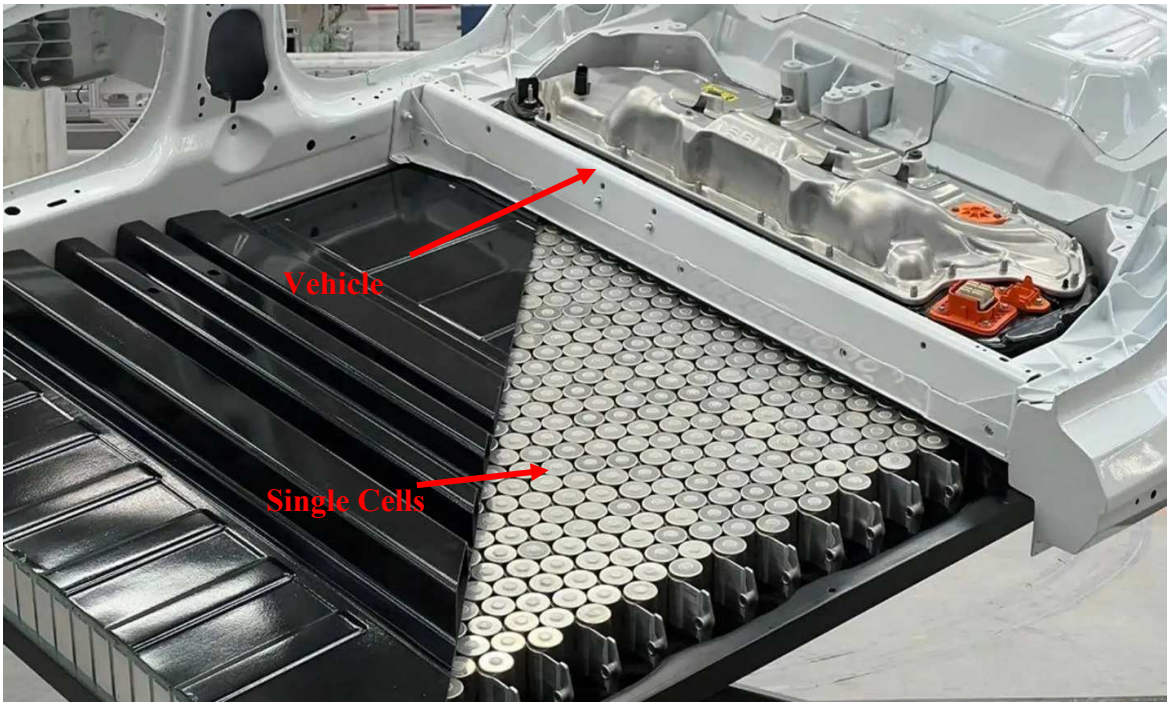

Figure 3.3: Tesla Model Y 4680 Cell-to-Chassis Design [27]

The CTC and MTC designs represent advancements over the CTP and MTP designs, with a key difference being the elimination of a separate battery pack housing. In these designs, battery cells are directly incorporated into the vehicle body using fillers or adhesive materials to absorb vibrations and support structural integrity. In 2022, Tesla introduced a CTC design using their 4680 cylindrical cells, 46 mm in diameter and 80 mm tall, as shown

in Figure 3.3. The primary advantages of CTC and MTC designs include enhanced energy density, streamlined manufacturing processes, and reduced vehicle weight, leading to the use of fewer materials and lower production costs [26].

However, there are concerns about the technical challenges associated with these designs, particularly the replacement, disassembly, and repurposing of the batteries due to the absence of a traditional pack enclosure [26]. Additionally, the filler material used to integrate the cells into the vehicle structure is challenging to remove, complicating the process of accessing or replacing damaged cells without compromising the main body structure. Therefore, battery packs designed with CTC and MTC are not ideal for reuse in second-life applications.

Table 3.1 lists a comparative analysis of the four battery pack designs discussed above.

Table 3.1: Battery Pack Design Comparison

Pack Design	MTP	CTP	MTC	CTC
Maintenance Voltage	30 – 90 V	100 V +	30 – 90 V	100 V +
Accessibility	High	Low	Low	Low
Energy Density	Low	High	High	High
Market Availability	High	High	Low	Low
Reusability Ranking	1	2	3	4

- **Maintenance Voltage** refers to the range of voltage that technicians work with when servicing a battery system, where a lower maintenance voltage enhances safety. Module-based battery packs are advantageous in this regard because they allow for the disconnection of series-connected modules, effectively reducing the maximum voltage across the battery pack to safer levels.

- **Accessibility** refers to how easily technicians can maintain and service the battery system. This includes the processes involved in removing the entire battery pack from the vehicle, accessing specific battery modules or cell groups, and the ability to remove or repair any damaged battery cells or modules. Therefore, the CTC and MTC designs complicate or prevent these tasks, making these types of batteries less desirable for second-life applications.

- **Energy Density** measures the amount of reusable energy that can be stored per unit of battery pack volume, which is important in applications with limited space. A higher

energy density is still preferable for some MBA systems as it allows for more energy storage in a smaller space.

- **Market Availability** reflects the ease of obtaining retired EV batteries of a particular design. This analysis is specific to the timeframe of this research project. Currently, CTP and MTP packs are more prevalent in the EV market, resulting in better availability. However, as more EV manufacturers shift towards CTC and MTC designs to increase energy density, the prevalence of MTP packs is expected to decrease over time.

Considering these factors, this research project has opted to integrate four MTP packs in the MBA demonstration unit, leveraging their market availability and accessibility to facilitate the research objectives. However, two MTP battery packs selected for this project still required significant labour work and excess materials during the repurposing process due to the restricted module design for second-life applications.

Understanding these varying characteristics of EV batteries is crucial for their successful repurposing process to the MBA framework. The diverse pack structure design, electrical layout, cell chemistry, cooling mechanisms, and performance characteristics present unique challenges and opportunities for each battery pack during the MBA system integration process, and these processes are detailed in Chapter 4.1.

3.2 BATTERY PACK INITIAL CONDITION ASSESSMENT

The battery energy storage industry has not yet widely adopted a specific regulatory framework for second-life battery applications; however, there are general principles in the battery energy storage industry for EV battery repurposing requirements. This research project aligns with these principles to prepare the EV battery packs for the demonstration MBA system. Moreover, the project incorporates several established testing procedures from the Renewable Energy Storage Lab (RESL), known for its second-life battery evaluations. These procedures are essential for ensuring the safe handling, storage, testing, and transportation of batteries, and they introduce additional safety measures and evaluation criteria focused on pack-level operations, forming the battery pack initial condition assessment procedure.

The initial condition assessment is designed to enhance the operation safety and evaluate the SOH conditions for potential operational limitations in second-life applications. As

such, the initial condition assessment includes a series of safety and performance testing procedures and a pack pre-conditioning procedure before commissioning the battery for the MBA operation environment. The testing procedure follows a specific sequence, where progression to the next step depends on the results obtained at the current step:

- Pack Structure Damage Check
- Pack Voltage at Receiving
- Internal resistance check
- Cell-level OCV measurements
- BMS communication check
- Self-discharge check

If the battery pack is retired due to an accident, a structural damage check will evaluate if the battery pack is still suitable for pack-level reuse applications via the MBA system. If structural damage is found, the battery pack often will not be suitable for pack-level reuse due to potential electrical damage and liquid coolant leakage issues. Hence, these battery pack types are unsuitable for the MBA system. However, they could still be valuable for other second-life repurposing applications at the module or cell group levels.

Suppose a cell group (or individual cell) fails during the testing process, and it can be safely bypassed without posing additional safety risks to the operator or the overall pack. In that case, the failed cell group will be bypassed from the battery pack (or extracted if necessary), and the testing process will proceed to the next step. This testing sequence evaluates the overall safety of the battery pack to determine its operational feasibility before allowing any current flow through the battery pack.

Upon successfully passing the initial condition assessment, the battery pack underwent a pre-conditioning procedure to prepare it for grid storage operations. This pre-conditioning procedure includes 3 low-power cycling processes, via a 4-hour rate or longer, to adjust the battery to the desired voltage, balance cell group voltage differences, and determine the pack SOH at the start of its second life. This pre-conditioning process is inspired by an existing battery testing process from RESL via Reference Performance Testing (RPT), initially for cell-level performance testing. Chapter 4.2 details the initial condition assessment process of two battery packs installed in this project. Chapter 4.5 outlines the RPT process and the pre-conditioning results for all battery packs installed in the demonstration MBA system.

3.3 DC-COUPLED VERSUS AC-COUPLED POWER ARCHITECTURE

The power architecture design is essential for accommodating various EV batteries in an MBA system. The two power architecture design options discussed below facilitate bi-directional power conversion between AC and DC during battery cycling. Still, each power conversion system utilizes distinct hardware, wiring configurations, and communication setups. Consequently, their DC voltage ranges, scalability and energy efficiency vary depending on the power architecture setups. The first design option features a DC-coupled power architecture, where the battery packs are grouped on the DC side of the power conversion system before being converted to the same AC voltage to feed to the grid. The second one uses the AC-coupled battery pack design. Despite these differences, both PCS convert different battery voltages to the nominal local AC voltages before merging onto the electrical grid.

The comparative study between DC-coupled and AC-coupled systems scrutinizes the variations in flexibility, wiring complexity, and energy efficiency since each coupling method brings different advantages and potential risks. The MBA power conversion system requires high flexibility to accommodate various battery packs with different DC voltage ranges and low wiring complexity to allow system capacity expansion or reduction. In addition, the PCS must maintain an acceptable energy efficiency during operation. According to the US Energy Information Administration (EIA), the average BESS roundtrip energy efficiency is 82% [28]. Based on the existing system installed in the US, EIA stated that most of the energy lost is caused by battery cell internal resistance, auxiliary system energy consumption, and wiring loss [28].

3.3.1 **DC-coupled Power Architecture**

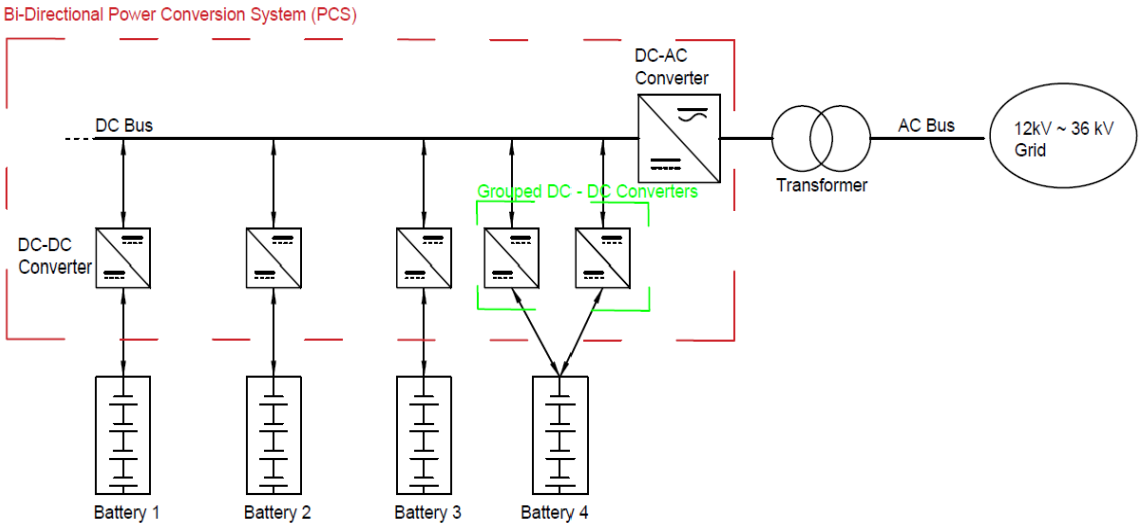

Figure 3.4: DC-coupled Battery System Single Line Diagram (SLD)

The DC-coupled power architecture, illustrated in Figure 3.4, utilizes modular DC-DC converters to regulate the DC bus voltage before connecting to a centralized DC-AC converter; therefore, the DC-coupled system incorporates both DC-DC and DC-AC converters within the PCS, as marked in the red box. Accordingly, battery packs with different voltage ranges are parallel connected after the DC-DC converters, demonstrated by batteries 1- 3 in Figure 3.4. Additionally, DC-DC converters can also be parallel-connected on the battery side to achieve a higher power rating if the battery pack can deliver, as highlighted in the green box. This approach allows for a flexible DC-DC converter sizing opportunity for each battery pack, avoiding DC-DC converter oversizing or power curtailment. Regardless of the battery coupling point, the centralized DC-AC converter only needs to work with one standard DC voltage from the DC Bus, ensuring a consistent energy efficiency performance.

The DC-DC converters have a wide DC voltage range on the battery side, allowing for various battery pack voltages within the MBA system. A suitable example of such a DC-DC converter is the Sinexcel PDS1-45M DC-DC, operating between 250 to 830 Vdc on the battery side and capable of outputting the DC voltage up to 830 Vdc on the DC bus side [29]. Each DC-DC module is rated for 45 kW with a peak efficiency of 99.4% [29]. Following this, the centralized DC-AC converter converts the DC bus voltage into 480 Vac. Hence, the centralized PCS must have sufficient power capacity to accept the sum of the power output from all preceding DC-DC converts. Sinexcel PWS1-500KTL-NA can

support up to 6 DC-DC modules in this setup, which has a 500 kW power capacity and 600 to 900 Vdc voltage range. This centralized DC-AC converter has a peak efficiency of 97% at maximum power capacity [30], as shown in Figure 3.5. Thus, the DC-coupled power architecture has four components of energy losses: battery energy efficiency, DC-DC and DC-AC converter power efficiency, and auxiliary components efficiency, which include wiring loss and transformer efficiency.

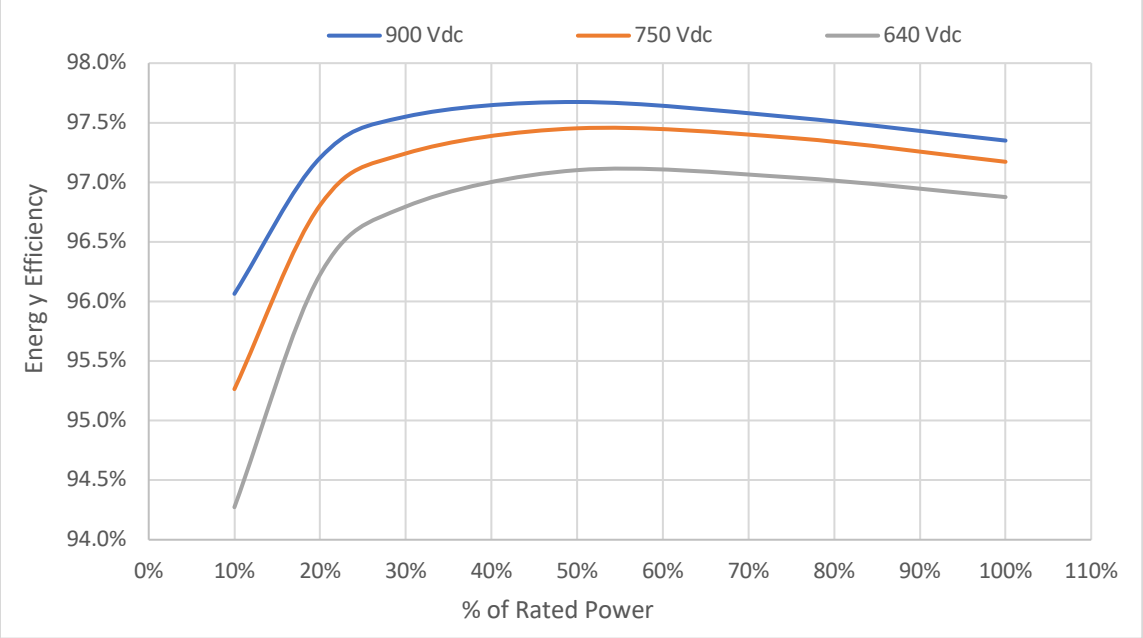

Figure 3.5: Sinexcel PWS1-500K Power Efficiency [30]

The power efficiency of the modular DC-DC converter peaks at the upper voltage level while operating close to the rated power, and it is less efficient when operating at the lower voltage due to the higher current input needed to maintain the constant power output. However, the centralized DC-AC converter demonstrated comparable power efficiency regardless of the output power once operated above 30% of the rated power, and the efficiency disparity at different voltage levels is less than 2%, rendering the overall impact on system performance almost insignificant, as shown in Figure 3.6.

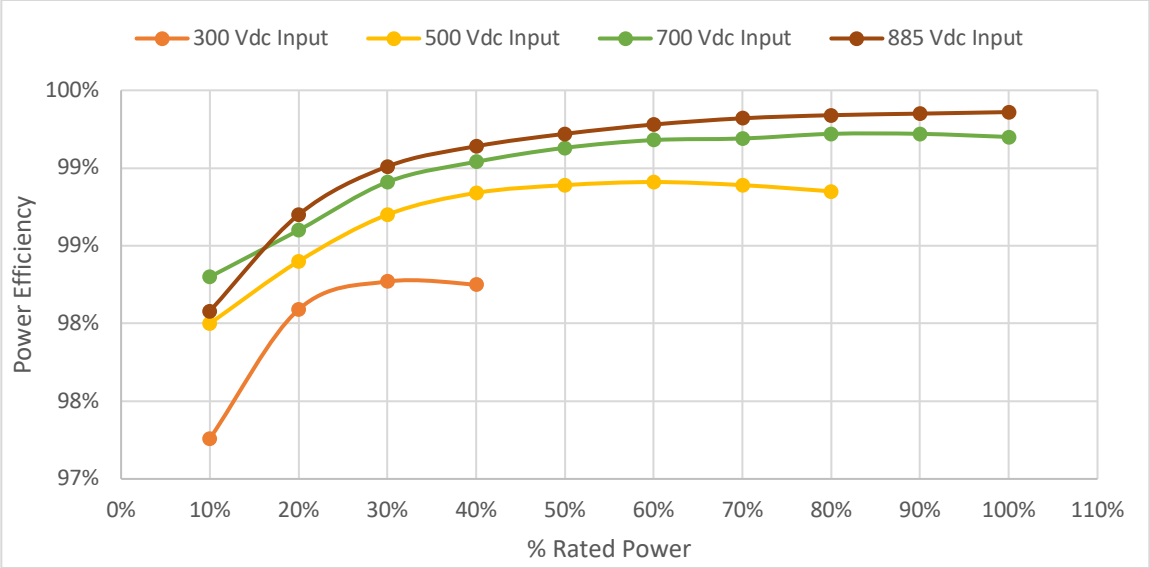

Figure 3.6: Sinexcel PDS1-45M DC-DC Power Efficiency [30]

Notably, both DC-DC and DC-AC converters have a significant power efficiency decrease below 20% of rated power. This decline was anticipated due to the auxiliary components consuming a fixed power load irrespective of the output power ratings, thereby driving down the overall power efficiency of the converter as the output power. The roundtrip efficiency of the DC-coupled interconnection system is calculated as follows:

Equation: 3-1

$$\eta_{DC-Coupled\ System} = \Sigma\eta_{Battery} \times \Sigma\eta_{DC-DC} \times \eta_{DC-AC} \times \Sigma\eta_{Auxiliary}$$

For reference purposes, assuming the battery pack used for the DC-coupled system is from the Tesla Model 3, which utilizes Panasonic 2170 cells, the battery DC energy efficiency will be 94.6% [17], as shown in Figure 2.1. Given the setup for the DC-coupled system, a suitable transformer is the 500 kVa unit from HPS Sentinel, catalogue number SG3A0500PK, which has a peak efficiency of 99.14%. Considering wiring losses and transformer efficiency, the auxiliary component efficiency is estimated to be 99%. Therefore, the expected energy efficiency of the DC-coupled power system is calculated as follows:

$$\eta_{DC-Coupled\ System} = 94.6\% \times 99.2\% \times 97\% \times 99\% = \mathbf{90.1}\%$$

3.3.2 AC-coupled Power Architecture

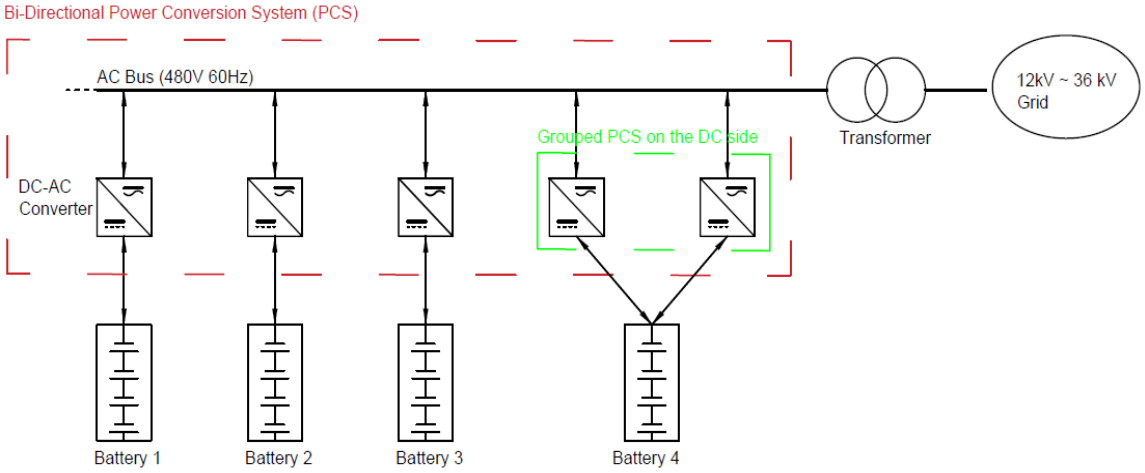

Figure 3.7: AC-coupled Battery System SLD

In the AC-coupled power architecture, as shown in Figure 3.7, DC-DC converters are not needed if the DC-AC converters provide a sufficient DC voltage range for the connected battery; thus, the PCS system only includes the DC-AC converters. Since the targeted EV battery packs for MBA systems have an expected energy capacity between 40 to 100 kWh (via typical passenger EV battery pack capacity), it is sensible for the AC-coupled system to employ modular DC-AC converters with power capacities ranging from 30 kW to 50 kW. This sizing strategy allows the DC-AC converters to provide a 1- to 4-hour discharge power rate from each battery pack while preventing oversizing the DC-AC converters. Figure 3.6 illustrates these AC-coupled DC-AC converters within the PCS, highlighted in the red box; meanwhile, the DC-AC converters can also be paralleled on the DC side to accommodate higher power outputs if the battery pack allows, as highlighted in the green box. When multiple DC-AC converters are grouped on the DC side, a master converter unit sets up internal communication links and manages their operations. Secondary units follow the control signals from the master unit to synchronize their actions. Consequently, the EMS only communicates with the master unit to control the entire array of converters. A representative DC-AC converter for the AC-coupled MBA system is the Sinexcel PWS2-30P-NA modular DC-AC converter. Each PWS2-30P-NA unit delivers a power output of 30 kW, operates within a DC voltage range of 150 to 750 V, and achieves a maximum efficiency of 96.5%. Moreover, this DC-AC converter supports paralleling up to ten units to attain a combined power output of 300 kW. Figure 3.8 shows the power

efficiency curve of the Sinexcel PWS2-30P-NA at different voltage levels according to the manufacturer.

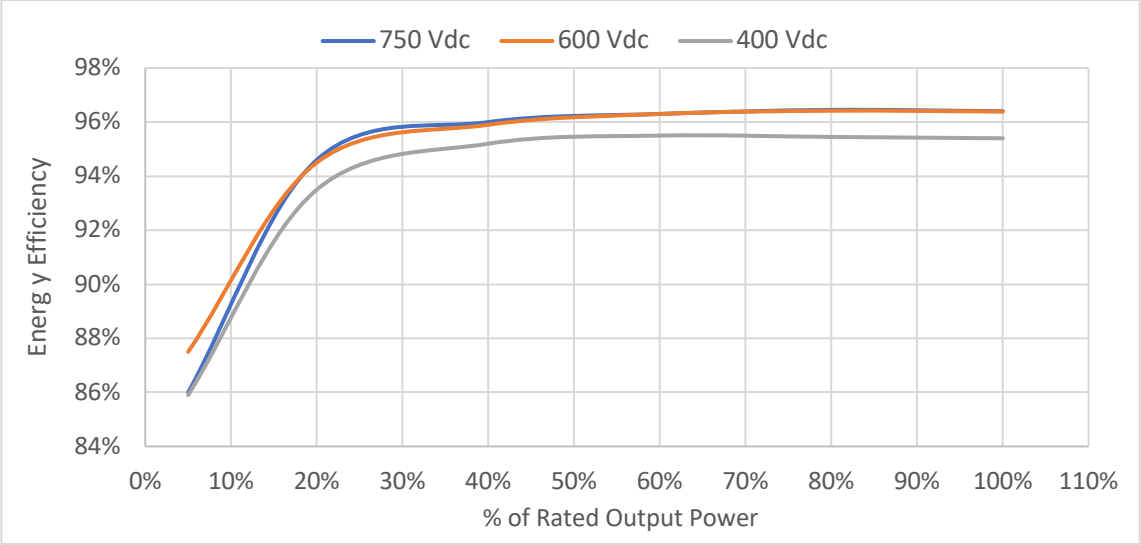

Figure 3.8: Sinexcel PWS2-30K Power Efficiency [30]

As shown in Figure 3.8, the power efficiency of the Sinexcel 30 kW DC-AC converter remains stable at 96% once the percentage power output is above 40%; however, the energy efficiency quickly drops below 90% when operating below 20% rated power. The efficiency drop below 20% rated power is also caused by the auxiliary component power consumption. Furthermore, lower operating voltages can also decrease energy efficiency by about 1.5% compared to higher voltages, potentially impacting overall system efficiency in the long term. Based on the power efficiency curve, the EMS should dynamically manage the power distributions among the DC-AC converters to avoid operating DC-AC units below the 20% power output threshold. This can be achieved by indexing and adjusting the number of active batteries and converters according to the power demands, ensuring that all units operate above 20% of their rated capacity at all times.

The energy efficiency between the DC-coupled and AC-coupled systems is expected to vary as the hardware used to achieve the connection differs. The energy efficiency for the AC-coupled system is calculated as follows:

Equation: 3-2

$$\eta_{AC-Coupled\ System} = \Sigma\eta_{Battery} \times \Sigma\eta_{DC-AC} \times \Sigma\eta_{Auxiliary}$$

Considering the same assumptions as for the DC-coupled system, where the battery efficiency is 94.6% from the Tesla Model 3 [17], and the auxiliary energy efficiency is 99%, including wiring losses and transformer efficiency, the energy efficiency of the AC-coupled system is calculated as follows:

$$\eta_{AC-Coupled\ System} = 94.6\% \times 96.4\% \times 99\% = \mathbf{90.3}\%$$

When the PCS operates above the 20% rate power capacity, the AC-coupled system should have higher energy efficiency compared to the DC-coupled system due to the energy loss from the DC-DC converters being eliminated. However, if the PCS system constantly operated below the 20% rate power rating, the DC-coupled system could be more efficient because the power efficiency is higher for centralized DC-AC converters at a lower power rate compared to the modular DC-AC converters, as shown in Figure 3.5 and 3.6. However, according to simulation results from Bauer et al. [14], the difference between the DC-coupled and AC-coupled PCS energy efficiency is minimal, at approximately 1%. This negligible difference suggests that energy efficiency alone is not a decisive factor in choosing between these systems for an MBA system.

3.3.3 DC-coupled versus AC-coupled Power Architecture

In addition to comparing energy efficiency between DC and AC-coupled power architectures, operation flexibility is also considered to accommodate various battery packs, particularly concerning converter operation limits such as DC voltage range and power capabilities. Moreover, the PCS must offer enhanced scalability to dynamically adjust system power capacity in response to evolving energy demand requirements. Finally, high reliability is crucial for MBA systems participating in grid-tie applications.

The DC-coupled power architecture facilitates quick integration by adding or removing active DC-DC converters as battery packs are connected or disconnected. DC-DC converters typically operate across a wider DC voltage range, accommodating most EV batteries; thus, a single type of DC-DC converter could potentially support the entire MBA system. However, the capacity of the DC-coupled system is constrained by the size of the centralized DC-AC converters, potentially resulting in power curtailments if too many batteries are connected. Hence, scaling up the DC-coupled system incurs higher capital costs due to the expensive centralized DC-AC converters. Furthermore, the centralized DC-AC converter introduces a single-point failure to the MBA system, affecting all connected

batteries until the DC-AC converter is replaced. Additionally, the DC-DC converters also need to establish constant communication with the EMS to support the energy demand from the DC-AC converter, complicating system operations since no commercially available DC-AC converters currently support autonomous power distribution downstream; hence, the EMS must manage it directly. Lastly, additional electrical components like wires, DC combiner boxes, and breakers are also necessary to facilitate DC bus connections in the DC-coupled architecture.

Conversely, the AC-coupled power architecture also supports quick integration by adding or removing modular DC-AC converters. However, DC-AC converters typically offer a narrower DC voltage range compared to DC-DC converters, which may necessitate using different models to support various battery packs at different operating voltages. Unlike the DC-coupled architecture, the AC-coupled system does not face capacity limitations from modular DC-AC converters, although the isolation transformers still restrict the overall system capacity downstream. The modular design of the AC-coupled system avoids the single-point failure risk inherent in centralized converters, significantly enhancing system redundancy and reliability. Moreover, the costs for repairing and replacing modular converters are lower, facilitating easier scalability for the MBA system. Additionally, linking multiple DC-AC converters to increase power capability does not require extra communication setup, reducing control complexity for the EMS and improving communication reliability. Thus, the AC-coupled system, with its modular DC-AC converter design, enhances system reliability and simplifies system expansions or reductions as needed.

Given the comparison study above, the AC-coupled PCS is selected for this project, and two different DC-AC converters with different operating DC voltage ranges are selected to address the voltage range limitation issues. Details on the integration process of the AC-coupled PCS are provided in Section 4.3.2.

Table 3.2 summarizes the comparison study between the DC-coupled and AC-coupled power architecture.

Table 3.2: DC-coupled System Vs. AC-coupled System

Connection Type	Pros	Cons
DC-Couple	✓ Facilitate easy system size adjustments. ✓ Wide DC voltage range. ✓ Higher energy efficiency at lower power output levels.	X Maximum DC power is limited by the DC-AC converter size. X The centralized DC-AC converter is a single point of failure. X DC-DC converter and EMS require communication systems. X Additional parts are needed, such as via wires, DC bus and breakers.
AC-Couple	✓ Simplified system layout. ✓ Enhanced capacity scalability. ✓ Higher redundancies. ✓ Simplified communication system.	X Limited DC voltage range.

3.3.4 Battery DC Voltage Range

In order to integrate EV battery packs into the MBA system, this research project must address the challenge of accommodating a broad spectrum of battery voltages, which extend from 150 to 1200 Vdc. The bestselling passenger EV in 2023, via Tesla Model Y and Chevrolet Bolt [31], operates on a 400 Vdc battery pack platform, which has a fully charged pack voltage of 403.2 V. This 400 V platform offers a good balance between daily range, power capabilities, and service safety, albeit at the expense of charging speed due to the limitations of the lower voltage level at around 260 Vdc.

Hence, the EV industry is progressively moving towards higher voltage platforms to satisfy the increasing demand for faster charging. The new tranche of passenger EVs, such as the Genesis GV60 and Porsche Mission E, utilize 800 to 900 Vdc platforms to deliver higher performance and provide faster charging capabilities. This upcoming shift to higher voltage platforms promises to improve energy efficiency and addresses the critical demand for rapid charging without compromising safety or practicality. However, this process might take longer for the EV industry due to the low-voltage requirements from the drive motors at the low speed, in which stepping down the 1200 V to as low as 20 V for low-speed rotations could be challenging for the electric motors.

Hence, A versatile PCS is vital to accommodate this wide range of voltages, from the current 400 V to 800 V battery pack platform. Given this, this research project employs

two modular power converters: the Sinexcel PWS2-30P operates between 150 to 750 Vdc, and the Oztek RS40 operates between 350 to 800 Vdc, ensuring support for both existing lower-voltage battery packs and anticipating the integration of higher-voltage systems. This strategic approach enables efficient power transition from diverse battery voltages to a unified AC bus voltage, paving the way for more adaptable and future-proof grid integration of EV battery packs.

3.4 BMS AND EMS INTEGRATION

The Battery management system monitors the battery status at all times during vehicle operation. Similarly, a BMS is also required in second-life applications for the same reason. However, the BMS integration does influence the second-life battery system performance and lifespan over time, due to cell-group voltage limitation and balancing settings. For instance, the cell-group voltage limitation set for EV applications might differ from that for energy storage applications. Expanding the cell-group voltage limitation could increase the discharge energy capacity of the battery pack but also accelerate the capacity degradation rate over time, according to Ellis et al.[23].

The communication architecture of the battery pack does not change from its original application, for which EV also requires a BMS. This BMS monitors battery cell group voltage, temperature, pack voltage and current for safety purposes and reports its active status to the vehicle control system through a messaging system via CANBUS [19]. In a BESS, BMS reports its active status to an EMS that controls the system operation. BMS also plays a crucial role in managing cell group voltage balance, which keeps the cell group voltage delta within a defined range. Naturally, battery cell group voltages should be consistent, as they receive the same current due to the series connections. However, some cells may charge or discharge differently due to manufacturing inconsistencies. Hence, minor discrepancies in cell group voltages can accumulate without a BMS active balancing process, gradually reducing the usable capacity and narrowing the operating voltage range [32]. No regulations or standards currently regulate the acceptable maximum voltage difference between cell groups. Yet, a common practice in the battery industry for an acceptable voltage delta is 5 mV for static voltage and 10 mV for dynamic voltage [33]. Other alarms, such as cell group under voltage, temperature over protection limited, current over the limit, and communication loss, are all captured by BMS and reported back to EMS

to ensure operation safety. In normal operations, EMS receives control signals from the electricity grid to execute charge or discharge actions from the AC side and adjust the operation limits based on the feedback from the BMS on the DC side. Table 3.3 shows a list of selected BMS data reported to the EMS for this research project.

Table 3.3: List of Data Reported by the BMS.

Data Transmitted	**Description**
Rolling Counter	A variable increment value is sent to the EMS to check the BMS live status.
Error Present	A 0/1 check value reports if the BMS detects any fault.
Balancing Active	A 0/1 check value reports if cell group balancing is active.
Pack Voltage (V)	BMS reports the instant battery pack voltage readings
Pack Current (A)	BMS reports the DC current readings to the EMS
Pack Power (kW)	The product of pack voltage and current.
Temperature Status (°C)	Maximum, mean, and minimum temperature measurements.
Temperature Status ID	The sensor ID reported the critical temperature status.
Voltage Status (V)	Maximum, mean, and minimum voltage measurements.
Voltage Status ID	Reports Cell group ID at the Max and Min values.
Temperatures (°C)	All temperature readings.
Cell group Voltage (V)	All cell group voltage readings.

3.4.1 OEM BMS

Most EV manufacturers integrate the Original Equipment Manufacturer (OEM) BMS within the battery pack to monitor the battery conditions during vehicle use; therefore, repurposed EV batteries typically come equipped with an OEM BMS. When the vehicle is on the road, the OEM BMS is responsible for reporting the battery status, such as voltage and temperature status, SOC, charge and discharge current, and any fault detected, to the onboard vehicle computer. However, when the vehicle is in the charging mode, the OEM BMS also communicates with the charge controller to manage the charging process at different stages, during which the BMS dictates the charging power based on the battery conditions. The charging process varies depending on the manufacturer; however, the current EV industry-standard charging process includes 2 main steps, which are separated

by the battery SOC and divided between a fast-charging step and a slow charging step. The OEM BMS allows the battery to be charged at the maximum capacity that the charging station can deliver until the battery SOC reaches about 80% SOC via the fast-charging step, then switch to a slower charging process to top up the SOC to 100% via the slow charging step. During the charging process, the BMS could adjust the charging power based on the battery pack temperature at any time to ensure vehicle safety and energy efficiency. Hence, the EV BMS shares many common duties and features with the BMS used for BESS; therefore, they can be repurposed for second-life applications.

The OEM BMS gathers data similar to what is delineated in Table 3.3, albeit with slight modifications to suit each EV manufacturer's specific battery operational thresholds. Therefore, EV manufacturers often develop their BMS in-house to balance cost-efficiency against the functionality of the system. Thus, the bespoke nature of the OEM BMS, conceptualized, developed, and rigorously tested by the EV maker, guarantees superior integration with the installed vehicle. Furthermore, the OEM BMS encompasses optimal wiring arrangements, steadfast communication, and efficient space management by the EV manufacturer. As a result, the OEM BMS comes pre-configured with advanced voltage balancing settings, finely tuned to the unique chemical makeup of the cells and anticipated degradation rates. Lastly, the installation location of the OEM BMS system was also carefully considered, promoting ideal balance wiring management while preventing the system from overheating. This meticulous approach not only enhances performance but also extends the longevity of the BMS board. Four types of OEM BMS are reviewed during this research project, including centralized, modular, master-slave, and distributed.

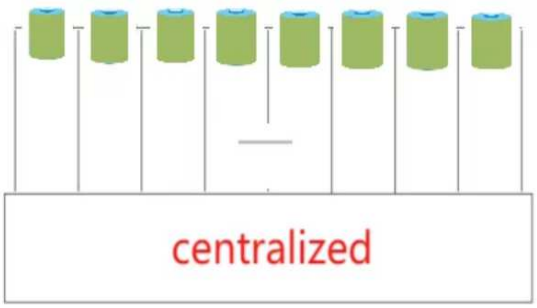

Figure 3.9: Centralized BMS [34]

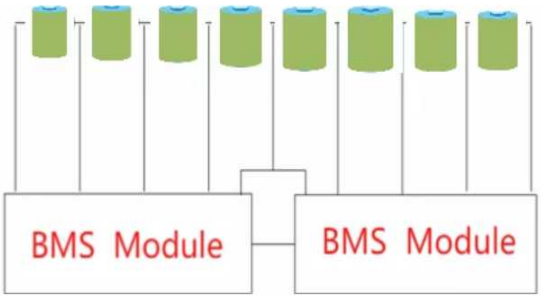

Figure 3.10: Modular BMS [34]

The centralized BMS is typically larger in format and consolidates all hardware within a single device, as illustrated in Figure 3.9. The centralized BMS solution offers significant

advantages for second-life applications, mainly due to its superior wiring adaptability with aftermarket adapters. All BMS wires converge at the same point, simplifying the integration of communication systems or the BMS replacement process. However, this architecture also introduces a considerable risk to MBA systems by creating a single-point failure for the entire battery pack. Should the centralized BMS fail, the whole battery will cease to function. Similarly, the centralized BMS structure presents another critical vulnerability: if a single cell group fails, the entire battery pack will stop operating due to the interconnected wiring of the battery cell groups, as presented in Figure 3.8. The Chevrolet Bolt is using a centralized BMS [34].

As illustrated in Figure 3.10, the modular BMS is similar to the centralized BMS but is divided into several segments based on the maximum number of battery cell groups each module can accept. Consequently, the modular BMS mitigates the risk of single-point failure and enhances the reusability of the battery pack in second life. In case a single BMS module or a cell group fails, only the cell groups associated with that particular module are impacted, allowing the rest of the battery pack to be repurposed. However, this modular architecture compromises wiring adaptability, resulting in a more complex BMS replacement process. Furthermore, the OEM BMS modules utilize a common CANbus to communicate with the onboard vehicle computer, which means that a single OEM BMS module cannot be substituted with a third-party module due to proprietary CANbus communication protocols among OEM parts. An example of modular BMS used in EVs is from the Tesla vehicles.

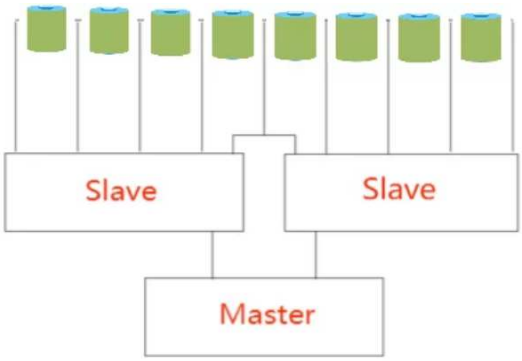

Figure 3.11: Master-slave BMS [34]

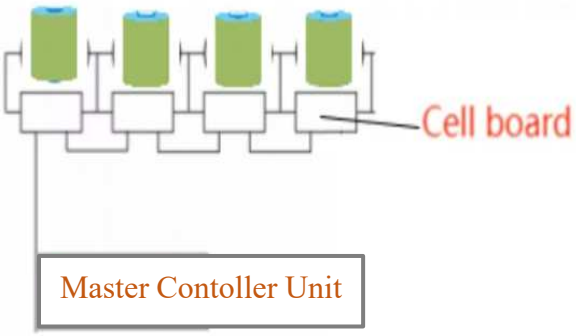

Figure 3.12: Distributed BMS [34]

In contrast, the master-slave BMS features a two-tier architecture, as demonstrated in Figure 3.11. The master BMS oversees battery pack status and facilitates communication

with the EV onboard computer. Meanwhile, slave BMS collects operational data from the battery cell groups, providing voltage balancing and protection mechanisms. Unlike the modular BMS design, the slave BMS units do not communicate with each other; instead, each one maintains an independent CANbus communication channel directly with the master BMS. This structure reduces the data transfer load on each CANbus, thereby enhancing the robustness of the communication. Although this system still bears the risk of a single-point failure at the master BMS, replacing the master unit is considerably more accessible compared to other BMS types. For replacement, the master unit only needs to be disconnected from the CANbus without altering the voltage or temperature harness. Moreover, should a slave BMS or a cell group fail, the master BMS can be reprogrammed to bypass the impacted slave BMS and continue operation, thus reducing the operation costs and improving the overall reusability of the battery pack. The master-slave BMS is less common in the EV industry because of its key advantages in low wiring costs and high scalability. Yet, EV battery packs do not require scalability since the battery cell number is fixed once the battery pack leaves the manufacturer. However, master-slave BMS is well adopted by the energy storage industry since the master BMS can expand or reduce the number of slave-BMS units based on the BESS capacity requirements.

Lastly, the distributed BMS, while architecturally similar to the master-slave BMS, as shown in Figure 3.12, offers limited protection and decision-making capabilities at the cell board level. The master control unit (MCU) establishes a CANbus communication line with all cell boards, handling balancing decisions, data monitoring, and protection mechanisms. Each cell board collects cell-level voltage and temperature measurements and executes voltage balancing as the MCU directs. In addition, each cell board typically manages fewer cell groups compared to the modular BMS, resulting in a higher number of cell board units per battery pack. This configuration shares the same advantages as the modular and master-slave BMS, such as mitigating the risk of BMS cell board and battery cell group failures, but it allows for more precise isolation of failed battery cell groups, thus minimizing collateral damage to the entire pack.

For instance, Tesla vehicles use a modular BMS configuration for their battery packs, which include four battery and BMS modules. Consequently, if a single cell or BMS module fails, the battery pack loses 25% of its total usable capacity. In contrast, Hyundai

EVs utilize a distributed BMS with 32 cell boards across the battery pack. Therefore, if a single cell or cell board fails, the battery pack would only lose approximately 3% of its usable capacity. This feature significantly enhances the reusability of the battery pack in second-life applications.

Table 3.4 lists the summary of the comparison of the OEM BMS discussed above.

Table 3.4: OEM BMS Comparison Summary.

BMS Type	Advantages	Disadvantages
Centralized	✓ Good wiring connecter adaptability. ✓ Easier BMS replacement and third-party BMS integration.	X Risk of single-point failure.
Modular	✓ No single-point failure risk. ✓ Enhances battery reusability.	X Less wiring connecter adaptability X Complex communication setup X Limited BMS replacement options.
Master-Slave	✓ Reduces wiring costs. ✓ Reduces risk of single-point failure. ✓ Allows scalable BMS configurations. ✓ Simplifies replacement of master unit.	X Less common in the EV battery packs.
Distributed	✓ Reduces risk of single-point failure. ✓ High precision in isolating failed cells. ✓ Excellent for maximizing battery pack reusability in second life.	X Requires more components via a higher count of cell boards.

However, most independent BESS integrators face significant challenges accessing the OEM BMS system due to EV manufacturers not releasing their CANbus communication protocols. This lack of access complicates the reuse of the OEM BMS. Even when manufacturers do share their protocols, integrators often encounter additional difficulties. For example, variations in physical connections across different models, model years, and manufacturers frequently necessitate protocol adjustments. As a result, independent BESS integrators aiming to use these OEM BMS must continually update their communication databases to accommodate the newest EV models.

Furthermore, inherent operational limitations within the OEM BMS can obstruct the effective use of battery packs in second-life applications. The OEM BMS are programmed explicitly for EV applications, incorporating stringent protection mechanisms to ensure vehicle safety. However, these safety protocols can prevent the battery from operating if the BMS detects any issues. For instance, the OEM BMS might activate a battery cell failure alarm, halting the operation of the entire battery pack until the defective cell is replaced. Moreover, the BMS might trigger voltage protection alarms if the pack-level voltage operations vary in second-life scenarios. These combined challenges make the OEM BMS less suitable for MBA systems. Figure 3.13 shows a Tesla Model 3 Long-Range (M3LR) Pack with OEM BMS installed.

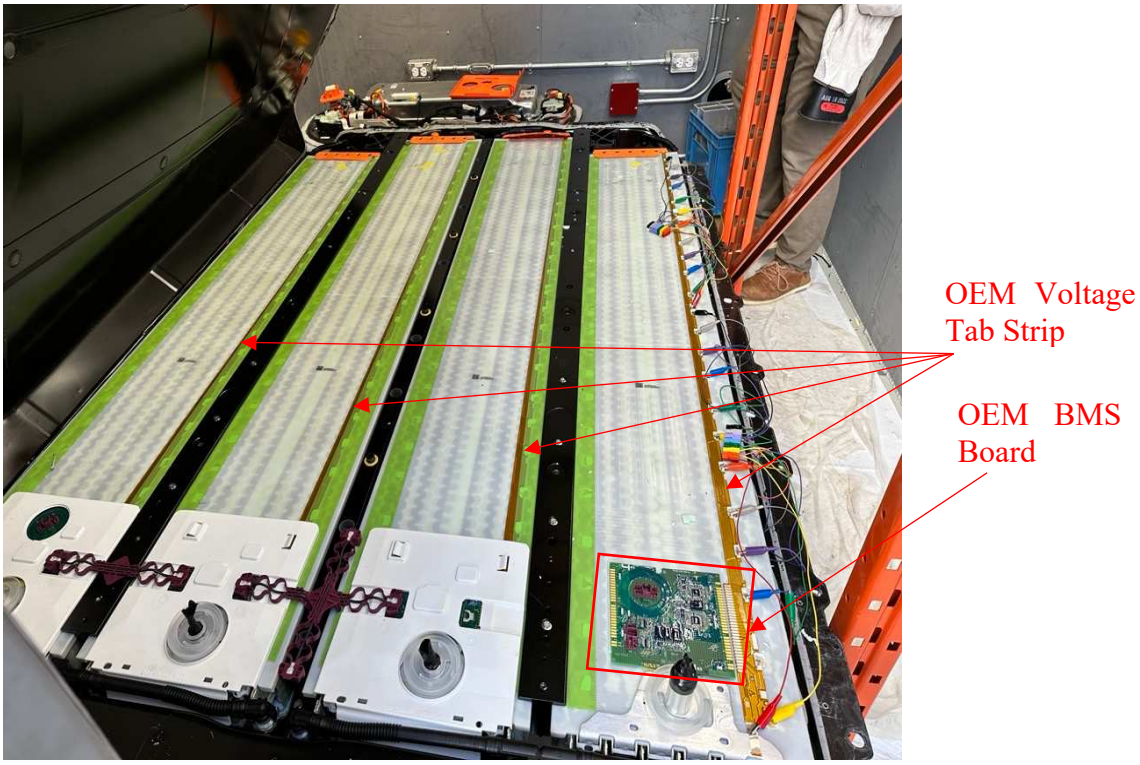

Figure 3.13: Tesla Model 3 Long-Range Pack Internal

3.4.2 Third-Party BMS

Independent BESS integrators can also choose to deploy a third-party BMS to acquire the necessary information from the EV battery packs. Third-party BMS options support self-installations for various battery configurations, including second-life EV battery packs. These universal third-party solutions offer extensive adaptability, allowing voltage and

temperature monitoring extension to achieve system-wide diagnostics. They also support customizable CANbus messages to facilitate active communication with the EMS.

The wide range of battery compatibility offered by third-party BMS systems often includes features that surpass the needs of second-life EV batteries, resulting in underutilized capabilities. As a result, investing in a third-party BMS constitutes a significant portion of the capital costs involved in repurposing batteries. Additionally, replacing the BMS is a complex process that typically cannot be standardized across different manufacturers. This procedure involves opening the battery pack, removing the OEM BMS, rewiring the connectors, and programming the new third-party BMS to match the specific pack configuration. It is also important to note that most commercial EVs employ liquid cooling for effective thermal management, with OEM temperature sensors optimally positioned within the battery pack to monitor thermal conditions. Therefore, if the third-party BMS is compatible, it is advisable to reuse the OEM temperature sensors to maintain accurate temperature monitoring in the MBA system.

Figure 3.14 shows the same M3LR pack from Figure 3.12 after the BMS replacement process. The M3LR pack comprises 96 cell groups linked in series, necessitating 97 new voltage tap installations to monitor the cell group voltage information. Additionally, eight new temperature sensors were added to the module surface to gather temperature data since the OEM temperature sensors were inaccessible. However, this BMS replacement approach is not universally applicable due to variations in battery pack designs; therefore, the MBA system must create tailored BMS wiring schemes for different EV batteries.

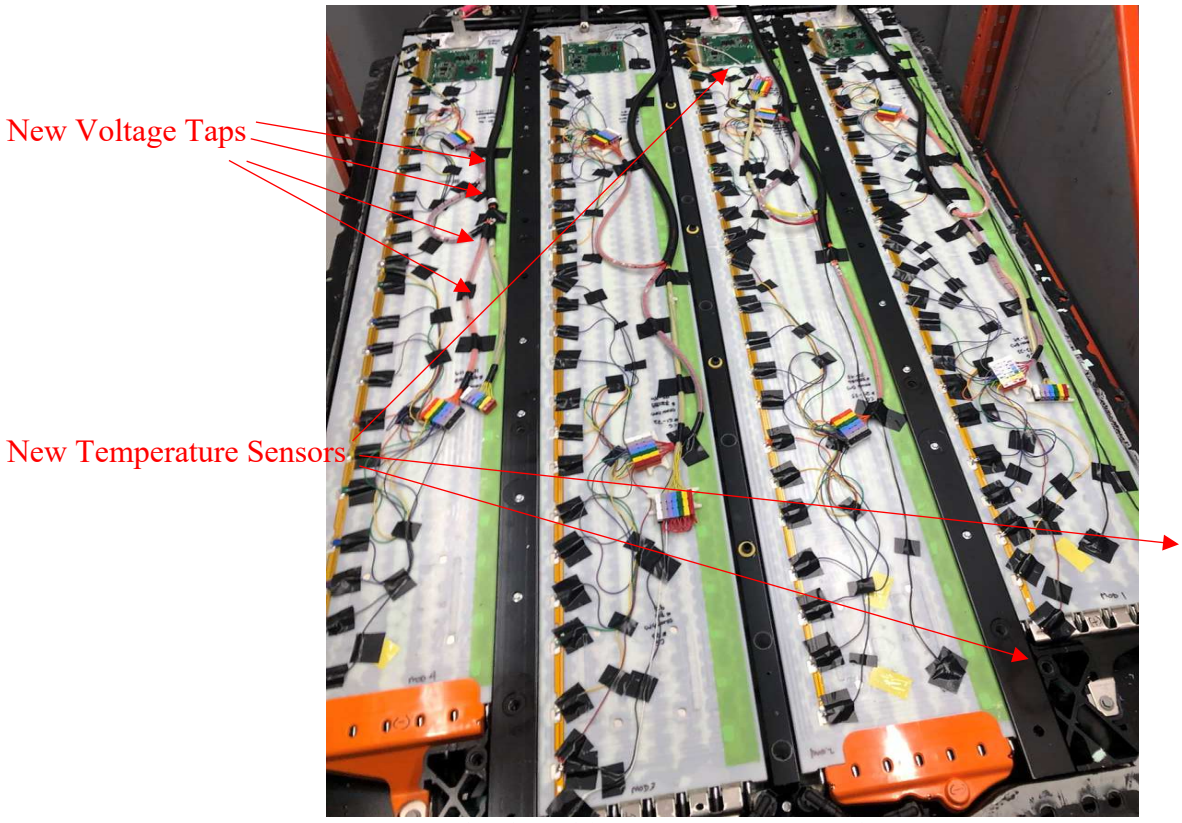

Figure 3.14: Rewired Tesla Model 3 Long-Range Battery Pack

3.4.3 OEM Versus Third-party BMS Integration

Considering the diverse array of EV battery packs accommodated by the MBA system, the chosen BMS solution must adapt to second-life applications while balancing costs and integration challenges. Specifically, reliability, flexibility, and accessibility are highly prioritized in the integration process. The preferred BMS should feature a robust communication system, precise measurement capabilities, and an effective voltage-balancing function that can be reprogrammed for various energy storage applications. Additionally, the BMS should allow for some rewiring flexibility by independent integrators in the event of modifications at the cell or module level. Given these considerations, a third-party BMS might be more suitable for the MBA system due to its versatility in accommodating different battery packs and providing full access to battery pack conditions once installed. Table 3.4 outlines other critical factors considered in this comparative study between OEM and third-party options.

Table 3.5: OEM BMS Vs. Third-Party BMS

BMS Type	Pros	Cons
OEM BMS	✓ Superior integration with the EV battery. ✓ Highly tested functionality and reliability. ✓ Advanced balancing profile tailored to the cell chemistry. ✓ Modular BMS offers better repurpose fixability. ✓ No additional costs. ✓ Plug-in and Play integration process if OEM shares full CANbus access.	X Limited information and functionality access if the OEM does not provide technical support. X High maintenance is required on the BMS database to stay updated. X Existing safety protocols might not be suitable for second-life use. X Centralized BMS creates a single failure point. X Very sensitive to cell group failures.
Third-Party BMS	✓ Full access to battery conditions. ✓ Highly adaptable to various battery configurations and repurposing needs. ✓ Flexible voltage and temperature monitoring. ✓ Flexible second unit expansion capability.	X Complex and non-repeatable installation process X Features may exceed second-life EV battery needs, leading to underutilized functionalities. X Significant costs for replacement.

After assessing the advantages and disadvantages of each BMS option, this project decided to adopt a centralized third-party BMS for all installed battery packs, replacing the OEM BMS. This decision was primarily driven by the limited accessibility offered by the OEM systems. During the replacement process, various installation approaches for the third-party BMS were investigated. The details of these installation processes are thoroughly documented in Section 4.3.1. This section provides an in-depth analysis of several critical aspects, including the rewiring plan for each battery pack, the development of CANbus messages between the BMS and the EMS, and the testing of voltage balancing functions for each battery.

3.4.4 EMS Development

An EMS was developed during this project to monitor and control the overall system operations. A CANbus communication network was also constructed to facilitate communication between the BMS and EMS. In addition, the EMS inherited the Modbus

communication protocol from the PCS to gain control access over the system. Upon receiving battery information from the BMS, the EMS directs the corresponding PCS units to either charge or discharge the battery as needed. Figure 3.15 illustrates the communication flowchart among the BMS, PCS, and EMS.

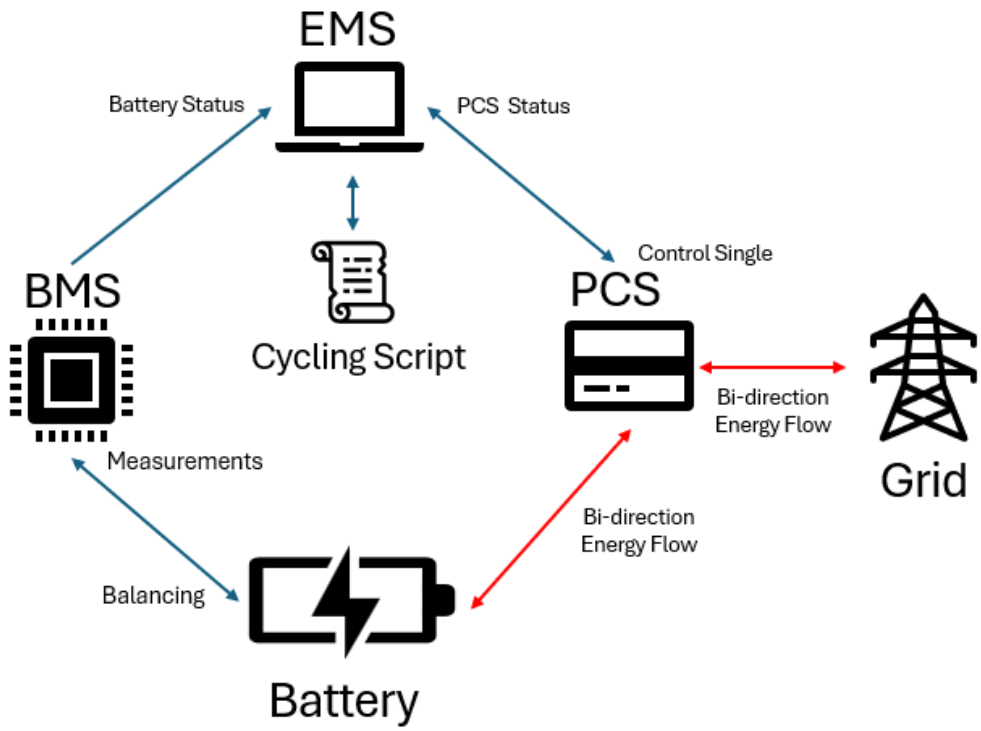

Figure 3.15: MBA Communication & Power Flow Diagram

The most significant challenge in integrating the EMS within the MBA system arises from the variable conditions of the EV battery packs. In contrast to commercial BESS setups, where each battery string maintains consistent voltage ranges, energy capacities, and PCS, allowing uniform energy demand distribution, the MBA system operates differently. The EMS must manage each EV battery pack based on its specific operational window and power capabilities relative to the demand signals for the MBA system. As a result, most commercially available EMS solutions lack the flexibility necessary to meet the specific demands of the MBA system. Additionally, EMS integration challenges in this project are further compounded by the need to develop a script cycling function to evaluate battery pack performance under various grid support scenarios.

Thus, the EMS developed during this research project overcame those challenges and facilitated the basic EV battery system-level research requirements. Specifically, the script

cycling function allows the EMS to operate the multiple batteries simultaneously under controlled conditions while recording the battery information for subsequent analysis. Additionally, the EMS establishes voltage and temperature limits for each battery pack and continuously compares them with real-time values during operation. This constant monitoring enables the EMS to make informed termination decisions, ensuring the safe operation of the system. Figure 3.16 illustrates the user interface of the EMS developed for this research project.

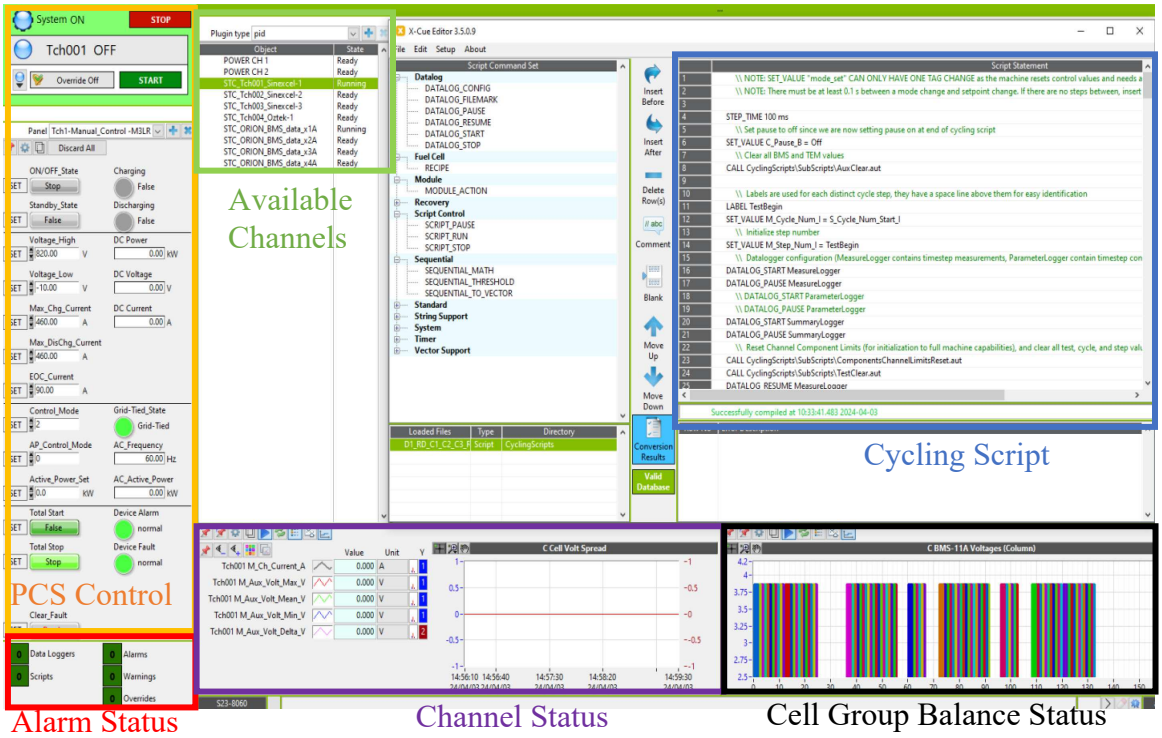

Figure 3.16: Energy management system based on Green Light Innovations Emerald Software

3.5 BATTERY THERMAL MANAGEMENT SYSTEM REVIEW

As discussed in the previous chapter, the temperature of battery cells significantly influences the energy efficiency, capacity degradation, and operational safety of the MBA system. Thus, selecting an effective thermal management system (TMS) is crucial, as it directly affects the maximum power rate, energy efficiency and the lifetime of the MBA system.

The primary function of the TMS is to keep battery pack temperatures within the optimal range of 15 to 35 °C and manage heat generation during the charge-discharge cycles, which allows the battery packs to operate efficiently [34]. Constantly operating the battery system below the optimal temperature range will impact battery performance by reducing usable

energy capacity. Conversely, operating above the optimal temperature range could improve energy efficiency performance but would also increase the energy capacity degradation rate overtime, according to White et al. [22]. However, the temperature control challenge escalates with varying heat generation rates among EV battery packs. Furthermore, since the MBA system operates multiple battery packs simultaneously, the heat emitted by one pack can influence the temperatures of adjacent packs, adding further complexity to the thermal management process.

There are two types of TMS for battery systems: passive and active. A passive TMS operates independently of the EMS and adjusts to an ambient temperature set point to provide necessary heating or cooling across the entire battery system. Thus, batteries under a passive system are either heated or cooled based on ambient temperature conditions without active intervention. Conversely, an active TMS depends on control signals from the EMS to ensure a safe and efficient environment. As such, the EMS actively monitors and adjusts battery pack temperatures based on feedback from the BMS; hence, the active TMS offers better heating and cooling rates and greater temperature uniformity for each battery pack. This research project investigates three potential TMS options for the MBA system: a passive cooling system, a forced-air active system, and a liquid cooling active system. Each system presents distinct advantages and challenges in terms of implementation and thermal performance.

3.5.1 Passive Cooling

The passive cooling method simplifies the TMS, opting out of the OEM battery pack liquid-cooling system and relying entirely on natural convection for heat dissipation. The heat exchange rate for passive cooling can be enhanced by removing the top cover from the battery pack and reducing the ambient temperature surrounding the batteries. Yet, passive cooling still has the lowest heat exchange efficiency of all thermal management solutions. As such, the passive cooling thermal management system will limit the MBA applications to low power rates for 4 hours or longer. Examples of applications include backup energy storage solutions or scheduled load-shifting operations, where the demands on power throughput are relatively modest.

Despite these limitations, passive cooling presents a set of compelling advantages, particularly from a financial and operational standpoint. The absence of complex

mechanical cooling systems translates into lower operational costs. This factor can be particularly appealing in the context of second-life applications where the cost-effectiveness of the energy storage solution is a primary consideration. Furthermore, the simplicity of passive cooling systems enables faster turnover rates for the deployment of MBAs, enhancing their viability for rapid reconfiguration or redeployment in various scenarios.

Figure 3.17 illustrates the passive cooling thermal management setup employed in the MBA system for this project. In this configuration, the battery pack is situated in the battery chamber with the top cover removed, and a heat pump maintains the ambient temperature. The heat pump unit at the top right of the chamber maintains a stable ambient temperature of 25°C. This setup underscores the feasibility of effective thermal management through passive means, emphasizing the balance between maximizing energy efficiency and minimizing system complexity and capital costs.

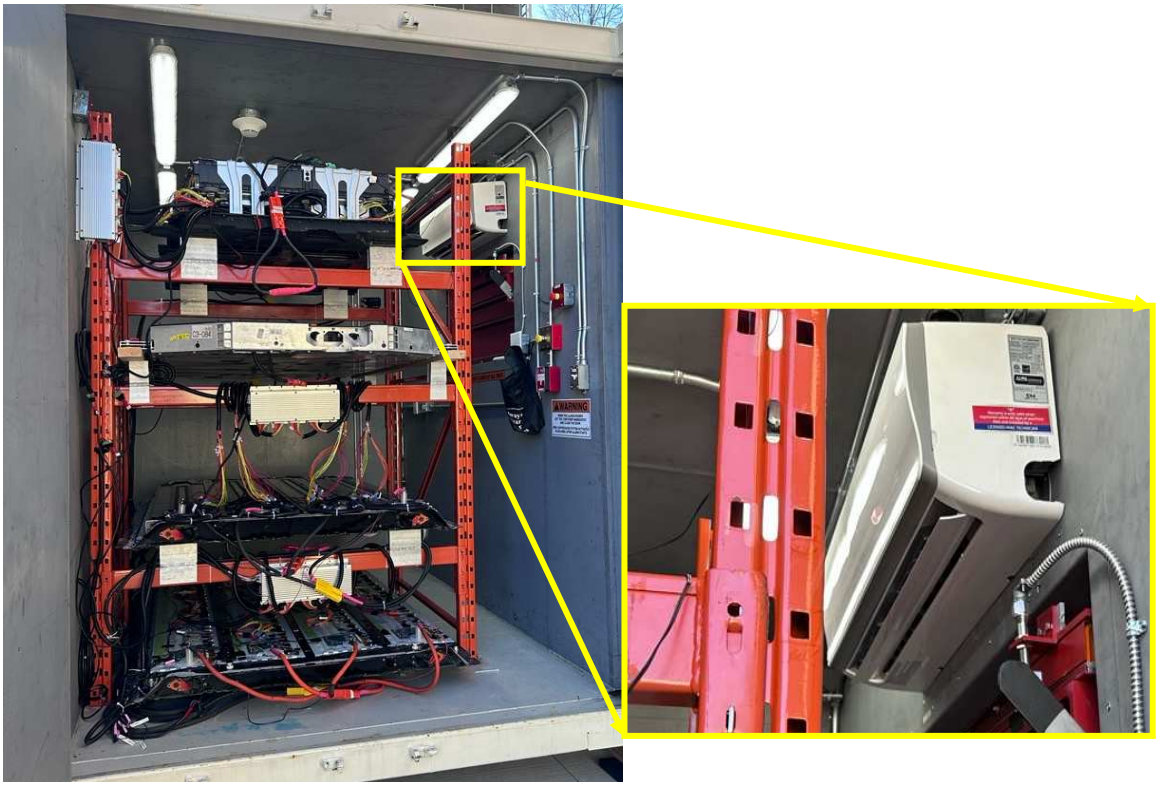

Figure 3.17: Passive Cooling Method

3.5.2 Forced Air Cooling

The forced air thermal management system, frequently adopted in stationary BESS, employs air conditioning to circulate heated or cooled air via ducting to regulate the

temperature of each battery module. Enhancing heat exchange efficiency necessitates using supplementary fans for sustained air movement and a sophisticated control mechanism by the EMS for precise air temperature adjustments. Forced air thermal management stands out for its improved heating and cooling capabilities, which are attributed to increased air circulation and more versatile control over ambient temperatures compared to the passive cooling method. Hence, the forced air thermal management system would allow higher power rate operation while maintaining lower cell temperature.

Commercial BESS often incorporates battery modules equipped with integrated fans to direct airflow and optimize the heat exchange rate. This setup involves air being channelled from the heat pump through the ducting system to each battery module, exiting the system as depicted in Figure 3.18.

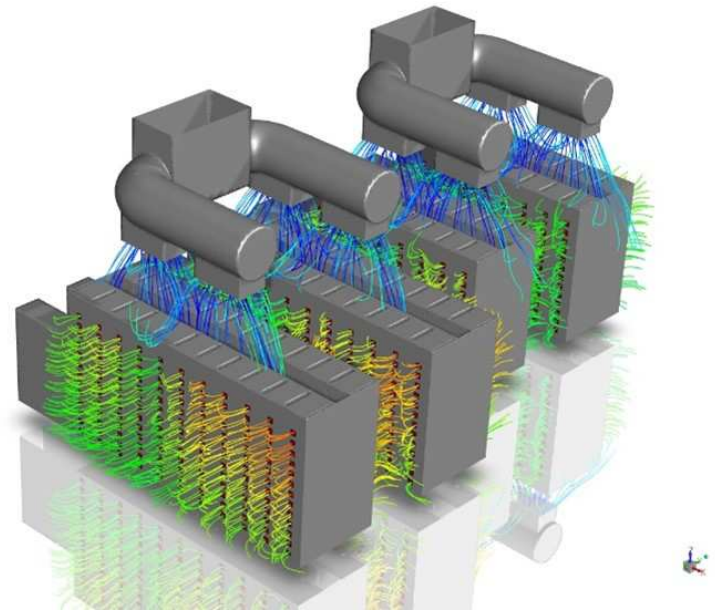

Figure 3.18: BESS Forced Air Flow Diagram [35]

This configuration is unsuitable for MBA applications because it requires extra fans to ensure sufficient air circulation for effective temperature regulation of each battery. To implement a forced air-cooling system, a redesign of the battery rack is necessary to accommodate the complex ducting system. Specifically, a central air duct channel must be added to guide airflow directly to the front of the MBA rack. This setup divides the air at every battery level and incorporates additional fans at the rear of the racks to pull air across the battery surfaces.

Moreover, the space between each rack level must be sealed to maintain airflow direction, preventing air leakage and ensuring consistent cooling across all batteries. This sealing process would involve installing barriers and gaskets, which add to the installation complexity and cost. Additionally, the added fans and ducting would occupy valuable space within the battery chamber, which is already limited. The spatial constraints of the MBA system make it challenging to fit the necessary components without compromising the overall design and functionality.

Furthermore, the forced air-cooling efficiency depends on precise airflow management, which can be difficult to achieve in a compact and densely packed battery chamber. Inconsistent airflow can lead to uneven temperature distribution, causing some battery cells to overheat while others remain under-cooled. This inconsistency can reduce the overall efficiency and lifespan of the battery packs, potentially leading to safety issues.

Considering these factors, including the need for additional parts, the complexity of the air duct design, and the insufficient space within the battery chamber, the forced air-cooling system is deemed unsuitable for MBA applications. Consequently, this project excluded the forced air thermal management system from further consideration.

3.5.3 Liquid Cooling

Liquid cooling is widely adopted in the EV industry and utilized in a few stationary battery energy storage systems, such as the Tesla Powerwall and Megapack [36]. Liquid cooling is significantly more effective than other thermal management methods at heat exchange from the battery pack, allowing high power rate operations. Adopting a liquid cooling system in the MBA system requires additional hardware, such as pumps, liquid reservoirs, pipes, and a large volume of coolant to circulate. However, the internal cooling plates are already built into the battery pack and have direct contact with the cell surfaces. Hence, Liquid cooling facilitates heat transfer through thermal conduction rather than convection. Moreover, the internal cooling pipe layout is designed to efficiently remove the maximum amount of heat during high-power demand periods while maintaining better temperature uniformity across the entire battery pack. Figure 3.19 shows a Tesla Model 3 battery pack cooling flow with four inlets and outlets.

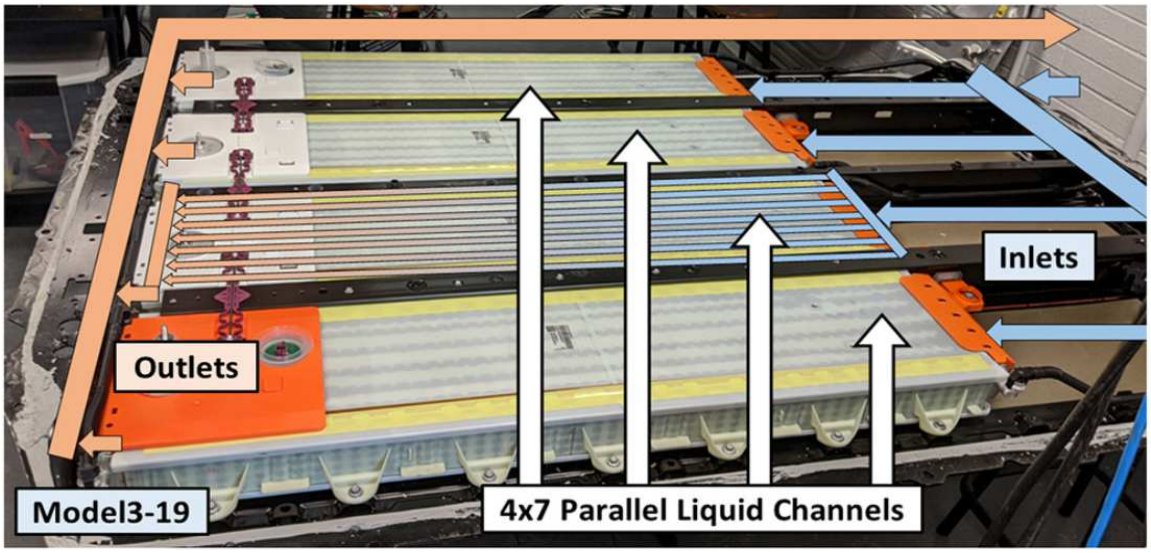

Figure 3.19: 2019 Tesla Model 3 Battery Pack Liquid Cooling Design [37]

The OEM liquid cooling systems are designed for EV packs operating in automotive environments face significant challenges, including extreme temperature variations (-30 to +45°C), exposure to vibrations, and physical stress. In contrast, an MBA system operates in a more controlled environment, which reduces the impact of ambient temperature fluctuations and places less thermal stress on the liquid cooling system. Additionally, the cooling load required for maximum power delivery during fast charging in automotive applications often exceeds the cooling load for most grid support applications. Consequently, the OEM-designed thermal management system will provide ample cooling capacity for the battery pack during its second-life application.

In the MBA system, the liquid cooling system requires a heat pump, a liquid pump, and a complex network of pipes to channel coolant to each battery pack. This configuration allows for liquid circulation, which can be either cooled or heated, with its temperature and flow rate controlled by the EMS. This arrangement facilitates active adjustments of the fluid temperature and flow rate entered in the battery packs and keeps the battery pack in optimal operating conditions. Although the liquid cooling thermal management system significantly boosts energy efficiency, reduces battery degradation, and enhances operational safety, it has drawbacks. Challenges such as the risk of coolant leaks, spatial constraints, the complexity of the control process, and increased auxiliary power usage could undermine the thermal benefits, particularly in scenarios of low power demand.

3.5.4 Thermal Management System Review

In the context of thermal management for MBA, passive cooling, forced air cooling, and liquid cooling each serve distinct operational needs, balancing application demands against cost, complexity, and heat exchange efficiency. Passive cooling, leveraging natural convection, excels in low-demand scenarios like daily energy storage, offering simplicity and cost-effectiveness but is limited under lower power conditions. Forced air cooling enhances heat exchange with additional fans but is unsuitable for MBA due to complex design changes. Liquid cooling, the most effective method, is ideal for high-demand applications, providing superior heat removal through direct contact cooling plates, but it necessitates a complex and costly infrastructure. Table 3.5 lists other factors considered for this comparison study.

Table 3.6: Thermal Management System Comparison

Cooling Method	Pros	Cons
Passive Cooling	✓ Low operational costs. ✓ No complex control system. ✓ No auxiliary energy consumption.	X Limited heat exchange capacity. X Insufficient cooling at high power rates. X Temperature inconsistency at the different rack levels.
Forced Air Cooling	✓ Better heating and cooling capabilities. ✓ Allow higher power rate operations. ✓ Advanced air temperature control.	X Increases system complexity. X Require battery rack modifications. X Require frequent maintenance. X High auxiliary energy consumption.
Liquid Cooling	✓ Significantly more efficient at heat exchange, enabling high power rate operations. ✓ Direct contact with cell surfaces allows for effective heat transfer. ✓ Adaptive thermal control capability.	X Coolant leaks pose a potential safety hazard. X Complex control process. X High auxiliary energy consumption. X High operating costs.

Hence, this project selected the passive cooling thermal management system due to the space limitations and sufficient cooling rate at the current testing stage.

4 DEMONSTRATION MIXED BATTERY ARRAY SYSTEM SETUP

4.1 BATTERY PACK INSTALLATION

The MBA system accommodates a wide variety of battery packs sourced from private passenger EVs because of its adaptable electrical, racking, and communication configurations. Consequently, the technical specifications of these battery packs, including factors like cell chemistry, pack size and configuration, operational voltage, and usable capacity, dictate the design parameters of the MBA system.

Hence, the battery pack technical specifications were evaluated and reviewed during the development of the demonstration MBA system. This assessment focused on four key factors: structural design, cell chemistry, rated capacity, and market availability. This selection process ensured a diverse battery pack array for this research project, facilitating meaningful comparisons and contrasts in battery pack integration for MBA systems. For instance, while many EV battery packs share a similar external layout, variations in structure and size exist among them. These distinctions can significantly impact the integration requirements for the MBA system. Thus, the subsequent sections delve into the technical nuances of the chosen battery packs, elucidating the disparities in their designs and how these variances translate into distinct installation requirements for the demonstration MBA system.

Given this, four EV battery packs were selected for the MBA demonstration system, which are the 2019 Tesla Model 3 Long-Range, 2021 Tesla Model 3 Standard Range, 2017 Chevrolet Bolt, and 2021 Genesis GV60. Based on the findings of the installation process, battery packs featuring a flat-pad design, compact module size, and operating voltages of 400 or 800 volts are identified as better-suited options for large-scale MBA systems.

4.1.1 2019 Tesla Model 3 Long-Range (M3LR)

The M3LR battery pack uses the MTP pack structure design, composed of four modules with 96 cell groups in total. The positive electrode cell chemistry used in this M3LR is Nickel Cobalt Aluminum Oxide (NCA), and the negative electrode cell chemistry is graphite with silicon added in all cells to boost energy capacity. NCA cells are known for their low energy efficiency yet high energy density.

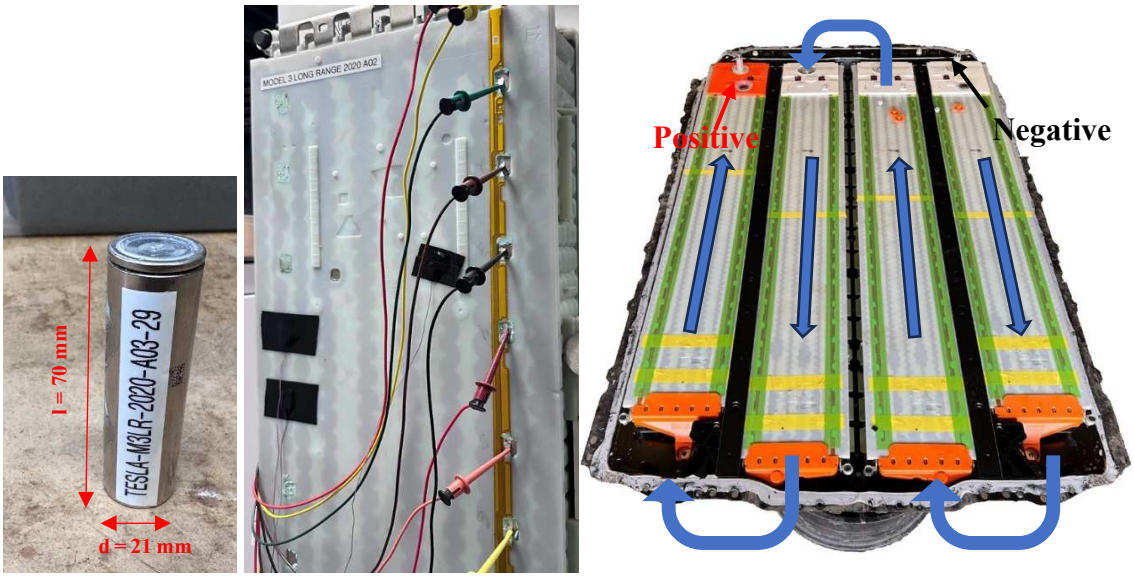

Figure 4.1: a) Tesla NCA Cell (Left); b) M3LR Module (middle); c) M3LR Pack (Right)

The internal structure can be observed upon removing the top cover and electrical components, as illustrated in Figure 4.1(c); the blue arrows present the current flow during the discharge process. Figure 4.1(a) highlights the 21-70 cylindrical cells used in the battery pack, which has a 4.35 Ah energy capacity, and Figure 4.1 (b) shows the honeycomb-like internal arrangement within the modules. A thermally conductive filler between cells mitigates vibration and enhances heat dispersion to the cooling serpentine tubes. M3LR pack features two smaller outer modules, each containing 23 series-connected cell groups, and two inner modules house 25 cell groups each. Forty-six cylindrical cells are paralleled and connected within each cell group, making a total of 4416 NCA cylindrical cells used in the entire M3LR pack. The M3LR battery module is equipped with liquid cooling tubes, BMS voltage, and temperature sensors under the plastic cover. Although the M3LR battery pack design is optimized for energy density, structural integrity, and thermal management, it also resulted in a problematic repurpose condition for its second-life application.

As shown in Figure 4.1c, M3LR battery cell groups are covered under a plastic sheet, as well as the voltage and temperature harnesses. This module design has caused two significant issues for the second-life applications. First, cell groups are not removable from the battery module, causing approximately 25% of total capacity to be lost if one cell group fails. Second, no access point is available to replace the OEM BMS, as the original BMS wires are covered under the plastic sheet. Hence, installing third-party BMS without damaging the battery module is nearly impossible. Therefore, repurposing the M3LR

battery pack has high labour costs and low-risk tolerance for cell-level damages. Thus, the current pack design from the M3LR is not a good repurpose option for second-life applications.

4.1.2 2022 Tesla Model 3 Standard Range (M3SR)

The Tesla Model 3 Standard Range (M3SR) battery pack has been redesigned since the 2022 model year. This revision entailed a transition in cell positive electrode cell chemistry from NCA to Lithium Iron Phosphate, known as LFP, while the negative electrode cell chemistry stayed at graphite carbon. The cell format switched from 21-70 cylindrical to prismatic, and the battery module was redesigned to accommodate the new cell format. Despite these changes, the overall pack dimension remains consistent with previous designs, as illustrated in Figure 4.2(c), which showcases the M3SR pack with the top cover removed.

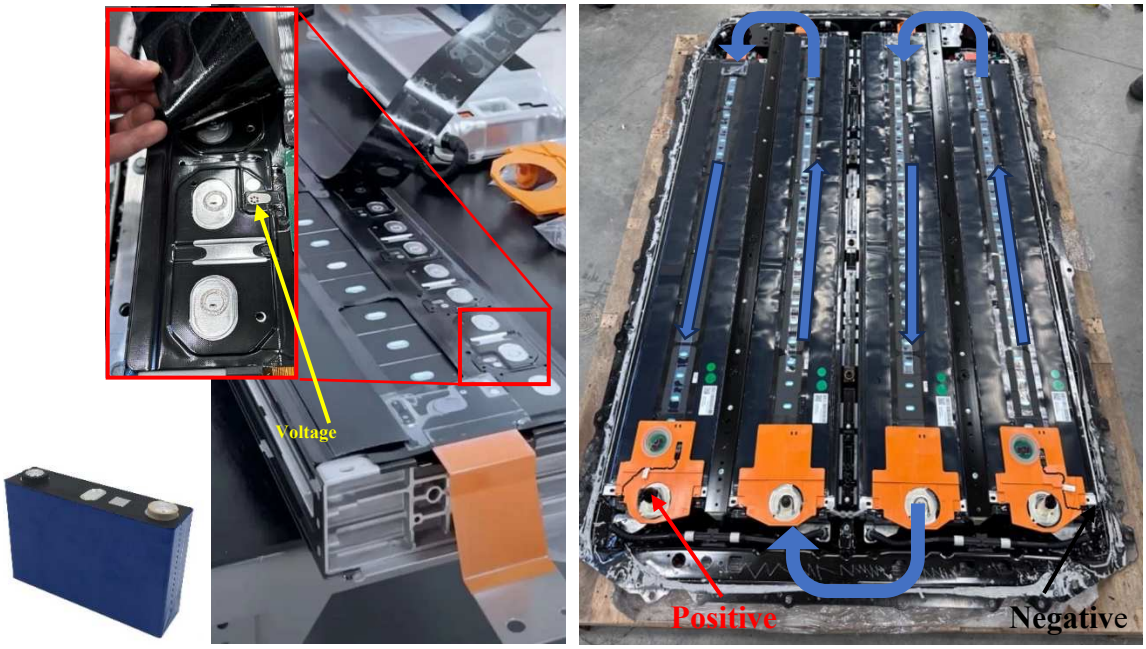

Figure 4.2: a) Tesla LFP cell (Left); b) M3SR Module (Middle); c) M3SR Pack (Right)

The revised M3SR pack is still composed of the four-module design, with the two outer modules containing 25 LFP cells and 28 for the two inner modules, adding up to 106 cells connected in series across the entire pack. Considering that the M3LR only has 96 cell groups connected in series from the same manufacturer, this requires high connectivity flexibility from the after-market BMS to work with these differences. The LFP prismatic

cell used in the M3SR has 161 Ah energy capacity, which is 37 times more than the single 21-70 NCA cell, which resulted in drastically fewer cell counts in the battery pack.

Tesla introduced an updated module design alongside the transition to the LFP cell format, as depicted in Figure 4.2(b). This redesign simplifies the module structure, eliminating the need for heat-conductive filler between cells and the module enclosure while ensuring pack-level integrity. Meanwhile, a cooling plate is added under the battery module, with heat-conductive filler applied between the plate and the cell surface to improve heat transfer and mitigate vibrations from vehicle movement. Furthermore, with the new prismatic cell format featuring the cell terminals on top, all the OEM voltage taps are consolidated on top of the cells. Consequently, the OEM BMS voltage wires were also redesigned, integrating them into a thin ribbon cable layer. This ribbon cable is then directly laser-welded to the cell terminals, as highlighted in Figure 4.2 (b). This redesign significantly simplifies the manufacturing process, reducing assembly time and component count compared to the M3LR pack design.

The updated M3SR battery pack enhances its suitability for second-life applications, also owing to the new cell format. Firstly, the M3SR cell terminals are easily accessible, facilitating the ability to jump over failed cells rather than necessitating the removal of the entire module. Consequently, this new module design improved the cell-level fault tolerance, minimizing potential capacity loss from 25% to just 1% in the event of a single cell failure within a module. Secondly, the OEM ribbon cable connector utilizes an industry-standard connection interface, simplifying the OEM BMS replacement process.

Despite the positive enhancements in the M3SR pack, it also presents new challenges for MBA system integrations. Specifically, the LFP cells operate within a voltage range (2.5 to 3.65 V) different from that of other commonly used EV battery cells (2.5 to 4.2 V). This variance in cell-level voltage necessitates the third-party BMS to operate on a distinct profile, affecting voltage balance settings and cell voltage limit alarms. Consequently, the demonstration MBA system also developed a specified BMS operation profile for the M3SR pack to safeguard the LFP cell voltage range.

In comparison to the M3LR battery pack, the revised M3SR battery pack offers notable improvements in second-life reusability, primarily due to its increased tolerance for single-cell failures and simplified process for OEM BMS replacement. Nevertheless, the higher

energy concentration per module continues to present a potential drawback, as removing an entire module from the battery pack may still result in a loss of up to 25% of its usable capacity.

4.1.3 2017 Chevrolet Bolt

The Chevrolet Bolt incorporates the "module-to-pack" design, featuring ten battery modules with a unique double-decking design at the rear of the vehicle. The positive electrode cell chemistry used in the Bolt is Nickel Manganese Cobalt oxides (NMC), and the negative electrode cell chemistry is graphite. Figure 4.3 (a) shows the NMC pouch cell used in the Bolt. The positive electrode chemistry competition in this 2017 Bolt is 622, in which the nickel content takes up to 60% of the total positive electrode volume, and manganese and cobalt each take 20% of the total positive electrode volume. The NMC chemistry composition impacts the cell performance character in terms of energy density, lifetime, and thermal performance. As such, NMC cells with higher nickel content offer higher energy density (kWh/L) than NCA and LFP cells; therefore, NMC cells are the most used cell type in electric passenger vehicles. Figure 4.3 (c) illustrates the Bolt battery pack without the top cover.

Figure 4.3: a) Chevrolet Bolt NMC Cell (Left); b) Bolt Module (Middle); c) Bolt Pack (Right) [38]

With a higher module count, each module contains fewer cell groups than the Tesla MTP design. Figure 4.3 (b) showcases a single battery module in the Bolt pack. The six modules on the lower level (yellow zone) have 10 cell groups connected in series and 3 cells connected in parallel per cell group. The 4 double-decked battery modules (green zone) feature a different cell group configuration, containing 36 cell groups in total. Thus, 96 cell groups and 288 pouch cells are in a Bolt battery pack. The higher module count also offers

several other benefits in second-life applications, including improved safety for the service technicians working on this pack, as the maximum voltage per module is less than 50 V. Moreover, the Bolt pack is more tolerable to damaged cells or modules, as each module only contains 10% of the total energy capacity; therefore, the Bolt pack would only lose 10% of its usable energy if a module is removed.

The double-decked module design optimizes space utilization beneath the rear seats, enhancing vehicle range without compromising overall size. However, despite this advancement, limitations in the fast-charging capability of the battery pack arise due to inadequate cooling capacity. During fast charging, the two modules on the second level risk overheating, which is attributable to the less surface area to dissipate the heat generation.

This MTP design allows for quick configuration change for the six modules on the lower level. Yet, the double-decked modules are less accessible as they are reinforced under a metal cover, as shown in Figure 4.3 (c). In addition, the double-decked design required more space on the MBA rack due to the excess high from the second-level modules, leaving wasted spaces in the front. Hence, this Bolt pack was placed on top of the MBA rack to compensate for the space requirement in this project.

The Bolt battery pack design reflects Chevrolet's effort to balance energy capacity with vehicle body size, leveraging battery module arrangement and cell chemistry. The higher module number offered better safety during pack modifications, and the energy capacity loss is much less sensitive to cell failure as each module only contains 10% of the total capacity. However, the double-deck design caused ineffective space utilization for the MBA system developed in this research project. Overall, the Bolt battery offers higher useability in second-life applications than the Tesla packs.

4.1.4 2021 Genesis GV60

The Genesis GV60 also used a "module-to-pack" pack design, containing 32 identical battery modules throughout the entire pack. While employing similar NMC cells with a 622 positive electrode chemistry competition as the Bolt, the GV60 cells exhibit slightly lower specific energy density. Nevertheless, the GV60 benefits from a flat-pad design, as depicted in Figure 4.4 (c), allowing it to utilize the least rack space among all packs in this project.

Figure 4.4: a) Genesis GV60 NMC cell (Left); b) GV60 Module (Middle); c) GV60 Pack (Right)

Each battery module, illustrated in Figure 4.4 (a) and (b), consists of 12 pouch cells, with 2 parallel cells connected per cell group and 6 cell groups connected in series, resulting in 192 cell groups within the GV60 battery pack. Compared to the Bolt pack, the increased module counts continuously improved module-level service safety, with the maximum module voltage remaining below 30 V. Consequently, the GV60 pack configuration has the highest cell failure tolerance among all selected battery packs for this project, with each module containing only 3% of the total energy capacity, hence, if a module fails, only 3% of usable energy will be lost. Additionally, integrating the liquid cooling plate under the battery modules ensures effective thermal conductivity, with all cells maintaining optimal thermal contact with the cooling plate, thus providing ample cooling capacity for high-power rate operations.

However, a notable distinction of the GV60 battery pack lies in the high number of cell groups connected in series, pushing the maximum voltage to 806 V. This renders the Sinexcel DC/AC converter inadequate to support the GV60 pack to its full voltage capacity, as the maximum DC voltage the Sinexcel unit supports is 750 V. Consequently, Oztek DC/AC converters are chosen to complement the GV60 pack, offering an extended DC voltage range reaching 820 V.

For several compelling reasons, the Genesis GV60 battery pack is the best choice for the MBA system. Firstly, its flat-pad design minimizes rack space utilization, which could

increase the number of battery packs installed in an MBA system. Secondly, thanks to the highest module count, the GV60 offered the best service safety and the highest tolerance to cell failures, enhancing its overall reliability in second-life applications. Thirdly, the NMC 622 cells have superior energy density compared to NCA and LFP cells, which also contributes to better power rate performance. Despite the need for a different PCS to support its higher voltage, the elevated pack voltage promises long-term energy efficiency gains due to reduced current and higher PCS power efficiency, outweighing its drawbacks.

4.1.5 Battery Pack Installation Review

This project demonstrated the MBA integration challenges from different battery packs, yet the MBA system overcame these challenges due to its flexibility in power structure. For instance, the M3LR pack showcases the complexity of the rewiring process for replacing the OEM BMS; the M3SR offers easier reusability with the new LFP cells yet requires an entirely different BMS operation profile; the Bolt pack features a double-deck design, which results in insufficient space utilization; finally, the GV60 required a different PCS to support its DC voltage range. These unique challenges from each EV battery shaped the design requirements of the MBA system and expanded its adaptability to other battery packs in the future. Table 4.1 lists the technical specifications of the four-battery pack installed in this project, and the distinctive integration requirements of each battery pack are highlighted in the list.

Table 4.1: Summary of Selected Battery Packs

Pack Number	1	2	3	4
Vehicle Manufacture	Tesla Model 3	Tesla Model 3	Chevrolet	Genesis
Year	2019	2021	2017	2021
Model	Long Range	Standard Range	Bolt EV	GV60
Cell Chemistry	NCA	**LFP**	NMC	NMC
Cell Format	Cylindrical-2170	Prismatic	Pouch	Pouch
Cell Capacity (Ah)	4.35	161	60	55.6
Cell Voltage Range (V)	2.5 – 4.2	**2.5 - 3.7**	2.5 – 4.2	2.5 – 4.2
# Cell Groups	96	106	168	**192**
Module Configuration	23S (25S)46P	25S (28S)1P	10S3P	6S2P
Pack Configuration	**4S**	4S	10S	32S
Pack Voltage Range (V)	240 – 403	265 – 392	250 – 420	**480 – 807**
Pack Dimensions with cover off (cm)	218x150x18	218x150x18	**Double-deck 180x128x35**	213x150x15
Packaging Type	MTP	MTP	MTP	MTP
Pack Wight (Kg)	480	440	435	~470
Rated Capacity (kWh)	75	55	60	77.4
Specific Energy (Wh/kg)	156	125	151	172
Energy Density (Wh/L)	134	98	74	162

4.2 SELECTED PACK ASSESSMENT RESULTS

Only the M3SR and GV60 battery packs underwent the initial pack assessment process because these two packs were new additions to the RESL battery inventory, and both packs were acquired from third-party dealers. The M3LR and the Bolt pack have been cycled and reconditioned from prior testing projects, and both packs are in good condition and ready for cycling. Hence, the initial results of the pack assessment for M3SR and GV60 are detailed below.

4.2.1 Tesla Model 3 Standard Range Battery Pack Assessment Results

Figure 4.5: Tesla Model 3 Stander Range LFP Pack at Receiving

The Tesla Model 3 Standard Range pack arrived at RESL in October 2023. Figure 4.5 shows the external condition upon arrival; no damage was observed. Immediately after its arrival, the top cover was removed for the initial evaluations, including structure damage inspection, battery pack voltage measurement, and preliminary cell and module level voltage assessments. The pack voltage at arrival was measured at 352.98 V, corresponding to an average cell voltage of 3.33 V, which is in the normal range for LFP cells. After removing the battery top cover, no internal damage or battery cell status issues were found at the cell or module level. Hence, no modifications were required except for the replacement of the OEM BMS. Due to the nature of the LFP cells, the battery cell voltage usually rests at 3.33 V regardless of the state of change unless the battery cells are fully charged or discharged. Therefore, the cell voltage imbalance was not visible during the initial inspections. However, the battery cells in the M3SR pack were later found out of balance after the battery pack was fully charged, and the Orion BMS2 performed the active balancing procedure at 3.5 volts per cell, bringing the maximum cell voltage delta down from 50 mV to 5 mV. Despite these minor voltage variations, the cell group voltage

readings showed uniformity across the entire battery pack, indicating all cells were in similar SOC conditions; thus, the M3SR pack was deemed ready for cycling.

4.2.2 Genesis GV60 Battery Pack Assessment Results

Figure 4.6: Genesis GV60 Battery Pack at Receiving

The Genesis GV60 battery pack arrived at RESL on February 13th, 2023. Initial inspection revealed no external damage to the battery pack, as shown in Figure 4.6. The initial assessment recorded the pack voltage at 676.8 Vdc, equating to an average cell voltage of 3.76 V upon arrival, which is normal for LFP cells. After removing the top cover, no internal structural damage was reported, and the layout of the battery modules is presented in Figure 4.7(a).

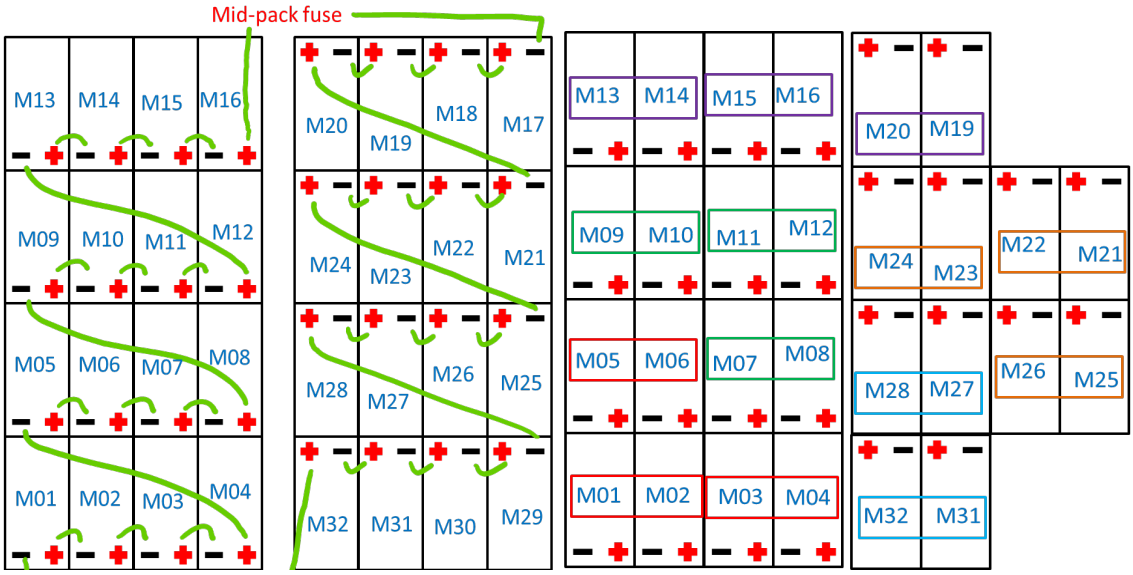

Figure 4.7: a) GV60 Module Configuration at Receiving (Left); b) GV60 Module Configuration Installed (Right)

During the module-level assessment, module 17 and module 18 displayed low voltage readings; therefore, these two modules were removed from the battery pack for further damage investigation. Once removed, the module 17 voltage reading fell to 0 V and module 18 measured at 14.27 V, below the anticipated 19.8 V per module. Thus, both modules were set aside for cell-level damage assessment, and the rest of the battery pack moved on to the next assessment step. In addition, modules 29 and 30 were removed later for internal studies at the cell and module level, focusing on degradation, energy efficiency, and state of health. Figure 4.7(b) shows the battery pack in its final reconfigured state for this research project, following the removal of the four modules. Hence, only 168 cell groups were successfully populated for the MBA system, which eliminated the need for the slave BMS as the master BMS can only take a maximum of 180 cell groups.

After the third-party BMS installation, the BMS reported the open-circuit voltage for the populated cell groups. The maximum voltage difference between cell groups was 11 mV, which deemed the battery pack unsuitable for cycling. However, after the BMS active balancing procedure for the GV60 battery pack, the maximum difference in cell voltage was reduced from 11 mV to 5 mV. Hence, the GV60 battery pack is ready for script cycling

at this state. Table 4.2 lists the cell group voltage status for M3SR and GV60 battery packs before and after the BMS balancing process.

Table 4.2: M3SR & GV60 Cell Group Voltage Status

	M3SR at Receiving	M3SR after BMS Balancing	GV60 at Receiving	GV60 after BMS Balancing
Maximum cell voltage (V)	3.33	3.492	3.761	3.956
Mean cell voltage (V)	3.33	3.492	3.760	3.956
Minimum cell voltage (V)	3.29	3.487	3.750	3.951
Maximum voltage delta (mV)	50	5	11	5

4.3 MIXED BATTERY ARRAY DEMONSTRATION SYSTEM EXPERIMENTAL SETUP

4.3.1 Standalone Test Container Layout

Figure 4.8: RESL Standalone Test Chamber

The proposed MBA system is housed in a custom-built 24 ft shipping container situated externally to the RESL lab, referred to as a Standalone Test Container (STC). The STC is subdivided into two designated zones: the PCS Chamber and the Battery Chamber, as shown in Figure 4.8.

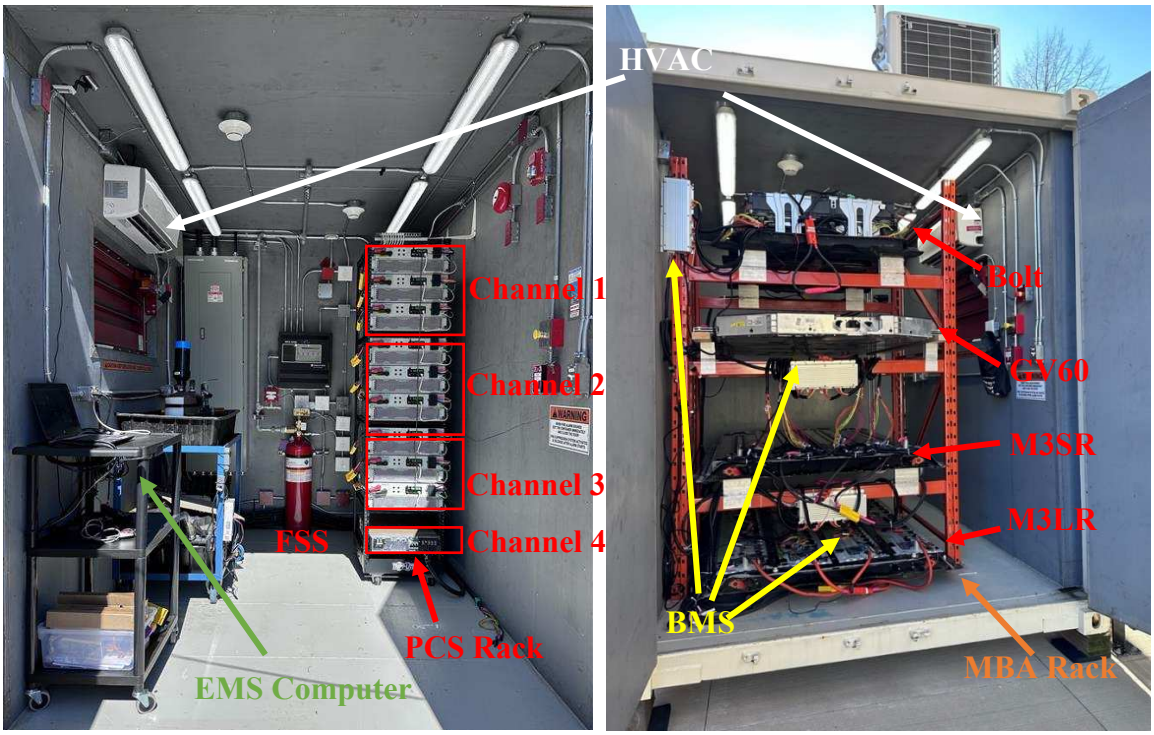

Figure 4.9: STC-PCS Chamber (Left); STC-Battery Chamber (Right)

As shown in Figure 4.9, two heat pump units are installed on both sides of the container for dual-zone climate control. Additionally, an isolation transformer is installed to convert the voltage from 600 Vac to 480Vac specifically for the PCS power supply, and a secondary step-down transformer further decreases the voltage to 208 Vac for auxiliary power supplies such as the heat pump, fire suppression system, and lighting. A six-inch steel wall in the middle of the container separates the two chambers. The battery chamber is allotted explicitly for battery pack installations, whereas the PCS chamber accommodates the PCS rack, EMS, and other auxiliary systems.

4.3.2 Orion BMS2 and CANbus Communication Setup

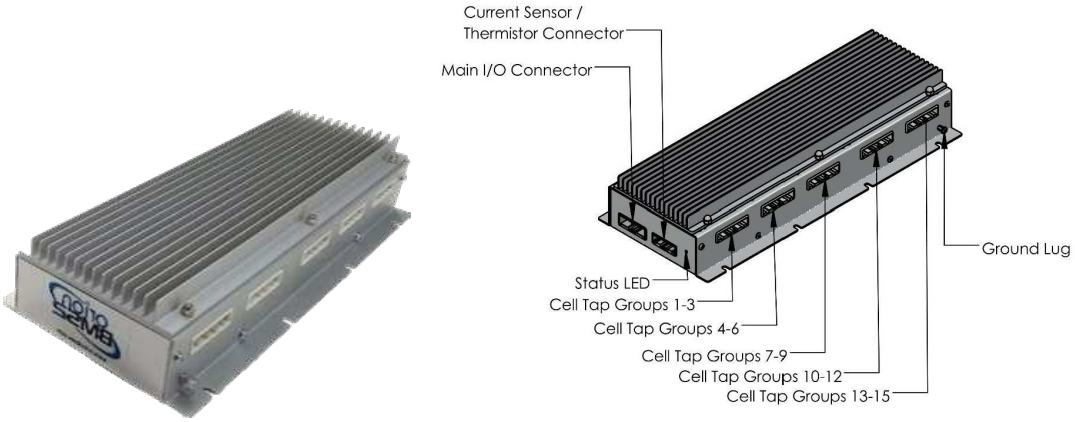

Figure 4.10: Orion BMS 2 [39]

The Orion BMS 2 is a centralized BMS, as depicted in Figure 4.10, providing battery pack status monitoring, cell balancing, and several safety features, offering good flexibility to integrate with third-party applications. It has 180 cell voltage measurement channels, eight temperature measurement channels, and a single current measurement channel. To accommodate a battery system containing more than 180 cell groups, Orion BMS2 can add a slave unit to expand the cell voltage channels. The 180 voltage channels are organized into 15 groups, each connected to a cell group capable of conducting up to 12 voltage measurements, as detailed in Figure 4.10 (right). Every three cell groups are further consolidated into one voltage harness with different colours (yellow/red/orange), as elaborated in Figure 4.11 (left). Hence, each voltage harness can measure up to 36 cell groups. The BMS also integrates a current sensor and eight temperature sensors into a unified wire harness, as illustrated in Figure 4.11 (middle). The Main I/O harness, as shown on the right side of Figure 4.11, includes the 12 V power cable, two CANbus lines, and various dry contacts for auxiliary power supply and EMS communication.

Figure 4.11: Cell Voltage Harness (Left); Current & Temperature Harness (middle); Mian I/O Harness (Right).

This research project developed a standard CANbus messaging system between the BMS and the EMS using the Orion BMS2 Utility software to accommodate constant communication. The CANbus message system includes six data frames transmitted to the EMS every 42 ms. The data transmitted in each frame has a unique address ID to identify the message type by the EMS, and the ID format is shown below:

$$ID\ Address\ = 0x\#\#(A/B)$$

- $0x$ marks the beginning of a new ID address.
- 1st Number (#) represents the battery Pack Number associated with the BMS, which is (1~4) for this project.

- Second Number (#) represents the message line number from this BMS via line 1 to line 6.
- (A/B) represents the master/salve BMS unit associated with the pack.

Given this CANbus messaging system structure above, table 4.2 shows the battery information transmitted by each frame, using an example from the first BMS.

Table 4.3: Orion BMS 2 CANbus Messages

ID	Data Transmitted				
0x11A	All cell group (CG) voltage measurements				
0x12A	Lowest CG Voltage	Lowest CG ID	Highest CG Voltage	Highest CG ID	Average CG Voltage
0x13A	Lowest Temperature	Lowest Temperature ID	Highest Temperature	Highest Temperature ID	Average Temperature
0x14A	Error Presented	BMS Balancing Active	Constant - 1	Rolling Counter	
0x15A	Pack Current		Pack Voltage		Pack Power
0x16A	8 Temperature Readings				

4.3.3 Orion BMS2 Installation Process

M3LR Pack BMS Installation

The M3LR pack had the highest labour intensity throughout the BMS replacement process due to its enclosed battery module and inaccessible OEM harnesses and connectors. The replacement process entailed a complete redesign of the BMS wiring framework and required dismantling the module enclosure to install the BMS measurements. The approach bypassed the existing OEM BMS data acquisition infrastructure, including the internal voltage and temperature taps, wires, and connectors. Consequently, understanding the OEM BMS wiring layout was not necessary to execute this replacement plan. Figure 4.12

provides a top-view comparison of the M3LR before and after the BMS replacement process.

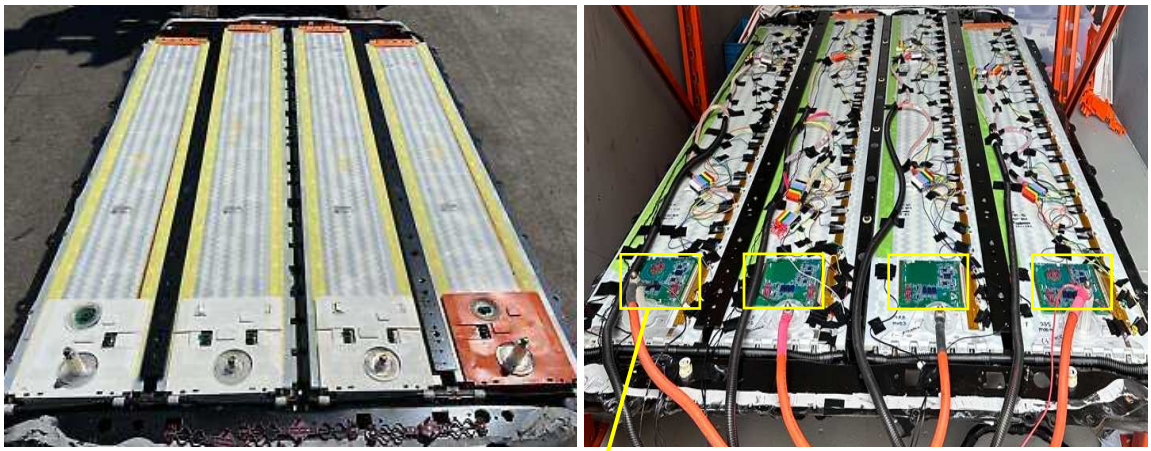

Figure 4.12: M3LR Pack Before Vs. After BMS Replacement

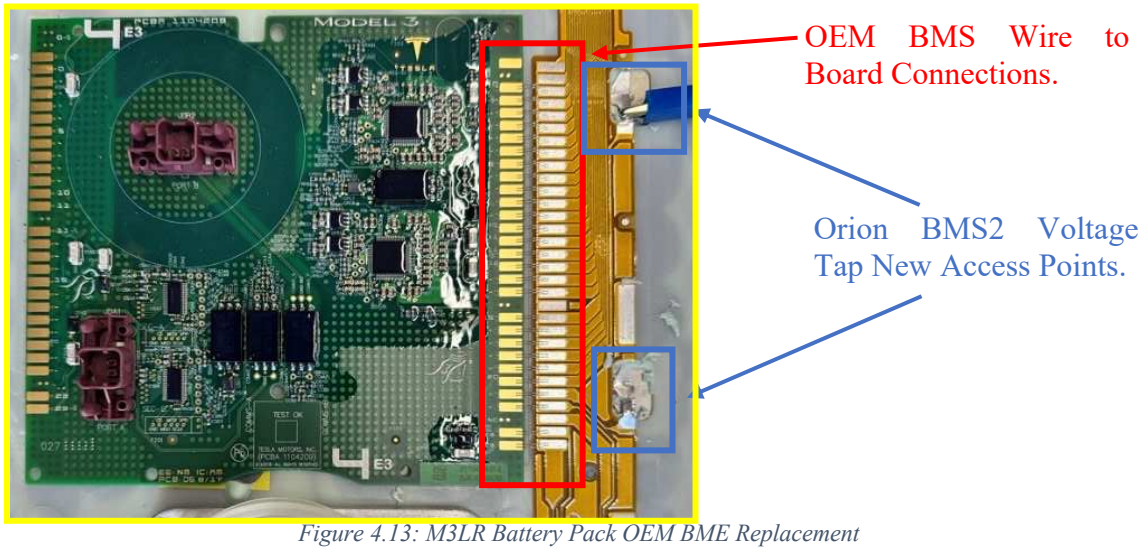

Figure 4.13: M3LR Battery Pack OEM BME Replacement

Figure 4.13 illustrates how the OEM BMS voltage measurement wires were initially soldered onto the BMS board, with the existing voltage tap wires concealed beneath the surface of the battery module, rendering them inaccessible to interact with. Small access points were cut into the module surface to obtain access to the cell group terminals. This adjustment necessitated additional extension wiring harnesses and connectors to span the entire module from top to bottom. A similar approach was applied to the installation of thermocouples on the battery module surfaces.

Although the complete replacement of the BMS affords unrestricted access to the battery for secondary life applications, the significant resource investment and increased risk

associated with modifying battery modules will limit the feasibility of this method for large-scale operations.

M3SR Pack BMS Installation

Unlike the M3LR pack, the M3SR pack required a less damaging process to replace the OEM BMS, where the original cell group wire harnesses were entirely repurposed to connect with the Orion BMS2. This integration is achieved using a TE Nano MQS connector, allowing direct reconnection using the OEM BMS connector head that came off the battery module. Although this is the least disruptive approach, it necessitates a detailed mapping of the voltage and temperature pins within the OEM BMS connector head, which ensures the new BMS correctly measures the voltage and temperature data. Each M3SR module utilizes two connectors, as depicted in Figure 4.14, illustrating the voltage and temperature mapping of the first module conducted during this research.

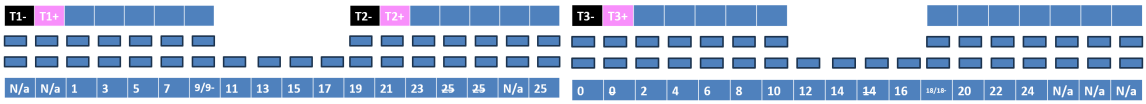

Figure 4.14: M3SR OEM BMS Connecter Mapping

The first module encompasses 25 voltage and 3 temperature measurements distributed across the two connectors, as shown in Figure 4.14. The voltage at each cell is measured at the positive terminal relative to the negative terminal of the preceding cell; hence, the voltage potential increase between these two terminals represents the open circuit voltage of the cell in question. It is crucial to map the correct pin position in the OEM connectors corresponding to the specific cell terminals so that the Orion BMS2 can correctly register the voltage readings. A similar approach is used to locate the pin positions for the temperature sensors. As such, the temperature sensor outputs a voltage reading across two pin positions. Hence, the temperature sensor pin position is determined by changing the temperature readings on the sensor and observing which two pins have voltage reading changes.

Figure 4.15 highlights the location of the OEM BMS connector head that reaches out by the end of the module after unplugging from the OEM BMS board, where the OEM BMS connector head (in blue) is disconnected from the OEM BMS board and subsequently

connected to a TE Nano MQS connector (in black housing) which came off the Orion BMS2.

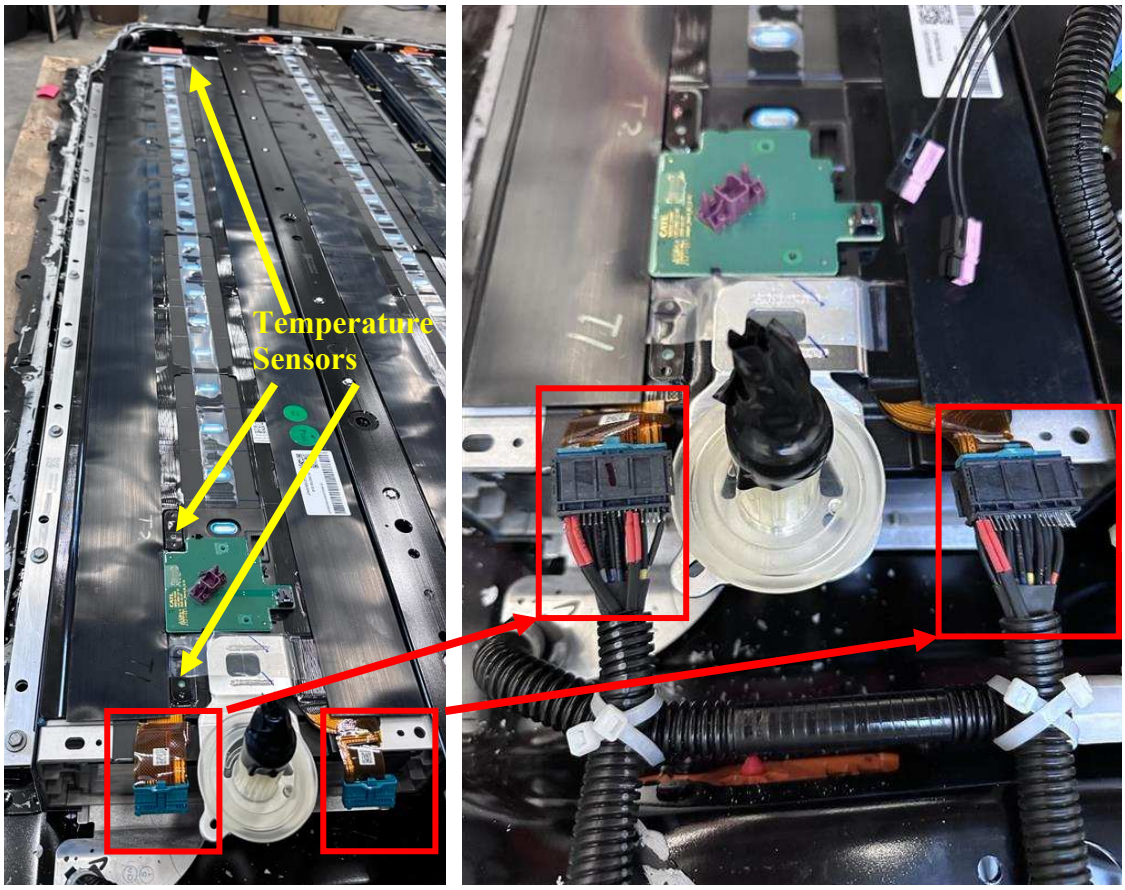

Figure 4.15: M3SR Orion BMS 2 Installation

Bolt and GV 60 Pack BMS Installation

The GV60 and the Bolt battery pack underwent a similar process to replace the OEM BMS. The self-developed BMS wire connectors used in these two packs are incomparable with industry-standard parts; however, all the wires leading up to the centralized OEM BMS are still accessible during the replacement process. Hence, these two packs are only required to replace the OEM connector heads while reusing the OEM wiring harnesses. This BMS replacement process modified the OEM wire-to-board connectors and replaced them with an industry-standard wire-to-wire connecter via Anderson PP15. This approach also requires a good understanding of the OEM voltage and temperature sensor map to adapt to Orion BMS2 successfully. The voltage and temperature sensor mapping process was the same for the M3SR pack but more accessible as the visible wire connections led to each module. Figures 4.16 and 4.17 illustrate the OEM connecter replacement process and the

transition from OEM parts to Anderson PP15 connectors. Contrary to the direct replacement method for the M3SR, this approach required a significantly longer process due to the extensive wire mapping and the meticulous connector installations.

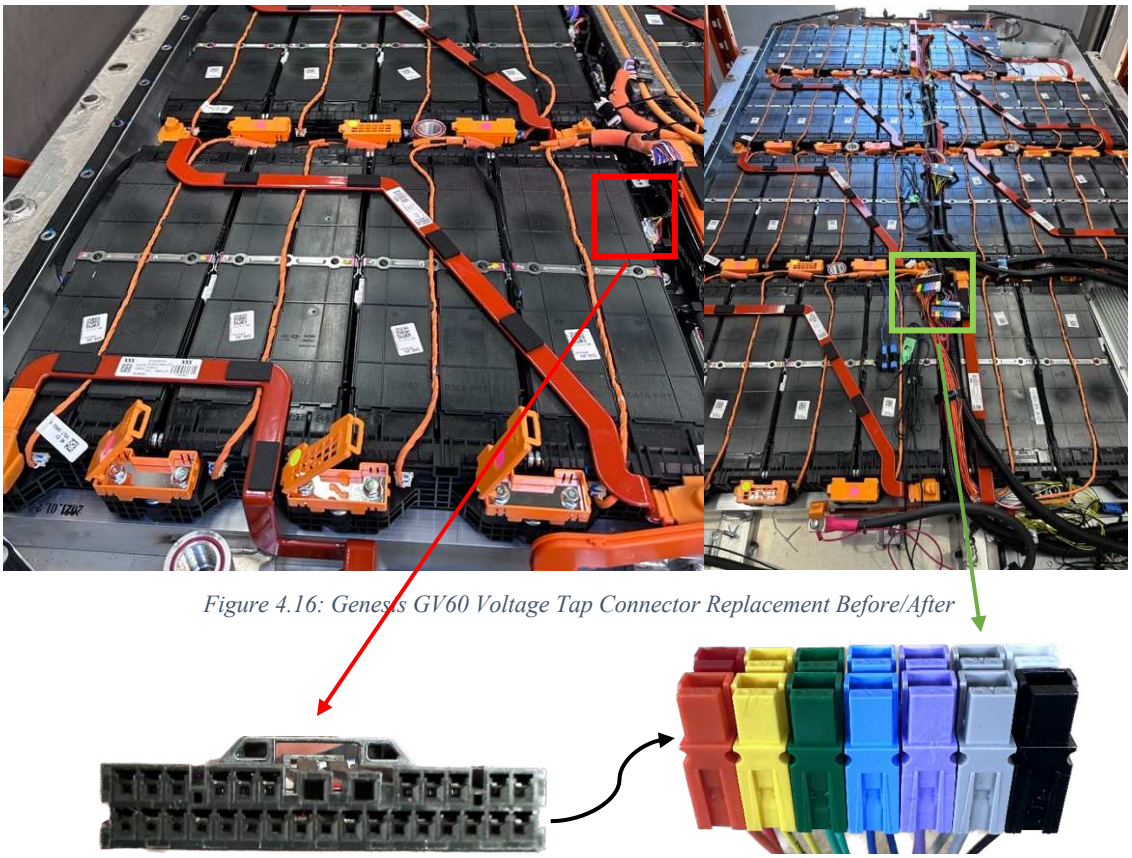

Figure 4.16: Genesis GV60 Voltage Tap Connector Replacement Before/After

Figure 4.17: GV60 OEM BMS Connecter (Left) Vs. Anderson PP15 Connectors (Right)

4.3.4 Power Conversion System Installation

Figure 4.18: Sinexcel 30 kW DC-AC Converter (Left); Oztek 40 kVa DC-AC Converter (Right)

The DC-AC converters are selected based on the DC voltage range mandated by the battery pack and power capabilities ranging from 30 kW to 50 kW per unit. Accordingly, 11 DC-AC converters are installed in the demonstration MBA system, composed of nine 30 kW units from Sinexcel and two 40 kW units from Oztek, as shown in Figure 4.18. Specifically,

every three Sinexcel units are arranged in a DC-coupled configuration to create three 90 kW AC power channels. Additionally, two Oztek units are similarly DC-coupled to form an 80 kW AC power channel. Consequently, the system accommodates four power channels. The single-line diagram (SLD) for Channel 1 is illustrated in Figure 4.19, with Channels 2 to 4 following identical configurations.

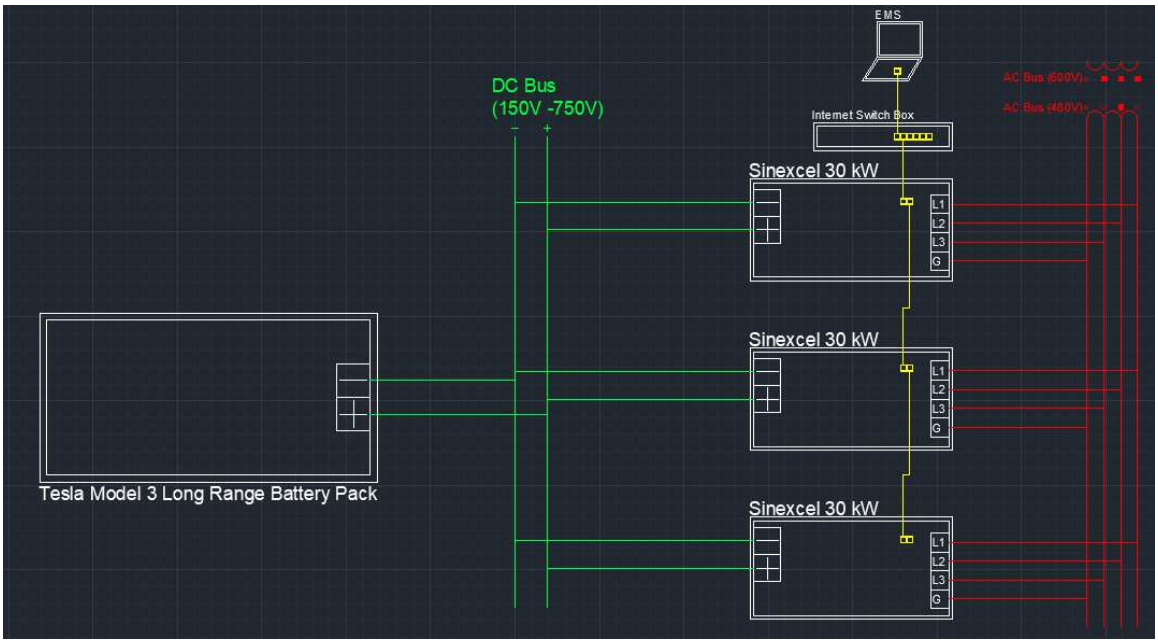

Figure 4.19: STC 90 kW Test Channel-1 SLD

The Sinexcel units operate within a voltage range of 150 to 750 Vdc, facilitating the discharge of battery packs at lower voltages. However, these units are unsuitable for the GV60 pack, as its maximum voltage reaches 806 Vdc. In contrast, the Oztek units can operate to a higher voltage spectrum, ranging from 330 to 820 Vdc, making them suitable to accommodate the higher cutoff voltage on the GV60. Therefore, the selection of PCS units for each channel is primarily influenced by the operational voltage range of the respective battery pack. Table 4.3 outlines the specifications for each test channel, providing an overview of the MBA system configurations.

Table 4.4: STC Power Channel Summary Table

Test Channel	1	2	3	4
PCS Unit Installed	Sinexcel	Sinexcel	Sinexcel	Oztek
# of PCS Units installed	3	3	3	2
PCS Model Number	PWS2-30P-NA	PWS2-30P-NA	PWS2-30P-NA	Ozpcs-RS40
Channel Rated Power (kW)	90	90	90	80

DC Voltage Range (V)	150 - 750	150 – 750	150 – 750	330 -820
Maximum DC Current (A)	270	270	270	150
Battery Connected	M3LR	M3SR	Bolt EV	GV60
Battery Voltage Range (V)	230 – 386.4	265 – 381.6	250 – 403.2	480 – 705.6
AC Voltage (V)	480			
AC Frequency (Hz)	60			
Power Factor	1~-1			
Communication Port	Modbus TCP			
Peak Efficiency	97.30%	97.30%	97.30%	97%
Weight per PCS unit (kg)	33	33	33	43

Sinexcel DC-AC Converter Power Efficiency Verification

This research project also tested the power efficiency on a single Sinexcel 30 kW DC-AC converter, and the measurement setup is presented in Figure 4.20. The DC measurements, including DC voltage and current, are captured by two Fluke 87V Industrial Multimeters. The AC measurements, including AC current, line 1 voltage, power, frequency, and power factor, are captured by a Fluke 190 Series III ScopeMeter.

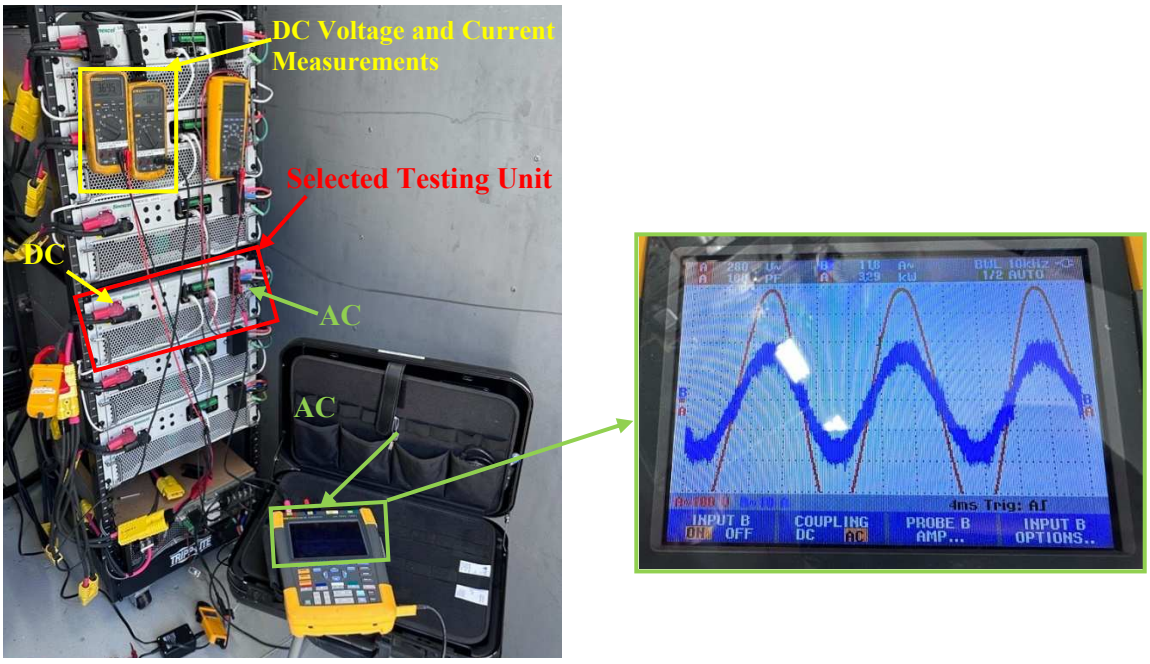

Figure 4.20: Sinexcel 30 KW DC-AC Converter Power Efficiency Verification Setup

The power efficiency of the DC-AC converter was evaluated for both charging and discharging processes, which is the ratio between DC and AC power. DC power is calculated from the product of DC current and voltage, while AC power is derived from

the sum of the line powers, as measured by the Fluke ScopeMeter. The results of these efficiency verifications are displayed in Figure 4.21. The test results indicate the peak power efficiency at 640 V is 98% and at 380 V is 96.5%, aligning with the efficiency claims by the manufacturer, as shown in Figure 3.7.

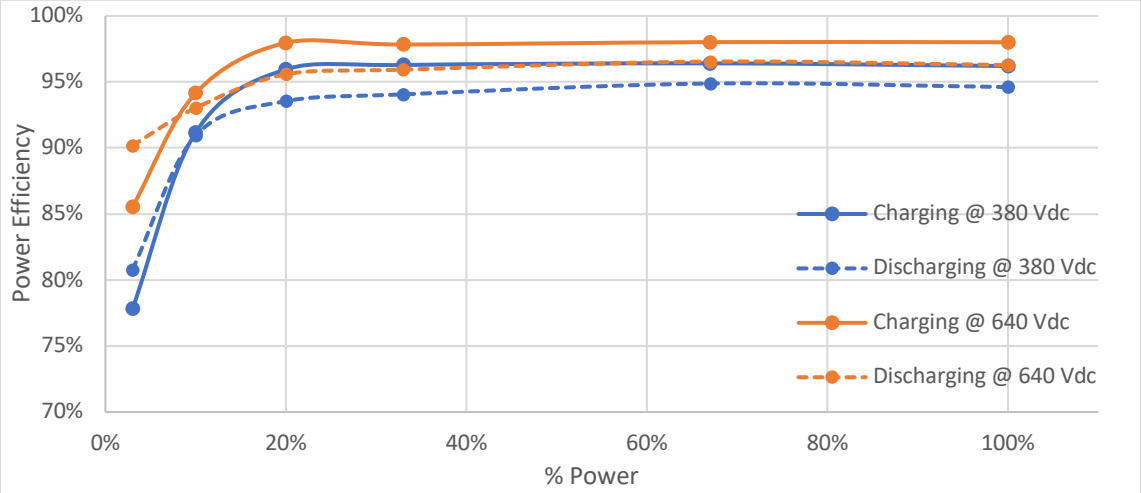

Figure 4.21: Sinexcel 30 kW Power Efficiency Test Results

4.4 ENERGY MANAGEMENT SYSTEM SETUP

The EMS developed during this research project via Emerald software regulates the overall operations of the MBA system. Emerald controls the operation status based on the data from the BMS while managing the power dispatch from each channel adaptively. Emerald is programmed to follow cycling scripts to achieve the research objectives at the current state. The single-line diagram of the system-level communication architecture is presented in Figure 4.22.

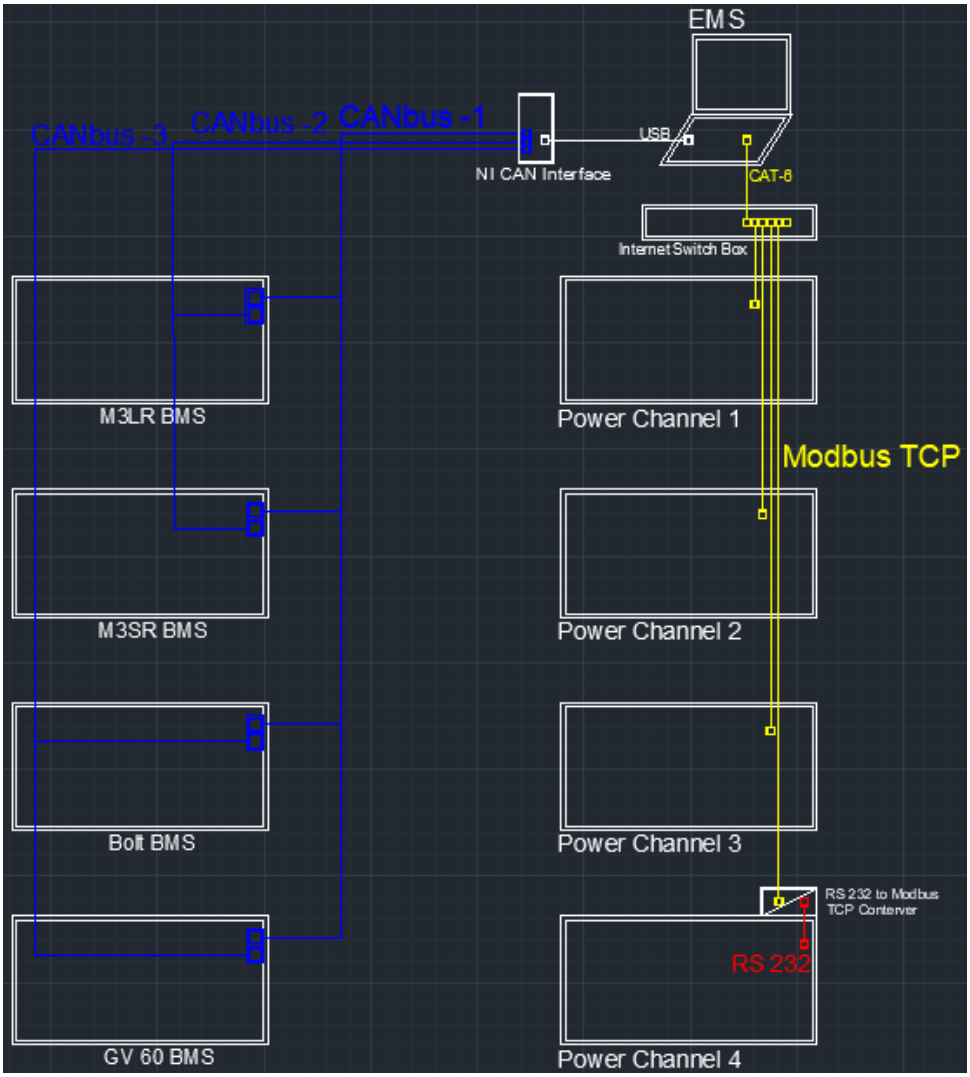

Figure 4.22: System Level Communication SLD

As discussed in the preceding section on BMS setup, each BMS sends out six frames of CANbus messages during regular operation. Therefore, the EMS receives 24 CANbus message frames from the four BMS units installed in total.

Figure 4.23: National Instrument CAN Interface [41]

Each CANbus message frame has a unique ID address, as presented in Table 4.3. The CAN messages first arrive at the National Instrument (NI) CAN Interface (shown in Figure 4.23) to be recognized and grouped based on the BMS units. Then Emerald receives the BMS data from the NI CAN interface and adds a prefix to each date frame to tag the data within the EMS. Figure 4.23 shows the processed BMS Data in Emerald.

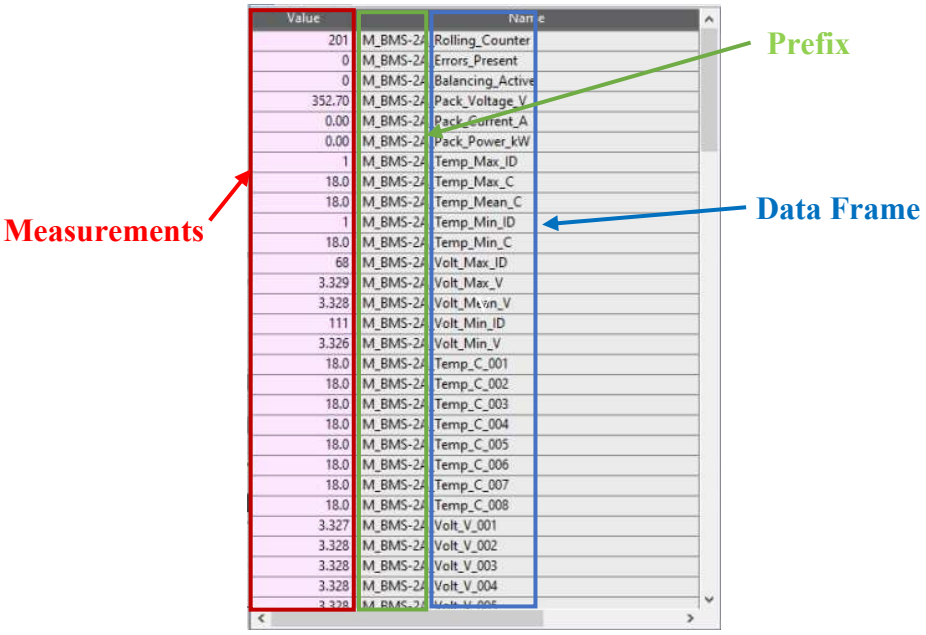

Figure 4.24: BMS Data Received at Emerald

The EMS and PCS use a similar data-transmitting process, but the Modbus-TCP communication protocol is used to link the EMS and the power channel. In this case, the PCS does not send data to EMS, but the EMS reads data from the PCS server. Thus, the communication message frames are adopted to the message register list defined by the PCS manufacturers. Given this, each power channel has a unique IP address and a Unit ID to identify its server location within the TCP network, where the EMS accesses it every 100 ms. In addition, the PCS manufacturer developed the Modbus register list, including all PCS data points, to assign a fixed register ID for each PCS data point. The EMS can read or write the PCS data points to achieve PCS status monitoring and control operations. Once the EMS obtains the updated PCS data value, a prefix is added to the data point name to tag data with the corresponding power channel. Figure 4.25 shows the processed PCS Data in Emerald.

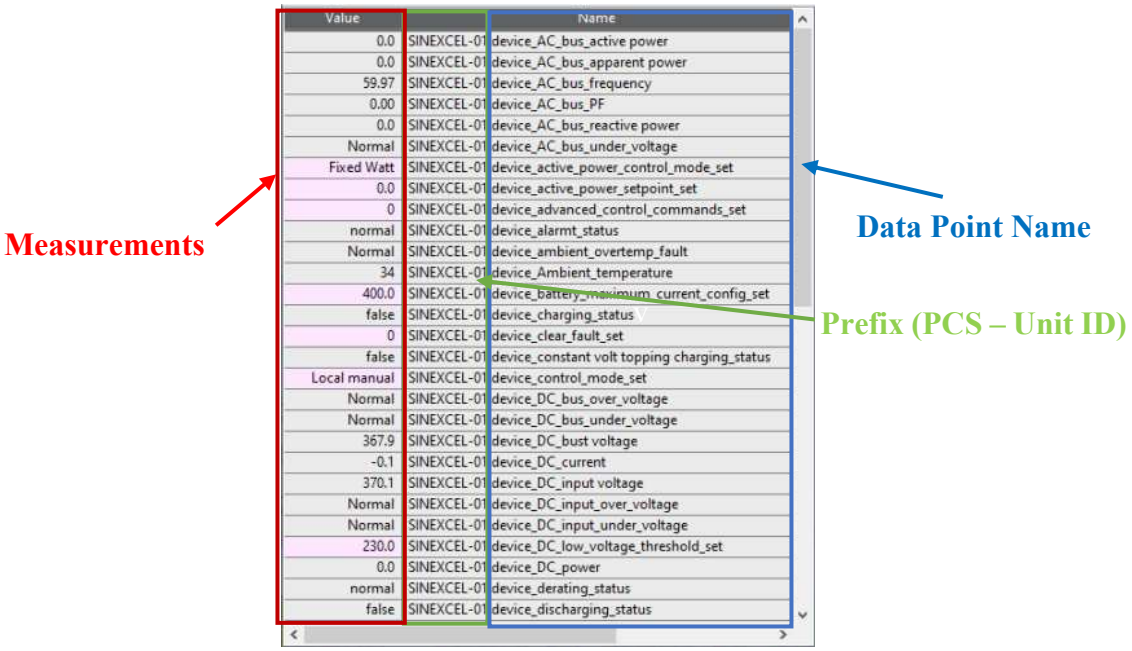

Value		Name
0.0	SINEXCEL-01	device_AC_bus_active power
0.0	SINEXCEL-01	device_AC_bus_apparent power
59.97	SINEXCEL-01	device_AC_bus_frequency
0.00	SINEXCEL-01	device_AC_bus_PF
0.0	SINEXCEL-01	device_AC_bus_reactive power
Normal	SINEXCEL-01	device_AC_bus_under_voltage
Fixed Watt	SINEXCEL-01	device_active_power_control_mode_set
0.0	SINEXCEL-01	device_active_power_setpoint_set
0	SINEXCEL-01	device_advanced_control_commands_set
normal	SINEXCEL-01	device_alarmt_status
Normal	SINEXCEL-01	device_ambient_overtemp_fault
34	SINEXCEL-01	device_Ambient_temperature
400.0	SINEXCEL-01	device_battery_maximum_current_config_set
false	SINEXCEL-01	device_charging_status
0	SINEXCEL-01	device_clear_fault_set
false	SINEXCEL-01	device_constant volt topping charging_status
Local manual	SINEXCEL-01	device_control_mode_set
Normal	SINEXCEL-01	device_DC_bus_over_voltage
Normal	SINEXCEL-01	device_DC_bus_under_voltage
367.9	SINEXCEL-01	device_DC_bust voltage
-0.1	SINEXCEL-01	device_DC_current
370.1	SINEXCEL-01	device_DC_input voltage
Normal	SINEXCEL-01	device_DC_input_over_voltage
Normal	SINEXCEL-01	device_DC_input_under_voltage
230.0	SINEXCEL-01	device_DC_low_voltage_threshold_set
0.0	SINEXCEL-01	device_DC_power
normal	SINEXCEL-01	device_derating_status
false	SINEXCEL-01	device_discharging_status

Figure 4.25: PCS Data After Processed at Emerald

Finally, Emerald offered the capability to design and implement system-level cycling scripts, closely simulating real-world power demands for various demand response strategies such as frequency regulation, energy arbitrage, and peak shaving. These scripts enable the research team to manage the status of any battery pack precisely, facilitating in-depth studies on performance and degradation. The versatile testing framework allows for incorporating diverse cycling profiles with multiple battery packs, subjecting the mixed battery storage system to realistic energy demand scenarios. This approach has significantly enhanced the understanding of system-level energy efficiency and thermal response at multi-pack operation, also offering valuable insights into MBA operational capability and resilience under varying load conditions.

4.4.1 MBA EMS Control Flow

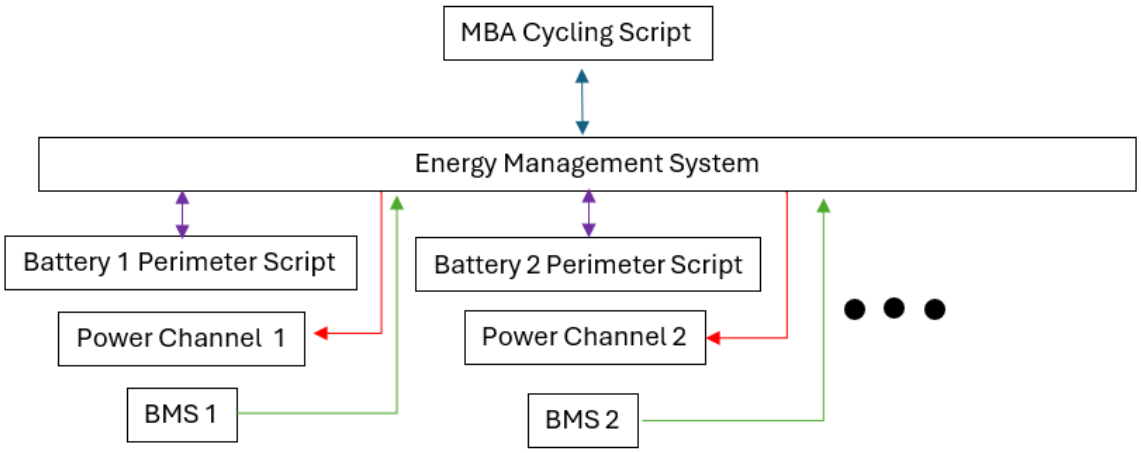

Figure 4.26: MBA Energy Management System Communication Topology Diagram

Throughout this research project, EMS control processes are developed around cycling scripts and the operational parameters of connected batteries. Specifically, the cycling script orchestrates the charging and discharging process for the power channel based on the test objectives. In contrast, the parameter script defines the battery pack operation window to ensure system safety. The EMS communication topology diagram is illustrated in Figure 4.26.

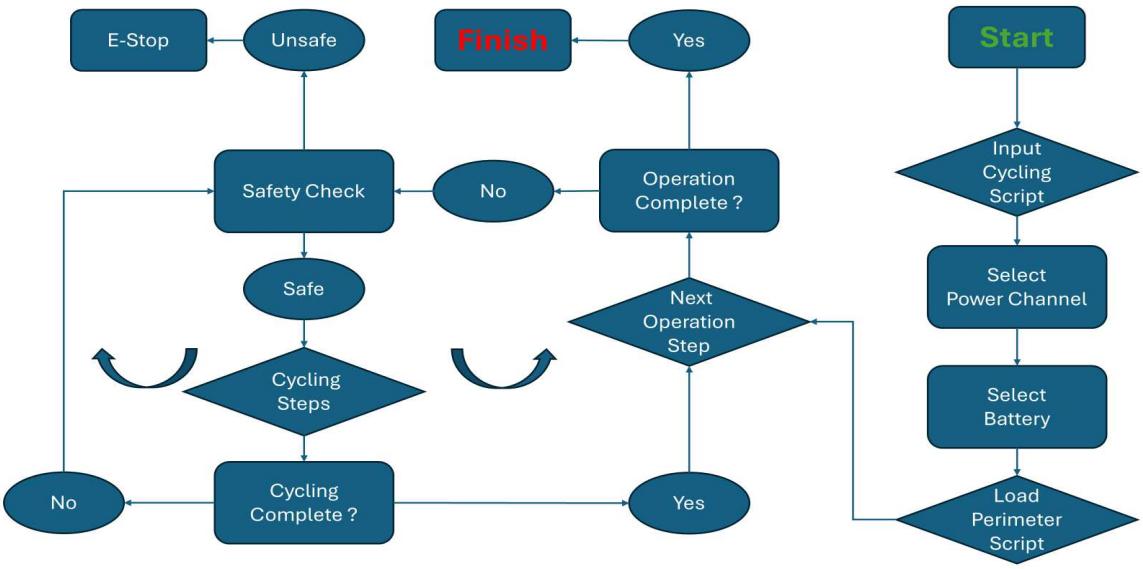

Figure 4.27: EMS Control Flow Chart

The control flow initiates with the EMS reading through the cycling script, which delineates the operational process for each power channel. This cycling script indicates the selection of the battery pack and power channel, the parameter script corresponding to the

selected battery, cycling steps, PCS control singles, and data recording setups. Following this, the EMS reads the parameter scripts to set up the battery operation limits and control the power channel to start cycling. The parameter script sets the operation limits, including the pack-level voltage range, cell-group voltage range, maximum and minimum current limit, and maximum temperature limit. Then, the EMS calls a while loop in the cycling script to compare the active data reported from the BMS with the set values from the parameter script to drive the cycling steps. Therefore, if a battery status arrives at the operation limit, the cycling script will trigger a follow-up command to the power channel to continue the cycling process, or an alarm will be set off, in which EMS will stop the cycling process. Thus, the parameters script is hard coded with each cycling script, establishing a safeguard to ensure operation safety. Once the cycling process is completed, the data logger compiles all the data points in an Excel file for further research analysis. The EMS control flow chart is shown in Figure 4.27. Appendix A shows the list of data logged by the EMS.

5 EXPERIMENTAL TESTING RESULTS

5.1 SINGLE BATTERY PACK SCRIPT CYCLING

All four battery packs underwent a constant power testing process to demonstrate the operational capabilities of the MBA system. The testing script guided the batteries through a sequence of operations, including three constant power cycling processes and a final depletion process to test the script cycling logic and the control reliability of the MBA system. This test represents the concluding step in the commissioning process for this project.

The cycling process for all four battery packs was identical; however, the parameter script was developed for each pack based on their respective operational ranges. The defined operational parameters for each battery pack are listed in Table 5.1. Appendix B provides details on the constant power cycling script.

Table 5.1: Constant Power Cycling Parameter Script Values

RPT Cycling Parameters	**M3LR**	**M3SR**	**Bolt**	**GV60**
Test Channel	1	2	3	4
Battery Pack Voltage Range (V)	240.0 – 403.2	265.0 - 376.3	240.0 - 403.2	420.0 - 705.6
Cell Group Voltage Range (V)	2.5 – 4.2	2.5-3.55	2.5 – 4.2	2.5 – 4.2
Operation Current Limits (A)	±50	±50	±50	±50
Temperature Limits (°C)	10 - 50			
Resting Temperature (°C)	30			
Charge/Discharge Power (kW)	20 / -20			
# of Testing Cycles	3			

Each battery pack was first discharged to the lowest cell group or pack-level voltage using a 20 kW constant power; then, the batteries were charged with a 20 kW constant power until the battery pack voltage reached the upper voltage limit. This cycling process was repeated three times. After the final charging step, the battery packs were discharged to 50% SOC to allow for long-term rest, minimizing capacity degradation and reducing safety

concerns. Figures 5.1 and 5.2 illustrate the M3LR pack voltage and cell group voltage profiles during this testing process and demonstrate the control logic of the EMS at each step.

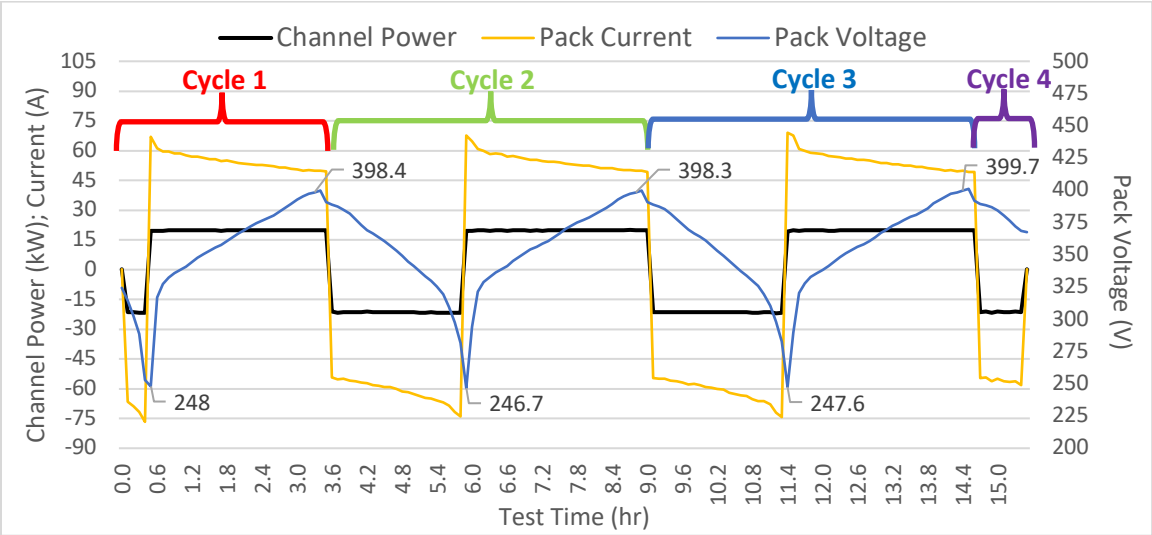

Figure 5.1: M3LR Constant Power Cycling Profile

As shown in Figure 5.1, the first cycle began with a discharge step, where Emerald commanded a -20 kW discharge power until the battery pack voltage reduced to 240 V or the minimum cell voltage arrived at 2.5 V; the discharging step in cycle 1 only took 0.5 hr due to the starting SOC was 20%. This was immediately followed by a charging step, applying 20 kW until the battery pack voltage ascended to 403.2 V or the maximum cell voltage reached 4.2 V. After three cycles, the battery pack voltage was discharged to 367.6 V, which is at around 50% SOC to exit the testing process.

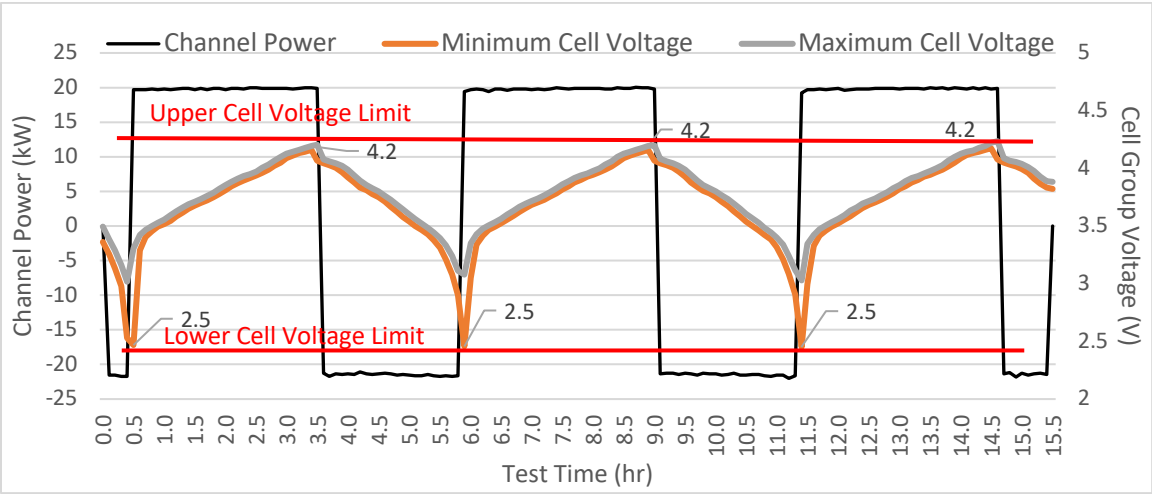

Figure 5.2: M3LR Constant Power Cycling Cell Group Voltage Profile

The power signal switch at the end of each cycling step is shown in Figure 5.2. As such, the cell voltage limit always triggers the discharge and charge termination logic earlier than the pack voltage limit due to the voltage imbalance between cell groups. Figure 5.2 also shows the cell group voltage profile during the testing process and the charging/discharging step limit marked in the red line at 2.5 V and 4.2 V.

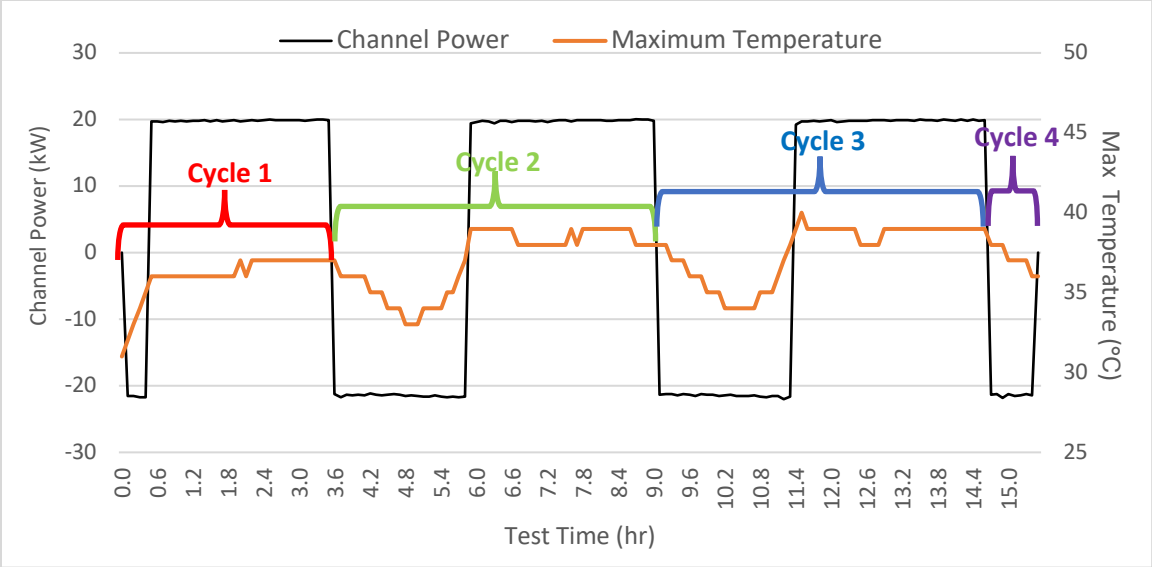

Figure 5.3: M3LR Temperature Response to 20kW Constant Power Cycling

Furthermore, the M3LR maximum temperature remained below 40 °C throughout the cycling process, as shown in Figure 5.3. However, a trend of increasing maximum temperature was noted as the cycle number grew, with about a 1 °C increase per cycle, attributed to the selected cooling method. Despite this, temperatures stayed within the safe threshold of 50 °C, though it was observed that passive cooling would not be sufficient for higher power rates cycling. A notable observation was the temperature increase when cell voltage dipped below 3.6V; this was caused by the increasing current during the discharge process to maintain the constant power at 20 kW.

Table 5.2: M3LR Battery Pack Constant Cycling Summary

Cycle Number	Max Pack Temperature (°C)	Discharge/Charged DC Energy (kWh)	DC Energy Efficiency	Discharge/Charged AC Energy (kWh)	AC Energy Efficiency
1	37	11.08/57.77	N/A	10.33/51.55	N/A
2	39	54.69/57.72	94.76%	51.81/58.98	87.81%
3	40	54.40/58.02	94.24%	51.55/59.03	87.33%
4	39	22.09/2.12	N/A	20/0	N/A

Table 5.2 presents data across four testing cycles, revealing insights into the pack and cell voltage ranges, maximum pack temperatures, energy metrics, and energy efficiency during each cycle. The first cycle displays a significantly lower DC energy efficiency (19.29%) due to the incomplete discharging process; therefore, this energy efficiency rate is disregarded. The second and third cycles achieve a DC energy efficiency rate of 94.76% and 94.24%, respectively. These efficiencies are noteworthy, given the pack voltage ranges maintained from 246.7 V to 400 V and consistent cell voltage ranges of 2.5 V to 4.2 V, which are ideal for this battery type. The fourth cycle does not apply to the standard metrics for energy efficiency calculation, hence the absence of a DC energy efficiency value.

AC energy efficiency for the M3LR during the second and third cycles consistently reached 87%, closely aligning with the expected results. Considering the DC-AC converter power efficiency at 67% rated power is 94.88% (via test results from Figure 4.21) and an additional 1% energy loss from wiring, the expected energy efficiency, derived from equation 3-2, is 89.0%, as shown in equation 5-1.

Equation 5-1: M3LR Constant Power Cycling AC Energy Efficiency Calculation

$$94.76\% \times 94.88\% \times 99\% = 89.0\%$$

Furthermore, the observed consistent discharged DC energy from cycle 2 to cycle 3 converts to an average of 77% SOH for the M3LR, given the OEM-rated capacity of 75 kWh. Hence, the usable energy capacity matched the expectation for a second-life EV battery pack. This observation does not guarantee other EV battery pack SOH conditions after their EV application, yet it does show the application potential for energy storage systems, which is why EV battery second-life research is valuable for the energy storage market.

Lastly, the slight increase in maximum pack temperature during cycling suggests a positive correlation between the thermal management method and operation power. It is imperative to note that maintaining or improving power rates in long testing cycles may necessitate a change in the thermal management method, especially if higher power rates are to be explored. Thus, 10 more cycles of constant power cycling at 3-hour and 2-hour rates are completed on each battery pack to further investigate the temperature response at different power rates.

5.1.1 M3LR Script Cycling Testing Result

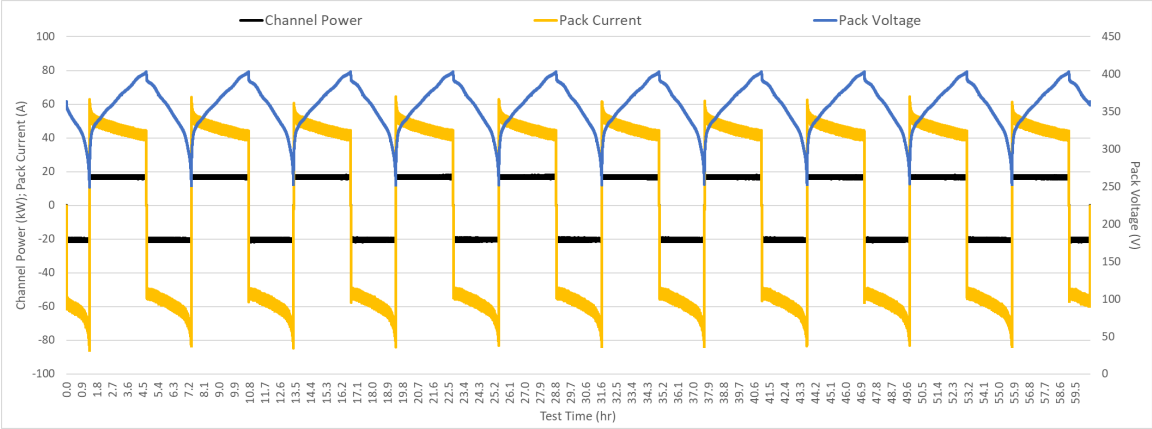

Figure 5.4: M3LR 3hr Constant Power Cycling Profile

Table 5.3: M3LR 3 hr Rate Constant Power Test Result

Cycle Number	Max Pack Temperature (°C)	Discharge/Charged DC Energy (kWh)	DC Energy Efficiency	Discharge/Charged AC Energy (kWh)	AC Energy Efficiency
1	32	28.0/56.2	N/A	25.6/58.3	N/A
2	34	54.3/56.4	96.2%	50.2/58.4	85.9%
3	35	54.4/56.5	96.3%	50.1/58.3	85.9%
4	37	54.5/56.8	96.0%	50.1/58.8	85.1%
5	38	54.8/56.8	96.4%	50.4/58.6	86.0%
6	37	54.9/56.7	96.9%	50.6/58.5	86.4%
7	36	54.6/56.7	96.5%	50.4/58.5	86.2%
8	37	54.6/56.6	96.5%	50.4/58.4	86.3%
9	37	54.6/56.4	96.8%	50.2/58.4	85.9%
10	36	54.5/56.4	96.6%	50.3/58.3	86.2%
Average	36	54.6/56.6	96.5%	50.3/58.5	86.0%

Table 5.4: M3LR 2 hr Rate Constant Power Test Result

Cycle Number	Max Pack Temperature (°C)	Discharge/Charged DC Energy (kWh)	DC Energy Efficiency	Discharge/Charged AC Energy (kWh)	AC Energy Efficiency
1	39	28.3/54.6	N/A	26.3/55.5	N/A
2	45	51.9/55.4	93.6%	48.1/56.5	85.2%
3	47	52.6/55.6	94.5%	48.8/56.7	86.1%
4	47	52.8/55.4	95.3%	49.1/56.4	87.0%
5	47	52.5/55.3	95.0%	48.8/56.4	86.5%
6	47	52.4/55.2	94.9%	48.7/56.3	86.6%
7	47	52.3/55.3	94.7%	48.7/56.4	86.4%
8	47	52.4/55.2	95.0%	48.8/56.3	86.7%
9	48	52.3/55.0	95.0%	48.6/56.1	86.7%
10	46	52.2/54.8	95.2%	48.4/56.2	86.2%
Average	46	52.4/55.3	94.8%	48.7/56.4	86.4%

5.1.2 M3SR Script Cycling Testing Result

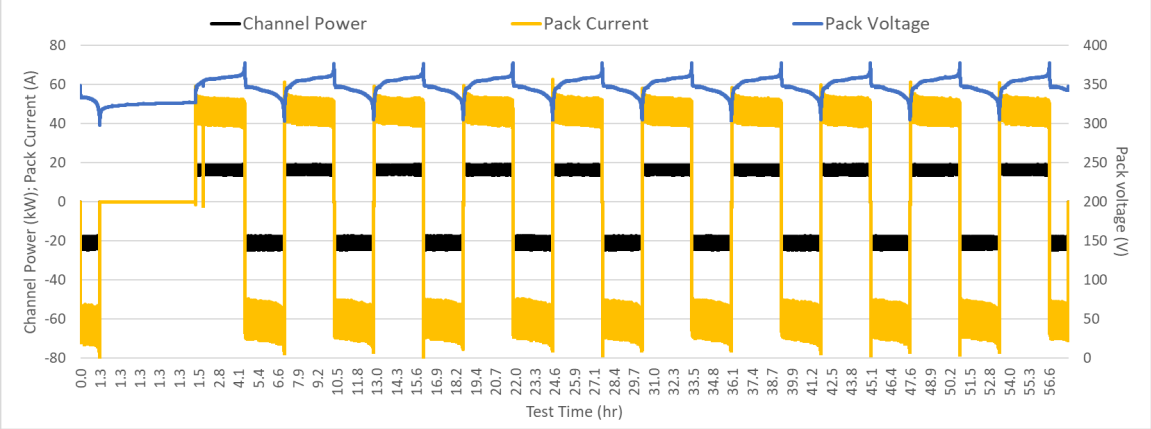

Figure 5.5: M3SR 3hr Constant Power Cycling Profile

Table 5.5: M3SR 3 hr Rate Constant Power Test Result

Cycle Number	Max Pack Temperature (°C)	Discharge/Charged DC Energy (kWh)	DC Energy Efficiency	Discharge/Charged AC Energy (kWh)	AC Energy Efficiency
1	30	26.0/54.2	N/A	24.3/56.9	N/A
2	32	52.4/54.5	96.2%	49.0/57.1	85.8%
3	34	52.6/54.5	96.6%	49.2/56.9	86.3%
4	35	52.8/54.4	97.1%	49.2/56.8	86.6%
5	35	52.7/54.4	97.0%	49.4/56.9	86.9%
6	34	52.7/54.4	96.9%	49.2/57.0	86.3%
7	34	52.6/54.3	96.9%	49.3/57.1	86.4%
8	35	52.7/54.3	97.0%	49.1/56.9	86.3%
9	34	52.7/54.3	96.9%	49.2/57.1	86.2%
10	33	52.6/54.3	96.9%	49.5/56.7	87.2%
Average	34	52.7/54.3	96.8%	49.3/56.9	86.4%

Table 5.6: M3SR 2 hr Rate Constant Power Test Result

Cycle Number	Max Pack Temperature (°C)	Discharge/Charged DC Energy (kWh)	DC Energy Efficiency	Discharge/Charged AC Energy (kWh)	AC Energy Efficiency
1	36	26.45/54.2	N/A	24.9/56.4	N/A
2	41	52.3/54.3	96.3%	49.1/56.6	86.7%
3	42	52.5/54.2	96.9%	49.9/56.6	88.1%
4	42	52.6/54.3	96.8%	49.5/56.6	87.5%
5	42	52.5/54.3	96.8%	49.5/56.7	87.3%
6	42	52.6/54.3	96.8%	49.4/56.4	87.6%
7	42	52.5/54.2	96.9%	49.5/56.6	87.4%
8	43	52.5/54.3	96.8%	49.5/56.6	87.5%
9	43	52.5/54.3	96.7%	49.4/56.6	87.3%
10	42	52.6/54.3	96.9%	49.5/56.4	87.7%
Average	42	52.5/54.3	96.7%	49.4/56.6	87.5%

5.1.3 Bolt Script Cycling Testing Result

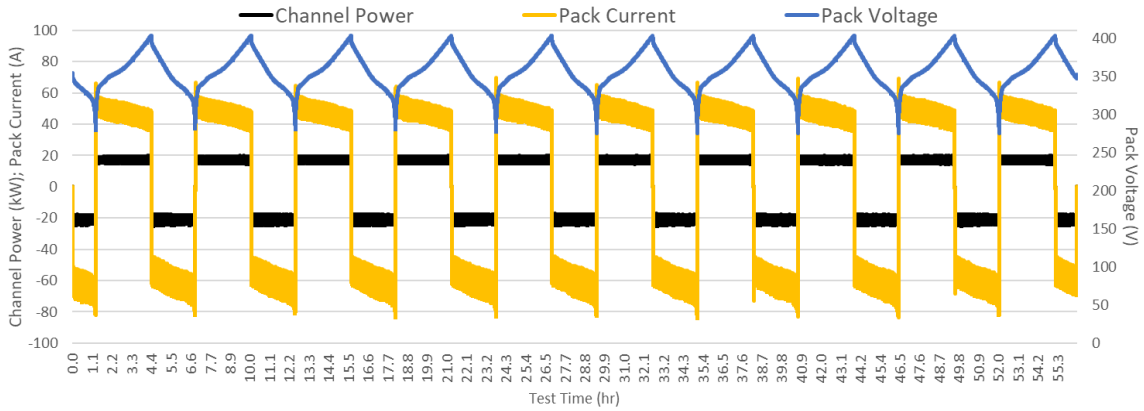

Figure 5.6: Bolt 3hr Constant Power Cycling Profile

Table 5.7: Bolt 3 hr Rate Constant Power Test Result

Cycle Number	Max Pack Temperature (°C)	Discharge/Charged DC Energy (kWh)	DC Energy Efficiency	Discharge/Charged AC Energy (kWh)	AC Energy Efficiency
1	32	27.4/53.4	N/A	25.8/55.9	N/A
2	36	51.7/53.6	96.5%	48.6/56.2	86.6%
3	38	52.1/53.8	96.8%	48.6/56.2	86.6%
4	40	52.2/53.8	97.0%	48.6/56.4	86.1%
5	42	52.4/54.0	97.1%	49.0/56.7	86.4%
6	42	52.5/54.0	97.3%	49.2/56.9	86.4%
7	41	52.4/54.0	97.2%	48.9/56.4	86.6%
8	40	52.3/53.9	97.2%	48.8/56.3	86.6%
9	41	52.3/53.9	97.1%	49.0/56.7	86.4%
10	41	52.3/53.8	97.2%	48.8/56.3	86.7%
Average	40	52.4/53.9	97.0%	48.7/56.6	86.4%

Table 5.8: Bolt 2 hr Rate Constant Power Test Result

Cycle Number	Max Pack Temperature (°C)	Discharge/Charged DC Energy (kWh)	DC Energy Efficiency	Discharge/Charged AC Energy (kWh)	AC Energy Efficiency
1	38	26.1/52.6	N/A	24.6/55.0	N/A
2	46	50.5/53.2	95.0%	47.4/55.6	85.4%
3	49	51.1/53.2	96.1%	48.1/55.7	86.4%
4	49	51.0/53.4	95.6%	48.1/55.9	86.0%
5	49	51.1/53.3	95.9%	48.1/55.6	86.5%
6	49	51.0/53.3	95.8%	48.2/55.7	86.6%
7	49	51.0/53.3	95.9%	48.1/55.7	86.3%
8	49	51.1/53.3	95.9%	48.2/55.6	86.7%
9	48	51.0/53.2	95.9%	48.2/55.6	86.7%
10	47	51.1/53.3	95.9%	48.7/55.7	87.3%
Average	48	50.8/53.1	95.7%	48.3/55.7	86.4%

5.1.4 GV 60 Script Cycling Testing Result

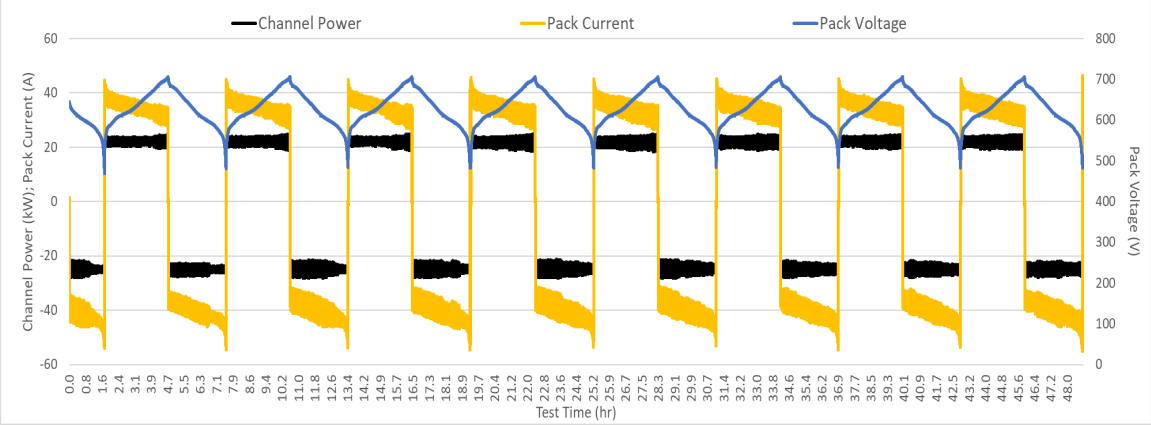

Figure 5.7: GV60 3hr Constant Power Cycling Profile

Table 5.9: GV60 3 hr Rate Constant Power Test Result

Cycle Number	Max Pack Temperature (°C)	Discharge/Charged DC Energy (kWh)	DC Energy Efficiency	Discharge/Charged AC Energy (kWh)	AC Energy Efficiency
1	29	41.6/68.8	N/A	40.0/72.9	N/A
2	30	68.3/68.8	99.3%	66.0/73.2	90.5%
3	30	68.2/68.9	99.0%	66.2/73.0	91.1%
4	31	68.2/69.1	98.7%	66.3/73.5	90.6%
5	32	68.6/69.2	99.1%	66.4/73.8	90.5%
6	33	68.5/69.3	98.8%	66.9/73.8	91.2%
7	32	68.3/69.2	98.8%	66.5/73.3	91.3%
8	31	68.2/69.1	98.8%	66.4/73.1	91.2%
9	32	68.4/69.1	99.0%	66.2/72.9	91.1%
10	32	68.3/69.2	98.7%	66.4/73.0	91.1%
Average	31	68.3/69.0	98.9%	66.4/73.3	90.7%

Table 5.10: GV60 2 hr Rate Constant Power Test Result

Cycle Number	Max Pack Temperature (°C)	Discharge/Charged DC Energy (kWh)	DC Energy Efficiency	Discharge/Charged AC Energy (kWh)	AC Energy Efficiency
1	30	45.3/69.7	N/A	43.8/73.3	N/A
2	37	66.4/69.5	95.7%	64.6/73.5	88.0%
3	38	67.5/69.6	97.0%	65.7/73.7	89.2%
4	39	67.7/69.9	96.9%	65.9/73.9	89.2%
5	39	67.7/69.7	97.2%	66.0/73.5	89.8%
6	39	67.7/69.7	97.1%	65.9/73.5	89.6%
7	39	67.7/69.7	97.2%	65.9/73.7	89.5%
8	39	67.7/69.6	97.1%	66.1/73.7	89.8%
9	39	67.7/69.6	97.2%	65.9/73.6	89.6%
10	39	67.7/69.6	97.3%	66.1/73.6	89.8%
Average	39	67.6/69.6	96.6%	65.8/73.7	89.4%

5.2 SINGLE-PACK CYCLING RESULT SUMMARY

All four battery packs completed ten cycles of 3-hour constant power cycling followed by another ten cycles of 2-hour constant power cycling. The summary of the test results is shown in Table 5.11. Since the usable energy varies for each battery pack, the discharge power also differed between packs to achieve the desired discharge hour rate.

Table 5.11: Single Pack Operation Testing Summary

	M3LR	M3SR	Bolt	GV60
3 Hour Discharge Power Rate (kW)	18.0	18.3	18.7	23.7
2 Hour Discharge Power Rate (kW)	28.5	27.3	26.0	34.5
Maximum Temperature @ 4hr Rate (°C)	32	31	35	31
Maximum Temperature @ 3hr Rate (°C)	36	35	42	33
Maximum Temperature @ 2hr Rate (°C)	46	43	49	39
Average DC Energy Efficiency @ 3hr Rate	96.5%	96.8%	97.0%	98.9%
Average DC Energy Efficiency @ 2hr Rate	94.8%	96.7%	95.8%	97.0%
Average AC Energy Efficiency @ 3hr Rate	86.0%	86.4%	87.5%	90.7%
Average AC Energy Efficiency @ 2hr Rate	86.4%	87.5%	86.4%	89.4%
SOH	77.2%	98.7%	89.8%	89.1%

All packs experienced an approximate 10 °C temperature increase as the discharge power increased, which is expected due to the higher current. The Bolt pack reported the highest temperatures at both power rates: 42 °C for the 3-hour rate and 49 °C for the 2-hour rate. The highest temperature reading in the Bolt pack was recorded at the bottom of the double-decked battery modules, which had limited heat dissipation compared to the rest of the battery pack. In contrast, the GV60 pack reported a maximum temperature that was 10 °C lower than the Bolt pack at the 2-hour rate due to the lower current required. Hence, the temperature difference between the hottest and coolest packs could lead to temperature gradients on the battery rack, resulting in insufficient thermal management with the passive cooling method. This issue can be mitigated by rearranging the battery pack positions and placing the warmer packs at the top of the rack so that the coldest air reaches them first. Therefore, the M3LR pack and GV60 pack should swap their rack positions.

In addition, the temperature response from each battery pack also impacted the DC energy efficiency. Packs reporting higher temperatures showed lower energy efficiency, as shown in Table 5.11. Given this, the M3LR had higher heat loss over the testing cycles compared to the M3SR and Bolt pack. The 2-hour power rate heat loss calculation for the M3LR pack over one cycle can be calculated as follows:

$$Q_{Heat\ loss} = DC\ Charged\ Energy - DC\ Discharged\ Energy$$

The energy required to remove the heat loss from the MBA system is calculated as follows:

$$E_{Cooling} = Q_{Heat\ loss} \div COP_{Heat\ Pump}$$

Hence, using the DC energy data from Tables 5.3 and 5.4, and an assumed conservative coefficient of performance (COP) of 3 for the heat pump, the cooling energy required to keep the M3LR pack under 50 °C can is calculated below:

$$E_{Cooling} = (55.3\ kWh - 52.4\ kWh) \div 3 = 0.97\ kWh$$

Therefore, 0.97 kWh of electricity is used to maintain the M3LR below 50 °C each cycle at the 2-hour rate. Similarly, only 0.67 kWh of electricity is needed to maintain the pack temperature below 40 °C for the 3-hour rate. Furthermore, the useful DC system efficiency per cycle can be calculated as follows:

$$DC\ System\ Eff = DC\ Discharged\ Energy \div (DC\ Charged\ Energy + E_{cooling}) \times 100\%$$

$$= 52.4\ kWh \div (55.3\ kWh + 0.97\ kWh) \times 100\% = 93.1\%$$

This calculation estimated the DC system efficiency for the M3LR pack at the 2-hour rate to be 93.1% which is very close to the measurand value from table 5.11. Table 5.12 lists heat loss and cooling energy required for the rest of the battery packs.

Table 5.12: Battery Pack Heat Generation and Cooling Energy Results.

	Pack	Heat Loss (kWh)	Cooling Energy (kWh)	DC System Efficiency
2-hour rate	M3LR	2.9	0.97	93.1%
	M3SR	1.8	0.60	95.8%
	Bolt	2.3	0.77	94.3%
	GV 60	2	0.67	96.2%
	Total	**9**	**3.00**	**94.9%**
3-hour rate	M3LR	2	0.67	95.3%
	M3SR	1.6	0.53	96.1%
	Bolt	1.5	0.50	96.3%
	GV 60	0.7	0.23	98.7%
	Total	**5.8**	**1.93**	**96.6%**

The M3SR pack required 0.6 kWh and 0.53 kWh of heat rejection power for the 2-hour and 3-hour rates, respectively. The Bolt required 0.77 kWh and 0.5 kWh of energy for heat rejection for the 2-hour and 3-hour rates. Therefore, higher DC energy efficiency does reduce the heat rejection as expected. Although the GV 60 had the highest DC energy efficiency, its heat rejection rate was still higher than the M3SR pack due to the higher usable capacity. As such, the electrical energy needed for heat rejection from the GV 60 pack at the 2-hour rate is 0.67 kWh and 0.23 kWh for the 3-hour rate. Given this, the GV 60 pack not only provided the highest energy efficiency but also required least cooling load from the heat pump due to its higher pack voltage design. This energy efficiency advantage can significantly impact the overall MBA system performance in the long term once scaled up in the future. Lastly, the total heat loss increased by 3.2 kWh pre-cycle moving from the 3 to 2-hour rate.

However, the DC energy efficiency difference between the 2-hour and 3-hour rates is less than 2% on average per cycle, which is practically negligible. Furthermore, the temperature increase caused less than 1% AC energy efficiency reduction because the DC-AC power efficiency also increased as the operation power rate reached above 20% rate power, as shown in Figure 4.21.

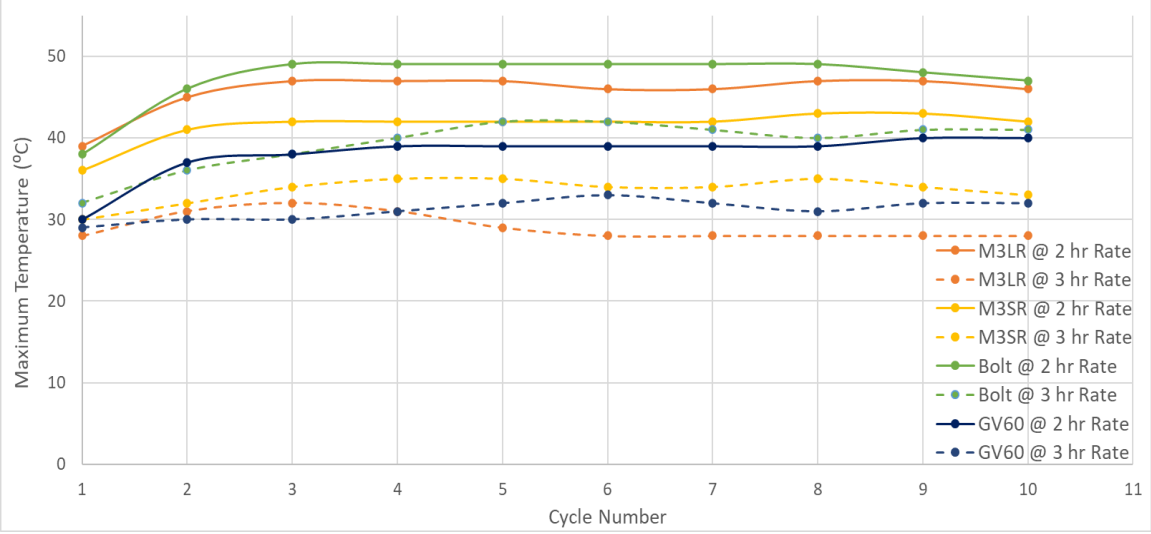

Figure 5.8: Battery Pack Temperature Response Over 2hr and 3hr Constant Power Cycling

Furthermore, the data plotted in Figure 5.8 show the maximum temperatures recorded during each cycle, where the starting temperature of each pack is approximately 30 °C for a 3-hour power rate and 40 °C for a 2-hour power rate. However, the actual starting

temperature for the battery packs is around 20 ± 5 °C, depending on the location of the battery pack. The battery pack at the bottom of the rack (M3LR pack) had the lowest starting temperature, while the battery pack at the top of the rack (Bolt pack) had the highest starting temperature. Consequently, all battery packs experienced a rapid temperature increase of about 15 °C after the first cycle at the 3-hour power rate and about 20 °C after the first cycle at the 2-hour power rate. However, the temperature rise plateaued after three cycles and remained relatively stable for the rest of the cycling process. Additionally, the M3LR, M3SR, and GV60 packs remained under the 40°C desired operating temperature, while the Bolt pack exceeded this threshold by 2 °C during the 3-hour constant power rate cycling. This temperature response suggests that the first three battery packs can operate at a maximum 3-hour rate using passive cooling thermal management. In contrast, the Bolt pack must operate at a rate below 3 hours to avoid overheating. Based on these test results, liquid cooling thermal management is highly recommended for all battery packs installed during this project when operating higher than the 2-hour power rate.

6 CONCLUSION AND FUTURE WORK

This thesis investigated the mixed battery array architecture using four repurposed electric vehicle batteries. Central to this research are four pivotal scopes: battery pack condition analysis, a comparison study between DC and AC coupled power structure, a comparison study of OEM BMS and third-party BMS, and the development of the energy management system, which marks a significant contribution to this project and future testing at RESL. An additional major contribution of this work lies in the exploration and strategic planning of thermal management systems, a critical factor in the operational efficacy and longevity of MBA systems.

Battery Pack Analysis and Grouping:

By selecting four distinct types of EV batteries, this study assessed and categorized battery packs based on their condition and performance capabilities. This foundational work underscored the potential of MBA systems to efficiently integrate batteries of varying states of health, capacities, and chemistries, presenting a robust framework for optimizing the energy efficiency and sustainability of energy storage systems.

DC versus AC Coupled Systems Comparison:

The research delineated a comparison between DC and AC coupling methodologies, ultimately advocating for an AC-coupled battery interconnection method. This choice was substantiated by the superior flexibility and compatibility with mixed battery arrays, which facilitate a broader application range and simplify the integration process for heterogeneous battery packs.

BMS and EMS Development:

A critical evaluation between OEM and third-party BMS revealed the strategic advantages of adopting third-party systems for MBA applications. This research project selected a third-party BMS, exemplified by the successful integration of a centralized system, which paved the way for enhanced communication, reliability, and adaptability in managing diverse battery technologies within the MBA framework. The development of the EMS is a hallmark achievement of this thesis. The EMS embodies a tailored solution for the complex operational demands of MBA systems, incorporating advanced algorithms and control strategies to optimize the performance and longevity of mixed battery arrays. This

bespoke EMS underscores the innovative approach to addressing the intricate dynamics of energy management in MBA systems.

Thermal Management System Design

This research explored three types of thermal management systems: passive cooling, forced air, and liquid cooling, each with unique benefits and applicability to MBA systems. This research project chose the passive cooling method for the current MBA system due to its control simplicity, cost-effectiveness, and sufficiency in cooling rates for low-power cycling. However, recognizing the limitations of passive cooling in handling higher power cycling intensities, the thesis recommends upgrading to a liquid cooling thermal management system for 2-hour or higher power rate cycling. This upgrade would significantly enhance the battery pack temperature management and operational flexibility, addressing one of the critical pathways for scaling MBA systems for more demanding applications. Therefore, the analysis of thermal management systems was a pivotal contribution of this thesis, highlighting the importance of appropriate thermal management solutions in optimizing the performance and sustainability of MBA systems.

In conclusion, this thesis not only delineates a practical and scalable approach to repurposing EV batteries for stationary storage applications but also contributes a novel set of tools and methodologies to the energy storage research community. The findings offer a valuable roadmap for future explorations, aiming to enhance the scalability, energy efficiency, and reliability of MBA systems. Looking ahead, the continued development of advanced diagnostic and predictive models for battery performance, alongside further exploration into regulatory and environmental frameworks, will be crucial for realizing the full potential of MBA technologies in contributing to a sustainable energy future.

6.1 FUTURE WORK RECOMMENDATIONS

6.1.1 Multi-Pack Script Cycling

Future investigations should prioritize multi-pack operational testing over single-pack assessments. This approach would provide a view of the MBA performance, particularly in thermal response and overall system efficiency. Single-pack tests, while informative, fall short of capturing the dynamic interactions within a multi-pack setup, where heat dissipation and thermal management demands differ significantly. A system-level perspective will not only elucidate the practicalities of deploying mixed battery arrays at

scale but also refine our understanding of how individual packs contribute to and influence aggregate system performance.

6.1.2 Development of FR and EA Signals for System-Level Operation

Reflecting the discussion from Chapter 2 on using Frequency Regulation (FR) and Energy Arbitrage (EA) cycling signals for evaluating battery performance and degradation from cell to pack level, it is imperative to extend these methodologies to system-level testing. The transition to a more holistic testing regime is expected to unveil nuanced insights into the operational efficiencies and potential inefficiencies inherent within MBA systems. Contrasts between pack-level and system-level energy efficiencies will likely emerge, primarily attributed to the complexities of managing a mixed battery array environment. By integrating FR and EA signals into system-level operations, this research can quantify their impact on individual battery packs and overall system performance, laying the groundwork for subsequent optimization and refinement of MBA configurations.

6.1.3 Enhanced Thermal Management Analysis

Performance Trade-offs between liquid and passive cooling methods, which investigate the efficacy of liquid versus passive cooling methods in thermal management, present a promising avenue for future research. Specifically, it would be invaluable to delineate the operational thresholds at which passive cooling suffices to maintain battery safety and efficiency and the critical junctures necessitating the transition to liquid cooling systems. This exploration should form a clear understanding of the power rates conducive to each cooling methodology, thereby optimizing the thermal management of MBA systems across various operational intensities. Such studies are essential for identifying the optimal cooling strategy that balances cost, complexity, and operational efficiency, especially as MBA systems scale up and encounter diverse environmental and operational demands.

6.1.4 Future EV Industry Battery Management System Integration

Looking ahead, the evolution of MBA should account for the evolution of emerging battery technologies such as future EV batteries via sodium-ion batteries. Given the sodium-ion cell operates at lower voltage levels, the future MBA system should also explore the possible PCS to better support the lower DC voltage range, or even reconsider the DC-coupled option to group sodium-ion batteries with lithium-ion batteries. In addition, future BMS designs might benefit from enhanced flexibility in programming, reporting, and

cabling, facilitating the bypassing of failed cell groups and allowing continued operation with OEM BMS. This adaptability would be crucial in extending the lifespan and utility of mixed battery arrays, ensuring they remain viable and efficient as newer battery chemistries and technologies become prevalent. Research should focus on developing a BMS that can dynamically adapt to the unique characteristics of various battery types, optimizing performance, safety, and reliability across a heterogeneous array of storage solutions.

REFERENCES

[1] "World Energy Outlook 2023 – Analysis," IEA. Accessed: Nov. 09, 2023. [Online]. Available: https://www.iea.org/reports/world-energy-outlook-2023

[2] "Lithium-ion battery demand forecast for 2030 | McKinsey." Accessed: Mar. 14, 2024. [Online]. Available: https://www.mckinsey.com/industries/automotive-and-assembly/our-insights/battery-2030-resilient-sustainable-and-circular

[3] "EV Battery Warranties and Exclusions | GreenCars." Accessed: Mar. 16, 2024. [Online]. Available: https://www.greencars.com/greencars-101/ev-battery-warranties-and-exclusions

[4] "What happens to EV batteries at the end of their useful life in a vehicle? - Electric Vehicle Council." Accessed: Jul. 02, 2024. [Online]. Available: https://electricvehiclecouncil.com.au/docs/what-happens-to-ev-batteries-at-the-end-of-their-useful-life-in-a-vehicle/

[5] L. Canals Casals, M. Etxandi-Santolaya, P. A. Bibiloni-Mulet, C. Corchero, and L. Trilla, "Electric Vehicle Battery Health Expected at End of Life in the Upcoming Years Based on UK Data," *Batteries*, vol. 8, no. 10, Art. no. 10, Oct. 2022, doi: 10.3390/batteries8100164.

[6] "1H 2023 Energy Storage Market Outlook," BloombergNEF. Accessed: Mar. 16, 2024. [Online]. Available: https://about.bnef.com/blog/1h-2023-energy-storage-market-outlook/

[7] X. Hu *et al.*, "A Review of Second-Life Lithium-Ion Batteries for Stationary Energy Storage Applications," *Proceedings of the IEEE*, vol. 110, no. 6, pp. 735–753, Jun. 2022, doi: 10.1109/JPROC.2022.3175614.

[8] "UL 1974 Ed. 1-2018 - Standard for Evaluation for Repurposing Batteries." Underwriters Laboratories Inc. (UL). Accessed: Nov. 09, 2023. [Online]. Available: https://webstore.ansi.org/standards/ul/ul1974ed2018

[9] "Electric vehicles, second life batteries, and their effect on the power sector | McKinsey." Accessed: Mar. 14, 2024. [Online]. Available:

https://www.mckinsey.com/industries/automotive-and-assembly/our-insights/second-life-ev-batteries-the-newest-value-pool-in-energy-storage

[10] F. Lambert, “BMW and Bosch open new 2.8 MWh energy storage facility built from batteries from over 100 electric cars,” Electrek. Accessed: Nov. 09, 2023. [Online]. Available: https://electrek.co/2016/09/22/bmw-bosch-energy-storage-facility-built-from-batteries-from-over-100-electric-cars/

[11] “Old Electric-Vehicle Batteries Are Getting a Second Life - WSJ.” Accessed: Nov. 09, 2023. [Online]. Available: https://www.wsj.com/articles/old-electric-vehicle-batteries-are-getting-a-second-life-11655114401

[12] C. Murray, “Tesla EV battery packs repurposed into energy storage systems in Finland and California,” Energy-Storage.News. Accessed: Mar. 30, 2024. [Online]. Available: https://www.energy-storage.news/tesla-ev-battery-packs-repurposed-into-energy-storage-systems-in-finland-and-california/

[13] B. S. S. Inc, “B2U Storage Solutions Commences Operations on Second Grid-Connected Hybrid Storage Facility Using Second Life Batteries in Santa Barbara County, CA,” GlobeNewswire News Room. Accessed: Mar. 14, 2024. [Online]. Available: https://www.globenewswire.com/en/news-release/2023/11/14/2780143/0/en/B2U-Storage-Solutions-Commences-Operations-on-Second-Grid-Connected-Hybrid-Storage-Facility-Using-Second-Life-Batteries-in-Santa-Barbara-County-CA.html

[14] M. Bauer, J. Wiesmeier, and J. Lygeros, “A comparison of system architectures for high-voltage electric vehicle batteries in stationary applications,” *Journal of Energy Storage*, vol. 19, pp. 15–27, Oct. 2018, doi: 10.1016/j.est.2018.06.007.

[15] “The circular economy of the electric car battery - Renault Group.” Accessed: Nov. 09, 2023. [Online]. Available: https://www.renaultgroup.com/en/news-on-air/news/the-circular-economy-of-the-electric-vehicle-battery/

[16] aitamrouche, “Stationary energy battery storage: three new projects in europe,” renaultgroup. Accessed: Apr. 14, 2024. [Online]. Available:

https://events.renaultgroup.com/en/2022/01/27/stationary-energy-battery-storage-three-new-projects-in-europe/

[17] S. Wolfe, “Startup spotlight: How Moment Energy gives EV batteries a new life,” POWERGRID International. Accessed: Mar. 14, 2024. [Online]. Available: https://www.power-grid.com/distributech/startup-spotlight-how-moment-energy-gives-ev-batteries-a-new-life/

[18] “Smartville - Sustainable Energy Storage Solutions,” Smartville. Accessed: Apr. 14, 2024. [Online]. Available: https://smartville.io/

[19] B. Thompson, “Repurposing Electric Vehicle Batteries in a Mixed Array for Grid Storage,” Thesis, 2018. Accessed: Nov. 09, 2023. [Online]. Available: https://DalSpace.library.dal.ca//handle/10222/73868

[20] M. Elliott, L. G. Swan, M. Dubarry, and G. Baure, “Degradation of electric vehicle lithium-ion batteries in electricity grid services,” *Journal of Energy Storage*, vol. 32, p. 101873, Dec. 2020, doi: 10.1016/j.est.2020.101873.

[21] C. White, B. Thompson, and L. G. Swan, “Repurposed electric vehicle battery performance in second-life electricity grid frequency regulation service,” *Journal of Energy Storage*, vol. 28, p. 101278, Apr. 2020, doi: 10.1016/j.est.2020.101278.

[22] C. White, B. Thompson, and L. Swan, “Comparative performance study of electric vehicle batteries repurposed for electricity grid energy arbitrage,” *Applied Energy*, vol. 288, p. 116637, Apr. 2021, doi: 10.1016/j.apenergy.2021.116637.

[23] B. Ellis, C. White, and L. Swan, “Degradation of lithium-ion batteries that are simultaneously servicing energy arbitrage and frequency regulation markets,” *Journal of Energy Storage*, vol. 66, p. 107409, Aug. 2023, doi: 10.1016/j.est.2023.107409.

[24] “BYD Blade LiFePO4 Battery,” Evlithium. Accessed: Apr. 17, 2024. [Online]. Available: https://www.evlithium.com/lifepo4-battery-news/byd-blade-battery-analysis.html

[25] D. LaChance, “Researchers: New class of adhesives driving increased EV battery pack efficiency,” Repairer Driven News. Accessed: Nov. 17, 2023. [Online]. Available:

https://www.repairerdrivennews.com/2021/12/28/researchers-new-class-of-adhesives-driving-increased-ev-battery-pack-efficiency/

[26] A. Johannisson, “Outlook of EV battery pack design trends”.

[27] “Panasonic To Begin Test Production Of 4680 Cells For Tesla: Report.” Accessed: Apr. 17, 2024. [Online]. Available: https://insideevs.com/news/565096/tesla-4680-cells-panasonic-testing/

[28] “Utility-scale batteries and pumped storage return about 80% of the electricity they store - U.S. Energy Information Administration (EIA).” Accessed: Mar. 16, 2024. [Online]. Available: https://www.eia.gov/todayinenergy/detail.php?id=46756

[29] “Bi-Directional DC-DC Optimizers | Solar + Storage.” Accessed: Apr. 18, 2024. [Online]. Available: https://alenconsystems.com/bidirectional-dc-dc/

[30] “Bi-directional DCDC & DCAC Inverter.” Accessed: Mar. 17, 2024. [Online]. Available: https://www.sinexcel.us/storage-inverters

[31] “The 15 Bestselling EVs of 2023,” Car and Driver. Accessed: Apr. 20, 2024. [Online]. Available: https://www.caranddriver.com/news/g46351238/bestselling-ev-2023/

[32] S. Touchette, S. Recoskie, G. Torlone, and D. MacNeil, “Lithium-ion battery safety primer: for use, storage and disposal,” National Research Council of Canada. Energy Mining and Environment. Battery Testing and Optimisation, Jun. 2021. doi: 10.4224/40002644.

[33] “Battery Pack Cell Voltage Difference and Solution Part 1 | Battery Monday.” Accessed: Nov. 21, 2023. [Online]. Available: https://www.grepow.com/blog/battery-pack-cell-voltage-difference-and-solution-part-1-battery-monday.html

[34] DNKPOWER, “Basics on Classifications of Battery Management System(BMS),” Lithium ion Battery Manufacturer and Supplier in China-DNK Power. Accessed: Jan. 08, 2024. [Online]. Available: https://www.dnkpower.com/li-ion-bms/

[35] “Battery Energy Storage System (BESS) Design using Ansys Fluent.” Accessed: Apr. 26, 2024. [Online]. Available: https://resources.randsim.com/rand-simulation-solutions-blog/battery-energy-storage-system-bess-design-using-ansys-fluent

[36] “Tesla Powerwall is the only home battery with thermal management,” Dunedin Solar. Accessed: Mar. 21, 2024. [Online]. Available: https://dunedinsolar.co.nz/knowledge-hub-posts/tesla-powerwall-is-the-only-home-battery-with-thermal-management/

[37] C. White and L. G. Swan, “Pack-level performance of electric vehicle batteries in second-life electricity grid energy services,” *Journal of Energy Storage*, vol. 57, p. 106265, Jan. 2023, doi: 10.1016/j.est.2022.106265.

[38] “Chevrolet Bolt Owner Has Battery Pack Replaced Twice | GM Authority,” GM Authority | General Motors News, Rumors, Reviews, Forums. Accessed: Apr. 07, 2024. [Online]. Available: https://gmauthority.com/blog/2019/02/chevrolet-bolt-ev-owner-reportedly-has-battery-pack-replaced-twice/

[39] “Orion BMS 2 | Orion Li-Ion Battery Management System.” Accessed: Mar. 17, 2024. [Online]. Available: https://www.orionbms.com/products/orion-bms-standard/

APPENDIX A: EMS DATA COLLECTION

List	EMS Data Collection and Generation
	Capacity (Ah or kWh):
1	Measured Capacity
2	Total charge and discharge capacity (Ah or kWh)
3	Energy Efficiency
	Current (A):
4	DC charge/ discharge current
5	AC charge/ discharge current (L1, L2, L3)
6	Maximum specified current limit
	DC Voltage (V):
7	Maximum charge voltage
8	Minimum discharge voltage
9	Average cell voltage
10	Maximum cell voltage (ID cell)
11	Minimum cell voltage (ID cell)
12	Maximum cell voltage Detla
	AC Voltage (V)
13	AC line-to-line voltage (AB/AC/BC)
14	AC line to ground voltage
	Power (kW):
15	DC Charge and discharge power
16	AC Charge and discharge power
	Temperature (°C):
17	Maximum and minimum cell temperature (ID cell)
18	Maximum and minimum cell temperature distribution
	Operational Data
19	Operation mode
20	Test Time
21	Cycle Time
22	Step Time
23	Cycle Number
~	**BMS Canbus Data (196 counts)**
~	**PCS Operational Data (56 counts)**

APPENDIX B: RPT CYCLING SCRIPT

```
STEP_TIME       100 ms
SET_VALUE       C_Pause_B       =       Off
CALL    CyclingScripts\SubScripts\AuxClear.aut
LABEL   TestBegin
SET_VALUE       M_Cycle_Num_I=  S_Cycle_Num_Start_I
SET_VALUE       M_Step_Num_I    =       TestBegin
DATALOG_START   MeasureLogger
DATALOG_PAUSE   MeasureLogger
DATALOG_START   SummaryLogger
DATALOG_PAUSE   SummaryLogger
CALL    CyclingScripts\SubScripts\ComponentsChannelLimitsReset.aut
CALL    CyclingScripts\SubScripts\TestClear.aut
DATALOG_RESUME  MeasureLogger
SET_VALUE       mode_set        =       1
WAIT    1 sec
SET_VALUE       mode_set        =       0
MESSAGE_BOX     TITLE = "Critical Task Checklist";
    ICON = 3;
    MB_TYPE = 3;
    MESSAGE = "You have executed TestBegin, now:
VERIFY (refer to Standard Operating Practice Document):
-Hardware: TCS, DAQ, BMS, TEM, Shunt, PC, Mid-pack Current Connector
-Emerald: Channel Selector, Automation Channel, Script Name
-Emerald: Customized EQUATIONS and DATA LOGGING
-Emerald: T ChX table for TestName, AuxTempMax, AuxVoltMax/Min
CHOOSE
Yes: Start Test (RestBegin)
No: Pause Mode (Pause, for user-adjustable steps and times)
Cacel: Quit and reset safety values (TestEnd)
NOTE: WAIT 10 SECONDS FOR PRE-CHARGE AT START OF TEST AND WHEN EXITING PAUSE";
    ACTION = Action;
        YES -> RestBegin;
        NO -> Pause;
        CANCEL -> TestEnd;
END_MESSAGE
CALL    CyclingScripts\SubScripts\StepClear.aut
LABEL   RestBegin
CALL    CyclingScripts\SubScripts\StepClear.aut
SET_VALUE       M_Step_Num_I    =       RestBegin
SET_VALUE       mode_set        =       0
DO
IF      C_Pause_B = On THEN
JUMP    Pause
END_IF
WHILE   M_Step_Time_h <= L_RestBegin_Length_h
    OR  M_Aux_Temp_Max_C >= L_Rest_TempHigh_C
    OR  M_Aux_Temp_Min_C <= L_Rest_TempLow_C
END_WHILE
CALL    CyclingScripts\SubScripts\StepClear.aut
LABEL   Dis1
IF      S_Dis1_Mode != Standby THEN
SET_VALUE       M_Step_Num_I    =       Dis1
CALL    CyclingScripts\SubScripts\ComponentsChannelLimitsDischarge.aut
```

```
SET_VALUE     mode_set          =          3
DO
IF         C_Pause_B = On THEN
JUMP    Pause
END_IF
SET_VALUE
   C_Ch_Current_A        =          S_Dis1_CC_A
   C_Ch_Voltage_V        =          S_Dis1_CV_V
   C_Ch_Power_kW         =          S_Dis1_CP_kW
END_SET
WHILE  M_Ch_Voltage_V >= L_Dis1_Volt_V
   AND M_Aux_Volt_Min_V >= L_Dis1_Aux_Volt_V
   AND M_Step_Time_h <= L_Dis1_Time_h
   AND M_Step_Cap_Dis_Ah <= L_Dis1_Cap_Ah
   AND M_Step_En_Dis_kWh <= L_Dis1_En_kWh
   AND M_Dis_Time_h <= L_Dis_Time_h
   AND M_Cycle_Cap_Dis_Ah <= L_Dis_Cap_Ah
   AND M_Cycle_En_Dis_kWh <= L_Dis_En_kWh
   OR    mode = 0
END_WHILE
END_IF
SET_VALUE     mode_set          =          0
CALL    CyclingScripts\SubScripts\ComponentsChannelLimitsReset.aut
CALL    CyclingScripts\SubScripts\StepClear.aut
LABEL  RestDis
SET_VALUE     M_Step_Num_I  =          RestDis
SET_VALUE     mode_set          =          0
DO
IF         C_Pause_B = On THEN
JUMP    Pause
END_IF
WHILE  M_Step_Time_h <= L_RestDis_Length_h
   OR    M_Aux_Temp_Max_C >= L_Rest_TempHigh_C
   OR    M_Aux_Temp_Min_C <= L_Rest_TempLow_C
END_WHILE
CALL    CyclingScripts\SubScripts\StepClear.aut
LABEL  Chg1
IF         S_Chg1_Mode != StandbyTHEN
SET_VALUE     M_Step_Num_I  =          Chg1
CALL    CyclingScripts\SubScripts\ComponentsChannelLimitsCharge.aut
SET_VALUE     mode_set          =          3
DO
IF         C_Pause_B = On THEN
JUMP    Pause
END_IF
SET_VALUE
   C_Ch_Current_A        =          S_Chg1_CC_A
   C_Ch_Voltage_V        =          S_Chg1_CV_V
   C_Ch_Power_kW         =          S_Chg1_CP_kW
END_SET
WHILE  M_Ch_Voltage_V < L_Chg1_Volt_V
   AND M_Aux_Volt_Max_V <= L_Chg1_Aux_Volt_V
   AND M_Ch_Current_Avg_A >= L_Chg1_Current_A
   AND M_Step_Time_h <= L_Chg1_Time_h
   AND M_Step_Cap_Chg_Ah <= L_Chg1_Cap_Ah
   AND M_Step_En_Chg_kWh <= L_Chg1_En_kWh
```

```
    AND M_Chg_Time_h <= L_Chg_Time_h
    AND M_Cycle_Cap_Chg_Ah <= L_Chg_Cap_Ah
    AND M_Cycle_En_Chg_kWh <= L_Chg_En_kWh
    OR  mode = 0
    OR  M_Step_Time_h <= 0.0000
    OR  M_SincePause_Time_h <= 0.0000
END_WHILE
END_IF
SET_VALUE   mode_set        =       0
CALL  CyclingScripts\SubScripts\ComponentsChannelLimitsReset.aut
CALL  CyclingScripts\SubScripts\StepClear.aut
LABEL RestChg
SET_VALUE   M_Step_Num_I    =       RestChg
SET_VALUE   mode_set        =       0
CALL  CyclingScripts\SubScripts\CycleCapacityandEfficiency.aut
DO
IF      C_Pause_B = On THEN
JUMP  Pause
END_IF
WHILE M_Step_Time_h <= L_RestChg_Length_h
    OR  M_Aux_Temp_Max_C >= L_Rest_TempHigh_C
    OR  M_Aux_Temp_Min_C <= L_Rest_TempLow_C
END_WHILE
CALL  CyclingScripts\SubScripts\StepClear.aut
LABEL Loop1
SET_VALUE   M_Step_Num_I    =       Loop1
SET_VALUE   mode_set        =       0
CALL  CyclingScripts\SubScripts\CycleClear.aut
EQUATION    M_Cycle_Num_I = M_Cycle_Num_I + 1
IF      M_Cycle_Num_I <= L_Cycle_Num_End_I  THEN
JUMP  Dis1
END_IF
SET_VALUE   mode_set        =       0
CALL  CyclingScripts\SubScripts\ComponentsChannelLimitsReset.aut
CALL  CyclingScripts\SubScripts\StepClear.aut
LABEL RestEnd
SET_VALUE   M_Step_Num_I    =       RestEnd
SET_VALUE   mode_set        =       0
DO
IF      C_Pause_B = On THEN
JUMP  Pause
END_IF
WHILE M_Step_Time_h <= L_RestEnd_Length_h
    OR  M_Aux_Temp_Max_C >= L_Rest_TempHigh_C
    OR  M_Aux_Temp_Min_C <= L_Rest_TempLow_C
END_WHILE
CALL  CyclingScripts\SubScripts\StepClear.aut
LABEL TestEnd
SET_VALUE   M_Step_Num_I    =       TestEnd
SET_VALUE   mode_set        =       0
END
```

APPENDIX C: COPYRIGHT AGREEMENTS

ELSEVIER LICENSE
TERMS AND CONDITIONS

Apr 03, 2024

This Agreement between Dalhousie University -- Ryan Ning ("You") and Elsevier ("Elsevier") consists of your license details and the terms and conditions provided by Elsevier and Copyright Clearance Center.

License Number	5761361287308
License date	Apr 03, 2024
Licensed Content Publisher	Elsevier
Licensed Content Publication	Journal of Energy Storage
Licensed Content Title	Degradation of lithium-ion batteries that are simultaneously servicing energy arbitrage and frequency regulation markets
Licensed Content Author	Bryan Ellis,Chris White,Lukas Swan
Licensed Content Date	Aug 30, 2023
Licensed Content Volume	66
Licensed Content Issue	n/a
Licensed Content Pages	1
Start Page	107409
End Page	0

ELSEVIER LICENSE
TERMS AND CONDITIONS

Apr 03, 2024

This Agreement between Dalhousie University -- Ryan Ning ("You") and Elsevier ("Elsevier") consists of your license details and the terms and conditions provided by Elsevier and Copyright Clearance Center.

License Number	5761370050264
License date	Apr 03, 2024
Licensed Content Publisher	Elsevier
Licensed Content Publication	Journal of Energy Storage
Licensed Content Title	Degradation of electric vehicle lithium-ion batteries in electricity grid services
Licensed Content Author	Mark Elliott,Lukas G. Swan,Matthieu Dubarry,George Baure
Licensed Content Date	Dec 1, 2020
Licensed Content Volume	32
Licensed Content Issue	n/a
Licensed Content Pages	1
Start Page	101873
End Page	0

ELSEVIER LICENSE
TERMS AND CONDITIONS

Apr 03, 2024

This Agreement between Dalhousie University -- Ryan Ning ("You") and Elsevier ("Elsevier") consists of your license details and the terms and conditions provided by Elsevier and Copyright Clearance Center.

License Number	5761370344965
License date	Apr 03, 2024
Licensed Content Publisher	Elsevier
Licensed Content Publication	Journal of Energy Storage
Licensed Content Title	A comparison of system architectures for high-voltage electric vehicle batteries in stationary applications
Licensed Content Author	Michaela Bauer,Julian Wiesmeier,John Lygeros
Licensed Content Date	Oct 1, 2018
Licensed Content Volume	19
Licensed Content Issue	n/a
Licensed Content Pages	13
Start Page	15
End Page	27